X-ray Scattering Studies on Protein Structure in Solution

1987

Yukio Morimoto

X-ray Scattering Studies
on
Protein Structure in Solution

A Doctoral Thesis Submitted

by

Yukio Morimoto

to

Faculty of Science

Osaka University

1987

APPROVALS

February, 1987

This thesis is approved
as to style and content
by

勝部幸輝

Member-in-chief

小高忠男

Member

寺本明夫

Member

高木俊夫

Member

田中信夫

Member

Acknowledgments

First of all, it should be mentioned that the work of this thesis has been carried out under the guidance of Professor Yukiteru Katsube of Institute for Protein Research, Osaka University.

The author is greatly indebted to Professor Yukiteru Katsube for his cordial guidance, advice and encouragement throughout this investigation.

The author is greatly indebted to Dr. Nobuo Tanaka for his continuous guidance and helpful advice throughout this investigation.

The author expresses his great gratitude to Professor Takayuki Ozawa, Dr. Masashi Tanaka and Dr. Yoshiharu Shimomura of Department of Biomedical Chemistry, Faculty of Medicine, University of Nagoya, for their useful discussion and biochemical advice for cytochrome oxidase and cytochrome $\underline{bc_1}$ complex from beef heart.

The author expresses his great thanks to Dr. Yoshiki Matsuura for their useful discussion for human immunoglobulin M.

The author expresses his deep thanks to Dr. Mamoru Sato Dr. Masami Kusunoki and Dr. Yasuo Hata for their kind guidance and discussion of X-ray structural study.

Thanks are due to Mr. Tatsuhisa Kato for his technical assistance of X-ray experiment.

The author would like to thank all members of Katsube laboratory for their friendship.

The author would like to acknowledge Mrs. Miyoko Morimoto for her assistance in preparing the manuscript.

Finally, the author thanks sincerely to his parents for their unfailing understanding and continuing encouragement.

森本幸生

Yukio Morimoto

February, 1987

CONTENTS

General Introduction 1

Chapter I

General theory of small-angle X-ray scattering

I-1 X-ray scattering from a single particle 4

I-2 Scattering from a solution composed of identical particles 8

I-3 Contrast variation method 12

I-4 Evaluation of the molecular parameters 17

1. Radius of gyration, Rg 17

2. Maximum dimension, Dmax 19

3. Volume, V 19

4. Molecular weight, Mw 20

5. Eccentricity, ω 21

Chapter II

Development of the experimental system of the solution X-ray scattering and the treatment of scattering intensities

II-1 Introduction 22

II-2 The small-angle X-ray scattering 24

II-3 The high resolution small-angle X-ray scattering . . 28

II-3-1 Design 29

II-3-2 Estimation of the new apparatus 34

a) Latex particle 34

b) Human immunoglobulin M (IgM) 36

c) Human α_2-macroglobulin (α_2M) 38

II-4 The middle- or large-angle X-ray scattering 40
II-5 Data treatments and analyses of the solution X-ray scattering intensities 41
a) Average of the scattering intensities 41
b) Correction for collimation effect (Desmearing) . . 43
c) Data analysis 45
II-6 Conclusion 46

Chapter III

Structural studies on cytochrome oxidase and cytochrome $\underline{bc_1}$ complex isolated from beef heart

III-1 Introduction 51
III-2 Experimental 55
III-2-1 Cytochrome oxidase and its complex with cytochrome $\underline{c}$ 55
III-2-1-1 Isolation and purification of cytochrome oxidase and cytochrome $\underline{c}$ 55
III-2-1-2 Cytochrome oxidase-cytochrome $\underline{c}$ complex 61
III-2-1-3 Preparation of samples for the contrast variation method 62
III-2-1-4 Measurement of small-angle X-ray scattering intensities 65
III-2-2 Cytochrome $\underline{bc_1}$ complex 67
III-2-2-1 Isolation and purification of cytochrome $\underline{bc_1}$ complex 67
III-2-2-2 Preparation of samples for the small-angle X-ray scattering measurement 72

III-2-2-3 Measurement of small-angle X-ray scattering intensities 73
III-3 Results 74
III-3-1 Cytochrome oxidase and its complex with cytochrome c 74
III-3-2 Simulation of model of cytochrome oxidase and its complex with cytochrome c 87
III-3-3 Cytochrome bc_1 complex 92
III-4 Discussion 99

Chapter IV
Secondary structure analysis of proteins by means of the solution X-ray scattering

IV-1 Introduction 108
IV-2 Experimental 110
IV-2-1 Preparation of protein solutions 110
IV-2-2 Large-angle X-ray scattering measurement 110
IV-2-3 Small-angle X-ray scattering measurement 111
IV-3 Results 112
IV-3-1 Data reduction 112
IV-3-2 Data analysis 116
IV-3-3 Simulation 123
IV-4 Discussion 133

Chapter V General conclusion 139

References 143

List of publications 147

General introduction

Polypeptide chains in a protein often form regular arrangements, that is, secondary structure, like α-helical or β-pleated sheet structure in certain regions, but these regions are always rather limited and the entire polypeptide chain is folded into complex tertiary structure which is three-dimensional structure with reference to the side chain types. In the tertiary structure, some regions of secondary structure frequently tend to aggregate as structural domains. The structure of such an aggregate is called a super-secondary structure and can be classified into several structural classes according to the arrangement of the secondary structure. It is known that biological functions of a protein are determined by its three-dimensional structure. In some cases, the protein functions by forming a quaternary structure which is the three-dimensional arrangement of more than one polypeptide chain. The biological function is very often dependent on the ability of such tertiary or quaternary structure to respond to the interaction with other molecules by conformational changes. Knowledge of the detailed three-dimensional structure is a key to the understanding of the biological function. At the present time, X-ray structure analysis of protein crystals is the only method by which detailed structural information may be obtained at the level of atomic resolution. However, the method has limitation and disadvantage, in that it is

applicable only to crystals. Therefore, structural studies of proteins in solution are required to compensate for this weak point in the crystal structure analysis. Solution X-ray scattering analysis is a technique for studying structural features of colloidal particles and can extract the structural information from the diffuse scattering intensity distribution profile around the incident X-rays. The intensity distribution profile is usually analyzed in two scattering angle regions , that is, small-angle and large-angle regions. The former distribution profile gives information about the overall structure of the protein molecule and the latter reveals the protein internal structure in solution. Recent developments of the X-ray source such as the synchrotron radiation and the one- or two-dimensional detectors have greatly shortened the measurement time and made it possible to detect the structural changes of some biological macromolecules.

In this work, we have dealt with a new way of studying protein structure in solution by means of solution X-ray scattering and the results applied to some enzymes. Chapter I describes the general theory of X-ray scattering and the structural parameters that can be obtained by the X-ray scattering method. Chapter II deals with the newly designed experimental system to learn the structure of proteins by the solution X-ray scattering method and with its data processing. In Chapter III, the structural studies on cytochrome $\underline{aa_3}$-type oxidase and $\underline{bc_1}$ complex from beef heart mitochondria by means of the small-angle X-ray

scattering are discussed. In Chapter IV, internal structures of some globular protein molecules of known structure, which have been determined by the large-angle X-ray scattering method, are discussed in terms of the secondary or super-secondary structure.

Chapter I

General theory of small-angle X-ray scattering

I-1 X-ray scattering from a single particle

X-ray diffraction gives the amplitude of radiation scattered by a point M_k in the direction defined by a unit vector $\vec{s}$,

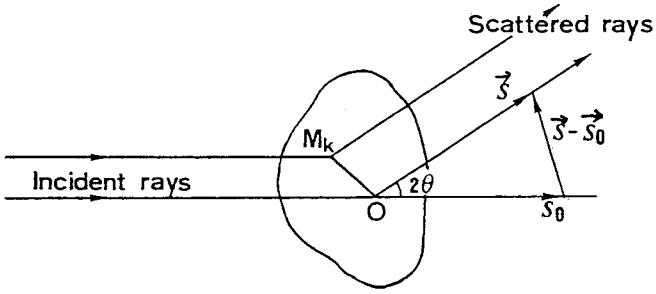

$$A_k = A_e f_k e^{-i\frac{2\pi}{\lambda}(\vec{s} - \vec{s}_0)\ \vec{OM}_K} \qquad (I\text{-}1)$$

where A_e designates the amplitude scattered by one electron, f_k the scattering factor of the mass point M_k, O an arbitrary origin used to describe the path differences among different rays, and $\vec{s}_o$ the unit vector defining the direction of the incident radiation. The scattering vector $\vec{h}$, in the reciprocal space, is $2\pi(\vec{s}-\vec{s}_0)/\lambda$. The magnitude of the vector $\vec{h}$ is $h=(4\pi\sin\theta)/\lambda$, in which 2θ represents the scattering angle and λ is the wavelength. The total amplitude of radiation scattered by a single particle is then,

$$A(\vec{h}) = \sum_k A_k(\vec{h}) = A_e \sum_k f_k \exp(-i\vec{h}\vec{OM}_k) \qquad (I\text{-}2)$$

and the scattered intensity, the product of the amplitude A and its complex conjugate A^*, is

$$I(\vec{h}) = A_e^2 \sum_k \sum_j f_k f_j \cos(\vec{h}\vec{r}_{kj})$$

$$= A_e^2 \{ \sum_{k=1}^{N} f_k^2 + \sum_k \sum_{j \neq k} f_k f_j \cos(\vec{h}\vec{r}_{kj}) \} \qquad \text{(I-3)}$$

where $\vec{r}_{kj}$ represents the vector from the point M_k to M_j.

The particle takes overall directions of r, so that $\cos(\vec{h}\vec{r})$ can be replaced by its average as following equation:

$$\langle I(\vec{h}) \rangle = I(h) = \sum_k \sum_j f_k f_j \frac{\sin(hr_{kj})}{hr_{kj}} \qquad \text{(I-4)}$$

where $\langle I(\vec{h}) \rangle$ designates the average of $I(\vec{h})$ in all directions of distance r. This is the fundamental formula due to Debye (1). Equation (I-4) can be rewritten by expanding the trigonometric function in powers of h^2,

$$I(h) = \sum_k \sum_j f_k f_j \{1 - \frac{h^2}{6} |\vec{r}_{kj}|^2 + \ldots\}$$

$$= \sum_k \sum_j f_k f_j - \frac{h^2}{6} \sum_k \sum_j f_k f_j |\vec{r}_{kj}|^2 + \ldots \qquad \text{(I-5)}$$

The first term of the expansion is equal to $(\Sigma f_k)^2$ which is I(0) (zero-angle scattering intensity). To describe the second term, a point O defining the center of mass of the particle is chosen so that $\Sigma f_k \vec{r}_k = 0$. If all the atoms are the same, this electronic center of gravity coincides with the conventional center of gravity of the particle. If $\vec{r}_k$ is defined as the vector from the point O to M_k,

equation (I-5) can be rewritten as:

$$I(h) = \{(\sum_k f_k)^2 - \frac{2}{6}h^2 \sum_j f_j \sum_k f_k |\vec{r}_k|^2 + \ldots\}$$

or

$$I(h) = (\sum_k f_k)^2 \{1 - \frac{h^2}{3} \frac{\sum_k f_k |\vec{r}_k|^2}{\sum_k f_k} + \ldots\} \qquad (I-6)$$

Guinier introduced a parameter, Rg, defined by the following equation (2):

$$Rg^2 = \frac{\sum_k f_k |\vec{r}_k|^2}{\sum_k f_k} \qquad (I-7)$$

Equation (I-6) can be rewritten as equation (I-8) by use of equation (I-7) with a good approximation under the condition of small h :

$$I(h) = n^2 \exp(\frac{-h^2 Rg^2}{3}) \qquad (I-8)$$

where n ($=\Sigma f_k$) is the total number of electrons in the particle. This relation of equation (I-8) is called the law of Guinier. Consequently, the radius of gyration, Rg, of the particle can be estimated from the initial slope of a log $I(h)$-h^2 plot (Guinier plot).

Equation (I-4) can be replaced by integration over the whole volume V irradiated by the incident beam and when V is equal to unity:

$$I(h) = \int_V \int_V \rho(\vec{r}_k)\ \rho(\vec{r}_j)\ \frac{\sin(hr_{kj})}{hr_{kj}}\ d\vec{r}_k\, d\vec{r}_j \qquad (I-9)$$

where $\rho(\vec{r}_k)$ is an electron density at a point $\vec{r}_k$. With the distance r between the point M_k and the point M_j, equation (I-9) can be written as follows:

$$I(h) = \int_0^\infty \{ \int_V \rho(\vec{r}_k) \ \rho(\vec{r}_k+\vec{r}) \, d\vec{r}_k \} \frac{\sin(hr)}{hr} 4\pi r^2 dr \qquad (I-10)$$

Porod (3) introduced a characteristic function $\gamma(r)$ defined by:

$$\gamma(r) = \int_V \rho(\vec{r}_k) \ \rho(\vec{r}_k+\vec{r}) \, d\vec{r}_k \qquad (I-11)$$

The scattering intensity is represented by use of $\gamma(r)$ as:

$$I(h) = 4\pi \int_0^\infty \gamma(r) r^2 \frac{\sin(hr)}{hr} dr \qquad (I-12)$$

The $\gamma(r)$ represents the probability that a point at a distance r from a given point in the particle will be found in the particle.

The distance distribution function P(r) is expressed:

$$P(r) = r^2 \gamma(r) \qquad (I-13)$$

P(r) is defined as the function representing the distribution of distance r in the particle. By use of P(r), scattering intensity is also expressed as follows:

$$I(h) = 4\pi \int_0^\infty P(r) \frac{\sin(hr)}{hr} dr \qquad (I-14)$$

Then, the distance distribution of a particle is obtained by the Fourier transform of the scattering intensity,

$$P(r) = \frac{1}{2\pi^2}\int_0^\infty I(h)\,hr\sin(hr)\,dh \qquad \text{(I-15)}$$

I-2 Scattering from a solution composed of identical particles

If particles producing small-angle scattering are densely packed, not only the interference within individual particles but also the mutual interference between neighboring particles must be considered, just as the mutual interference between neighboring atoms has to be taken into account in extending the treatment of the X-ray diffraction by monatomic gases to the case of liquids.

A simple case can be described by the intensity of the X-rays scattered from a large number of identical atoms (i.e. all having the same atomic scattering factor, f_{atom}) separated by distance of the order of the atomic radius, as for example in liquid mercury. In this case, the scattering intensity can be written by the following equation similar to equation (I-3):

$$I(\vec{h}) = A_e^2 f_{atom}^2 \{ {}_{j=k}N + \sum_k^{k\neq j}\sum_j \cos(\vec{hr}_{kj}) \} \qquad \text{(I-16)}$$

where N is the total number of atoms in the irradiated volume. The problem here is to find a method of summing

the second term of equation (I-16) over almost infinite pairs of atoms. If the atoms are completely disordered, their statistical distribution may be assumed to be independent of the particular choice of an atom as the origin, and statistical methods are applied to the pairs of atoms.

If the total volume is V and the total number of atoms within the volume is N, the average volume occupied by one atom is $V/N=v_1$. The probability of finding an atom in a volume element dv is dv/v_1. The probability that a second atom will be found within a volume element dv at a distance and direction, r, from this atom should also be dv/v_1. This may be true only for values of r very much longer than the average interatomic distance. It is not true for liquids at small values of r; the atoms or molecules exhibit short-range order interactions over relatively short distances. In this case, the probability of finding an atom in volume dv at r should be expressed as $dW(\vec{r})$, where $W(\vec{r})$ is known as the radial density distribution function. The $dW(\vec{r})$ therefore can be rewritten as $W(\vec{r})dv/v_1$. $W(\vec{r})$ is a function which must clearly take the value of zero for r less than twice the contact radius of the atoms and which must tend to be unity for sufficiently large r. Intermediate values of $W(\vec{r})$ are oscillates above and below unity. For this reason, the double summation in equation (I-16) cannot be carried out by means of arithmetical addition with equal weight given to each pair of atoms. Instead a weight $(1/v_1)(W(\vec{r})-1)$ must be assigned to the vector $\vec{r}_{kj}$.

Moreover, as $\vec{r}_{kj}$ may be assumed to be continuously variable, summation can be replaced by integration. If the system is isotropic, $\vec{r}_{kj}$ is independent of the direction, and may be replaced by r. Then, the equation (I-16) can be rewritten as:

$$I(h) = A_e^2 f_{atom}^2 N\{1+\frac{1}{v_1}\int_0^\infty 4\pi r^2 (W(r)-1) \frac{\sin(hr)}{hr} dr\} \qquad (I-17)$$

The scattering intensity for monatomic liquids can be given the following expression:

$$I(h) = A_e^2 f_{atom}^2 N\{1+\int_0^\infty 4\pi r^2 (\rho_a(r)-\rho_0) \frac{\sin(hr)}{hr} dr\} \qquad (I-18)$$

where $\rho_a(r)$ is an atomic density of the solution and ρ_0 is its average density: $\rho_0=1/v_1$. This expression was introduced initially by Zernickel and Prins, and by Debye and Menke.

The scattering intensity from the solution of closely assembled spherical particles with uniform size (radius = R) can be expressed by the number n of electrons and scattering factor Φ of the sphere :

$$I(h) = A_e^2 Mn^2\Phi^2\{1+\int_0^\infty 4\pi r^2 (\rho(r)-\rho_0) \frac{\sin(hr)}{hr}\}dr \qquad (I-19)$$

$$\Phi^2 = \{ 3 \frac{\sin(hR)-hr\cos(hR)}{h^3R^3}\}^2$$

where M is the number of particles in the unit volume, ρ_0 the average particle density in the system and $\rho(r)$ the

particle density in the immediate environment of a particle.

In the solution system, the W(r) in equation (I-17) is related to the osmotic pressure p and the potential energy, Ψ, between the particles through the equation of state:

$$p = \frac{kT}{v_1} - \frac{1}{6v_1^2}\int_0^\infty W(r)\psi(r)4\pi r^3\, dr \qquad \text{(I-20)}$$

This relation was introduced by Green (4). When W(r) is zero, i.e. when particles are separated sufficiently, equation (I-20) is reduced to $pv_1=kT$ and the scattering intensity becomes $I(h)=A_e^2(h)Mn^2\Phi^2$. This scattering intensity represents that of a single particle. Then a first approximation to W(r) is:

$$W(r) = \exp(-\psi(r)/kT) \qquad \text{(I-21)}$$

To this approximation, the equation of state becomes

$$pv = kT\{1-\frac{(2\pi)^{\frac{3}{2}}}{2}\frac{\beta(0)}{v_1}\} \qquad \text{(I-22)}$$

and scattering intensity is

$$I(h) = A_e^2\, Mn^2\Phi^2\{1+\frac{(2\pi)^{\frac{3}{2}}}{v_1}\beta(h)\} \qquad \text{(I-23)}$$

where the function $\beta(h)$ is defined by the relation:

$$h\beta(h) = \frac{2}{\sqrt{2\pi}}\int_0^\infty r(\exp(-\psi(r)/kT)-1)\sin(hr)\, dr \qquad \text{(I-24)}$$

An approximate solution for hard spheres of radius R and volume v_0 has been obtained by Debye (5). With the probability function defined as:

$$W(r) = 0 \qquad 0 < r < 2R$$

$$W(r) = 1 \qquad r > 2R \quad ,$$

equation (I-23) becomes:

$$I(h) = A_e^2 \, Mn^2 \Phi^2(hR)\{1-\frac{8v_0}{v_1}\Phi(2hR)\} \qquad \text{(I-25)}$$

Equation (I-25) means that the scattering intensity from the solution depends upon the concentration, since the coefficient $8v_0/v_1$ corresponds to the number of particles irradiated by X-ray in a certain volume. It shows that interference between particles increases with concentration but approximates more closely to single particle scattering by decreasing of the concentration. This effect does not change in character even if the scattering body is rod-shaped or lamellar rather than spherical.

I-3 Contrast variation method

The theory of small-angle X-ray scattering explained above is adapted to the case of particles with electron density $\rho(\vec{r})$, where $\vec{r}$ is the distance from the electronic center of gravity of the particle. In the system where the particles diffuse into the solvent, it is required to exclude the effects of the solvent. The scattering

amplitude $A(\vec{h})$ is generally given by the Fourier transform of the electron density $\rho(\vec{r})$. Therefore, the intensity I(h) from a solution is written by:

$$I(h) = <\left|\int_V (\rho(\vec{r})-\rho_s)\exp(i\vec{h}\vec{r})\ d\ \vec{r}\right|^2> \qquad \text{(I-26)}$$

where the electron density of the solvent is assumed to be constant ρ_s. Equation (I-26) can be expanded in powers of h^2 to give equation (I-27) in the small-angle region, neglecting the third or higher power of h.

$$I(h) = (\Delta\rho V)^2\left(1-\frac{1}{3}\frac{h^2}{\Delta\rho V}\int_V|\vec{r}|^2(\rho(\vec{r})-\rho_s)\ d\ \vec{r}\right) \qquad \text{(I-27)}$$

$$\Delta\rho = \frac{1}{V}\int_V\rho(\vec{r})d^3\vec{r} - \rho_s = \bar{\rho} - \rho_s \qquad \text{(I-28)}$$

where $\bar{\rho}$ designates the mean electron density of the particle, $\Delta\rho$ is called the contrast and V stands for the volume of the particle. Equation (I-27) is effective when the center of gravity of the particle coincides with that of $\rho(\vec{r})$. The second term in equation (I-27) corresponds to the radius of gyration of a particle with electron density of the difference between $\rho(\vec{r})$ and ρ_s, and it can be written as:

$$Rg^2 = \frac{1}{\Delta\rho V}\int_V|\vec{r}|^2(\rho(\vec{r}) - \rho_s)\ d\ \vec{r} \qquad \text{(I-29)}$$

This relation means that Rg shows the effective envelope of the electron density of the particle in the solution where the particle is dispersed in the solvent. It is also clear that Rg of the particle is attributed to the contrast between the solvent and the particle.

The electron density of the particle, $\rho(\vec{r})$, can be divided into two terms:

$$\rho(\vec{r}) = \bar{\rho} + \rho_F(\vec{r}) \qquad \text{(I-30)}$$

where $\rho_F(\vec{r})$ represents the fluctuations around the mean electron density of the particle and its integration becomes zero.

$$\int_V \rho_F(\vec{r})\, d\vec{r} = 0 \qquad \text{(I-31)}$$

Fig. I-1 shows the relation of $\rho_F(\vec{r})$ to $\bar{\rho}$. Since the scattering intensity from the solution is given by equation (I-26), it can be rewritten with equations (I-28) and (I-30) as: (6)

$$I(h) = \Delta\rho^2 I_V(h) + \Delta\rho I_{VF}(h) + I_F(h) \qquad \text{(I-32)}$$

where

$$I_V(h) \simeq \left\langle \left| \int_V \exp(i\vec{h}\vec{r})\, d\vec{r} \right|^2 \right\rangle$$

$$I_F(h) \simeq \left\langle \left| \int_V \rho_F(\vec{r}) \exp(i\vec{h}\vec{r})\, d\vec{r} \right|^2 \right\rangle$$

$$I_{VF}(h) \simeq 2\left\langle \left| \left(\int_V \rho_F(\vec{r}) \exp(i\vec{h}\vec{r})\, d\vec{r} \right) \left(\int_V \exp(i\vec{h}\vec{r})\, d\vec{r} \right) \right| \right\rangle \qquad \text{(I-33)}$$

I_V is the scattering intensity from a particle with a uniform electron density, I_F reflects the fluctuation from the mean electron density of the particle, and I_{VF} is the

mixed term between I_V and I_F.

In the equation (I-33), I_F and I_{VF} contain $\rho_F(\vec{r})$ in their integrals, so that they become zero as $h \to 0$ because of the relation in equation (I-31). Consequently, for the intensity I(0) of zero-angle scattering using the contrast variation method, we have:

$$I(0) = \Delta\rho^2 I_V(0) \qquad \text{(I-34)}$$

This means that I(0) is zero when $\Delta\rho=0$. A plot of the square root of I(0) against $\Delta\rho$ may be a straight line and the point of intersection with the abscissa gives the mean electron density of the particle.

Luzzati and co-worker point out that the application of this method is generally based upon two assumptions: (a) the sample is a homogeneous solution of identical particles; (b) each particle has a scattering-power distribution which is independent of the scattering power of solvents. Therefore, this method is generally used on the assumption that the structure of the particle is not influenced by the change in the electron density of the solvent.

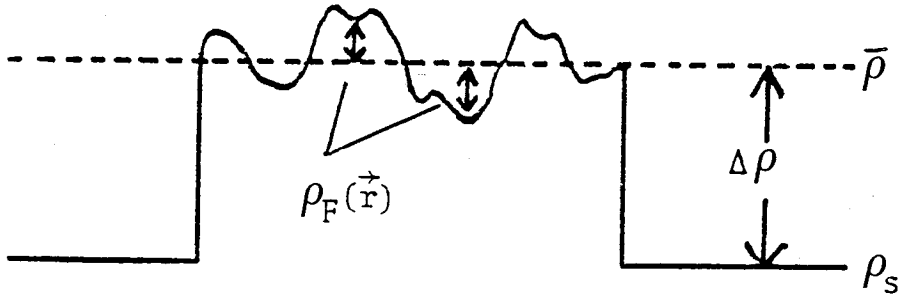

Fig. I-1. Schematic representation of $\bar{\rho}$, ρ_s, $\Delta\rho$ and $\rho_F(\vec{r})$; $\bar{\rho}$, ρ_s, mean electron density of the particle and the solvent; $\Delta\rho$, difference between the $\bar{\rho}$ and the ρ_s; $\rho_F(\vec{r})$, fluctuation of electron density of the particle.

I-4 Evaluation of molecular parameters

1. Radius of gyration, Rg

The radius of gyration, Rg, of a dissolved particle is one of the most important and precise parameter obtained by small-angle X-ray scattering and it can be determined in several different ways.

It is most commonly estimated by the law of Guinier described previously. The radius of gyration defined by A. Guinier (equation (I-7)) can be calculated from the slope of the straight line in the log I(h) versus h^2 plot. The plot of log I(h) versus h^2 is called the Guinier plot. This parameter is the same as the mean square distance from the center of gravity, if electrons are replaced for point masses. In this sense, this parameter is also the same as the mean-square radius of gyration, $\langle s^2 \rangle$, derived from the method of the light-scattering as the following expression:

$$\langle s^2 \rangle = \frac{1}{N^2} \sum_{i=1}^{N} \sum_{j=i+1}^{N} \langle r_{ij}^2 \rangle$$

where N is the number of scattering points for light and r_{ij} is a distance between i-th and j-th points.

The radius of gyration can also be determined from the distance distribution function, P(r). The approximate radius of gyration, Rg_A, is represented by the following equation (7):

$$Rg_A^2 = \int_0^{Dmax} r^2 P(r) dr / 2 \int_0^{Dmax} P(r) dr \qquad \text{(I-35)}$$

where Dmax is the maximum dimension of the particle. This method uses a whole scattering intensity which is described in equation (I-15), while the Guinier plot requires a innerpart (Guinier region) of the scattering intensity. In some cases, this method may be superior to the Guinier plot. It is especially so when a particle does not have the Guinier region in its scattering intensity distribution as in the case where the scattering intensity attributed to the overall structure of the particle disappears from the whole scattering distribution as the contrast is made zero. The radius of gyration depending upon the contrast is derived from the equations (I-29) and (I-30) as:

$$Rg^2 = Rg_V^2 + \frac{1}{\Delta\rho}\alpha - \frac{1}{\Delta\rho^2}\beta \qquad \text{(I-36)}$$

$$Rg_V^2 = \frac{1}{V}\int_V \vec{r}^2 \, d\vec{r}$$

$$\alpha = \frac{1}{V}\int_V \rho_F(\vec{r})\vec{r}^2 \, d\vec{r} \qquad \text{(I-37)}$$

$$\beta = \frac{1}{V^2}\int_V\int_V \rho_F(\vec{r})\rho_F'(\vec{r}')\vec{r}\,\vec{r}' \, d\vec{r} \, d\vec{r}'$$

Rg_V is the radius of gyration that may be observed for the particle at the infinite contrast. It represents the shape of the particle. The term α is a measure of the internal structure. In particular, if the particle can be approximated as a core surrounded by a spherical shell which is denser than the core, α is positive, and it is negative if the core has a higher density. The parameter β is always positive. It describes the displacement of the

apparent center of mass as a function of the contrast. For a simple shell-core particle, β increases as the distance between the centers of mass of the core and shell increases. β vanishes for a particle for which the electronic center coincides with the center of gravity. In a plot of Rg^2 which is obtained from the Guinier plot or the distance distribution function (equation (I-35)) versus $1/\Delta\rho$ (Stuhrmann plot), a point of intersection with the ordinate gives Rg_V^2, and the tangent of the curve in $1/\Delta\rho=0$ gives the term α.

2. Maximum dimension, Dmax

The distribution of the distance, r, in the particle is expressed by the P(r) function derived from the equation (I-15). It follows immediately from this definition that P(r) is zero for all distances larger than the maximum dimension of the particle. Therefore, the maximum dimension of the particle can be obtained by searching the distance, r, which makes the P(r) zero.

3. Volume, V

The electron density of the particle with uniform electron density is expressed as:

$$\rho(\vec{r}) = \rho = \text{const.} \qquad \text{(I-38)}$$

This assumption leads the equation (I-11) to the next equation:

$$\gamma(0) = \int_V \rho^2 dv = \rho^2 V \qquad \text{(I-39)}$$

Then, the following relation is derived by the Fourier inversion of the equation (I-12) and from the equation (I-39):

$$\gamma(0) = \frac{1}{2\pi^2}\int_0^\infty I(h)\ h^2 dh = \rho^2 V \qquad \text{(I-40)}$$

According to Porod (3), the following integral of scattering intensity is characterized as invariant and called Q:

$$Q = \int_0^\infty I(h) h^2 dh \qquad \text{(I-41)}$$

Scattering intensity at zero-angle, I(0), is in proportion to the summation of the number of electrons in the particle and can be expressed as:

$$I(0) \simeq n^2 = \rho^2 V^2 \qquad \text{(I-42)}$$

From the equations (I-40),(I-41) and (I-42), the volume of the particle can be obtained as:

$$V = 2\pi^2 I(0)/Q \qquad \text{(I-43)}$$

4. Molecular weight, Mw

If the partial specific volume of a particle is given by v(ml/mg), the molecular weight can be estimated as:

$$Mw = N_A V/v \qquad \text{(I-44)}$$

where N_A is the Avogadro's number.

5. Eccentricity, ω

The eccentricity of a particle can be estimated by the comparison of the experimental scattering intensity curve with a theoretical curve attributed to ellipsoid of revolution of a given axial ratios. Log I(h) versus log (hRg) plots are used frequently to illustrate these curves.

Chapter II

Development of the experimental system of the solution X-ray scattering and the treatment of scattering intensities

II-1 Introduction

An X-ray scattering experiment is to measure the variation of the intensity scattered by a sample as a function of the scattering direction, which is in general defined by two parameters. In the particular case that the scattering is circularly symmetric about an axis coincident with the incident beam, only one parameter, the scattering angle, is involved, and the experiment is the determination of the relative value of I(h), with $h=4\pi\sin\theta/\lambda$.

The method employed to realize the objectives discussed above is not different in principle from that used in all experiments in X-ray crystallography. However, special difficulties are encountered in investigating the scattering in very small angle region.

The scattering intensity in small angle is generally very weak, and moreover the path of the X-rays is several times as long as that in the X-ray crystallography. A powerful X-ray source is therefore required, and rotating anode X-ray generators are used. CuKα radiation is normally employed. The accuracy of the analysis increases with the decreasing slit width, increasing slit distance, and increasing specimen-to-detector distance. However, the small-angle scattering intensity simultaneously decreases.

Therefore the experimental conditions must be chosen carefully by considering the nature of the specimen and the purpose of the measurement. In order to investigate the structure of proteins, the instruments which are suitable for the measurement of intensities scattered from a protein solution are required to have sufficient accuracy. For this purpose, two kinds of experimental systems of small-angle scattering have been developed. One of them is the system which utilizes a commercially available camera. In this system, equipment such as data acquisition device and the specimen chamber have been developed originally. The other system has been designed so as to measure the scattering intensities at much smaller angle than that measured by the former system. The developed high resolution small-angle camera is available for the measurement of intensities scattered by some biological macromolecules with the large molecular size.

The investigation of the protein structure by means of the solution X-ray scattering can be made not only by the small-angle scattering but also by the large-angle X-ray scattering. The information on the internal structure such as the secondary or super-secondary structure and the distances between subunits would be reflected in the large angle region rather than the small angle region. These structural investigations require the system of the large-angle X-ray scattering, in which intensity distribution must be recorded up to such a resolution as the X-ray crystallographic analysis. A powerful and suitable

measuring system for the large-angle scattering has been developed.

A general treatment of the intensity distribution scattered by a protein solution and the evaluation of its accuracy will be described in this chapter. A correction technique for the effects of the slits and the methods of analysis of scattering intensity data are also described here.

II-2 The small-angle X-ray scattering

A schematic drawing of the experimental system of small-angle X-ray scattering method is shown in Fig. II-1. A commercially available small-angle scattering camera was modified as follows. The X-ray source is a 0.4 x 8 mm spot on the copper anode of a Phillips fine-focus X-ray tube equipped with a Rigaku Denki D9C X-ray generator run at 40 kV-30 mA. A line focus is used to obtain sufficiently intense X-rays. The spot is foreshortened to 0.04 x 8 mm at a glancing angle of 6°. The small-angle scattering camera (Rigaku Denki Co. Ltd.) installed in the X-ray beam has a single focusing mirror and two slits. The X-rays monochromatized by a 10 μm-thick nickel filter ($I_{K\beta}/I_{K\alpha} < 0.03$) are focused by a nickel-coated bending mirror (20 x 60 x 5 mm) and made to pass through the two slits. The first slit located just behind the mirror restricts the width and length of the X-ray beam reflected by the mirror and also stops the unreflected X-ray beam. The second

SCHEMATIC DIAGRAM FOR X-RAY SMALL ANGLE SCATTERING

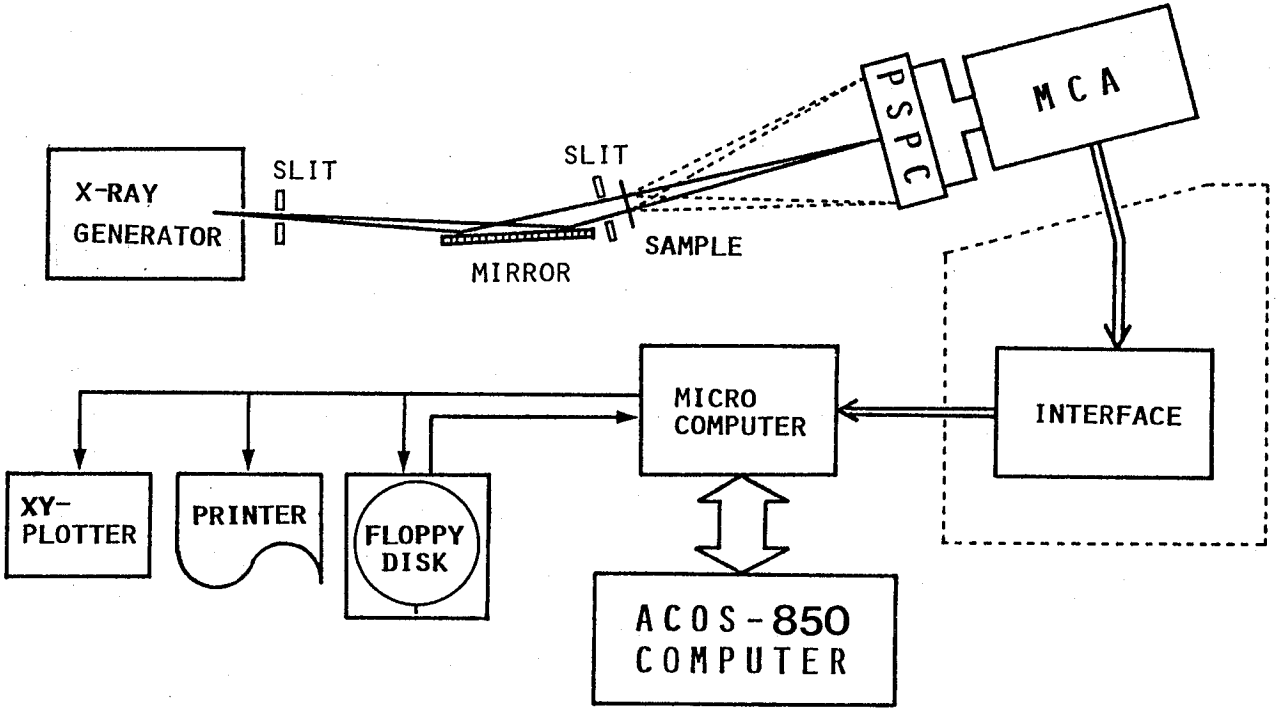

Fig. II-1. Schematic representation of small-angle X-ray scattering system; PSPC, position-sensitive proportional counter; MCA, multi-channel analyzer.

slit located just before the specimen cell prevents the parasitic scattering caused by the edge of the first slit from reaching the detector. A vacuum chamber is placed between the specimen holder and the detector to eliminate the air scattering.

X-ray scattering intensities are detected by a one-dimensional position sensitive proportional counter (PSPC). The effective slit area of the counter is 10 x 50 mm^2 with the depth of the counter of 11 mm. The PSPC (chamber) is filled with a gas mixture of 90% Ar and 10% CH_4 at the pressure of 2.2 Kg/cm^2. The spatial resolution of the PSPC is 0.1265 mm. A micro-computer (Hitachi, Level-III) controls a variety of measuring devices arranged in the experimental system, including the PSPC, a multichannel-pulse height analyzer and a process memory (64 K bytes).

In order to minimize the errors due to the specimen cell, it is required to keep it identical in the measurement of protein or buffer solution. Thus, a new specimen cell has been designed. The specimen cell was made of a quartz capillary in a form of a flow-cell. Each end of the capillary was connected to a plastic tube. This cell made it possible to replace a small volume of the sample solution, 50-100µl, without waste. An optimum thickness, d_{opt}, is represented as follows:

$$d_{opt} = \frac{1}{\mu}$$

where µ is the linear absorption coefficient. This

coefficient can be calculated approximately from the mass absorption coefficient of the individual elements of the material, by weighted summation according to the equation:

$$\mu = \left(\sum_{n=1}^{i} \left(\frac{\mu}{\rho}\right)_i \rho_i \right) \bar{\rho}$$

where ρ_i is the weight fraction of i-th element, $(\mu/\rho)_i$ the mass absorption coefficient of the i-th element and $\bar{\rho}$ the mean density of the entire sample at the measuring temperature. From a simple calculation, μ is approximately estimated to be 10 cm^{-1} in the case of copper Kα-radiation. Taking into account of the X-ray absorption of the protein solution, the capillary with 1.0 mm ϕ was chosen. A stopped-flow cell (Union Giken Co. Ltd.) modified for the X-ray scattering has been also prepared to measure the scattering intensities by means of time-resolved X-ray scattering. The instrument of the stopped-flow cell is also controlled by the same computer so that repeating measurements can be facilitated by use of this cell.

The temperature of the flow or the stopped-flow cell is controlled by circulating water with a constant temperature. The temperature of the cell is detected by a copper-constantan thermocouple located beside the capillary and is monitored on a recorder.

All the X-ray camera units are placed in a small chamber whose temperature is kept at 5°C (with a cooling unit), in order to prevent dew from appearing on the cell during low-temperature experiments. The sample-to-detector

distance is 305.0 mm, so that the scattering intensities can be collected in a range of scattering angles from 3.8 x 10^{-3} to 7.7 x 10^{-2} rad, corresponding to Bragg spacing from 400 to 20 Å.

II-3 The high resolution small-angle X-ray scattering

One of the structural parameters of the particles obtained by means of small-angle scattering is the radius of gyration, Rg. The value of the radius of gyration can be estimated by a log I(h) *versus* h^2 plot (Guinier plot). However the plot gives a straight line only in a region of $(h\ Rg)^2 < 1.2$, that is a Guinier region. This relation means that the Guinier region would be shifted to a smaller angle region if the particle becomes larger. For example, in order to estimate the radius of gyration of a particle of 60 Å, the scattering intensities must be measured in the range of scattering angle down to 4.5 x 10^{-3} rad. Therefore, the commercially available small-angle scattering camera described in section II-2 is not suitable for the measurement of the radius of gyration of such a particle by the method of the Guinier plot. However, the radii of gyration of biologically important macromolecules such as high molecular weight proteins, protein aggregates, viruses, membrane proteins and lipid proteins have usually large values. In order to measure the scattering intensities of such samples in very small angle region, a new high resolution small-angle scattering apparatus and

the system of the data processing were designed and developed. The details will be described below.

II-3-1 Design

An X-ray source is a 0.1 x 1 mm spot on the copper rotating anode of a Rigaku Denki (RU-200) X-ray generator operated at 40 kV-30 mA. The spot is foreshortened to 0.1 x 0.1 mm at a glancing angle of 6°. In the designing of the new apparatus, it can be assumed that a spherical protein which has a radius of gyration of 250 Å or larger is rare, because its molecular weight becomes to be about 1×10^{8} dalton assuming that the partial specific volume of 0.74. The new apparatus, for this reason, has been designed so as to detect scattering intensities in the Guinier region of such a large protein particle. Thus the small-angle resolution is required to be 1 mrad of scattering angle, corresponding to Bragg spacing of 1500 Å. A sample-to-detector distance of 1500 mm is necessary to attain the small-angle resolution of 1 mrad with a beam stop less than 3 mm in the width on a focal plane of a optics. The optics is in principle a focusing system by the use of reflections on a nickel- or a platinum-coated mirror. The focusing system can utilize whether a line-focusing system by use of a flat mirror or a point-focusing system by a toroidal mirror or two flat mirrors.

A reflecting angle on the nickel- or platinum-coated mirror is determined as in the following equation:

$$2\sin^2\left(\frac{\theta_1}{2}\right) \leqq \delta$$

where θ_1 is a critical angle for the reflection and δ is unit decrement of a reflection index. The δ can be expressed as follows:

$$\delta = ne^2\lambda^2/(2\pi mc^2)$$

where n is the number of electrons in a unit volume, e (esu) the electric charge of electron, λ (cm) the wavelength, m (g) the mass of electron and c (cm/s) the velocity of light in vacuo. From a simple calculation, the critical angle, θ_1, is given the values of 0.4217^{o} and 0.5871^{o} about the nickel and the platinum, respectively. The length of the platinum-coated mirror of which critical angle is 0.5871^{o} is determined to be 160 mm so that the width of the reflected beam becomes 1 mm which corresponds to the diameter of the specimen cell.

The focusing condition must be satisfied with a geometry as shown in Fig. II-2. F1 is a position on the focal plane of this optics and F2 is a position of the X-ray spot on the copper-target. The F1-F2 distance is a interfocal distance. If the M1 and M2 are both ends of the mirror, a center of the mirror of which length is $\overline{M1M2}$ must be placed approximately on the center of the interfocal distance so that critical angles on the two positions (M1,M2) can be satisfied effectively. And it results in that the distance between F1 and F2, full length of the apparatus, is longer than 3000 mm because of the distance of 1500 mm for the sample-to-detector distance. The depth of a groove of the platinum-coated toroidal mirror also can

be estimated to be less than 10 mm. Consequently, a beam conduit pipe made of stainless steel is 10 mm in inner-diameter and 1500 mm in length. Two slits are also available for this apparatus. They play unique roles of the restriction of the beam and the prevention of the parasitic scattering, each of which is located behind the mirror or before the specimen cell. The distance between the two slits is 340 mm. The width of the reflected beam becomes to be 1 mm at the specimen cell. The X-ray scattered by the sample passes through an aluminium pipe (120 ϕ x 1450 mm) and is detected by a position sensitive proportional counter (PSPC) as described in the section II-2. The effective area of the counter slit of the PSPC is 10 x 100 mm. The inner pressure of the camera chamber is usually kept below 5×10^2 Pa. to eliminate the air scattering. A nickel-foil of 10μm-thickness and a polycarbonate membrane are used for keeping vacuum inside the camera. The geometrical outline of the new apparatus is shown in Fig. II-3. The system of treatments of the scattered X-rays, that is, the data acquisition system is the same as that described in the section II-2. And the specimen cell and the control unit of its temperature are also same.

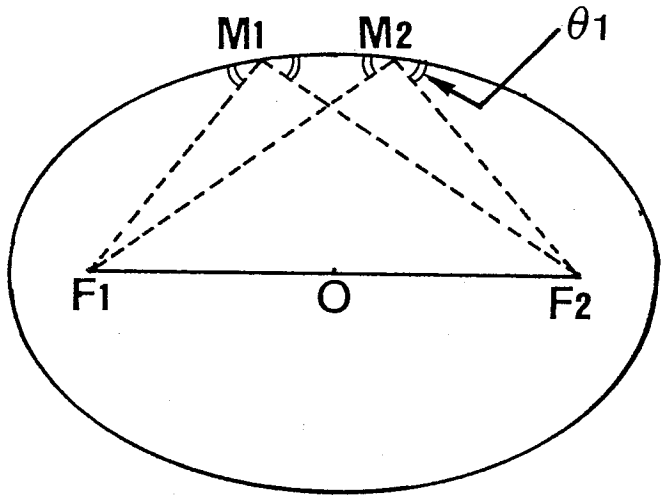

Fig. II-2. Geometry of the focusing X-rays; F1, F2, focusing positions on the focal plane and the copper target; M1, M2, both ends of the mirror; θ_1, reflecting angle; O, a center of F1-F2.

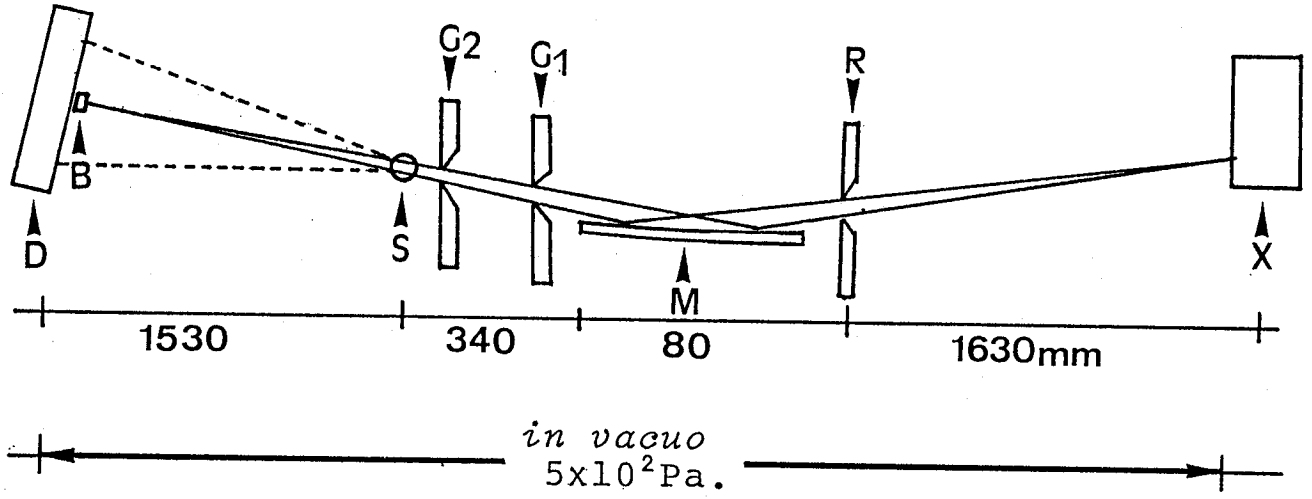

Fig. II-3. Schematic representation of high resolution small-angle X-ray scattering apparatus; X, X-ray generator; R, slit restricting incident X-rays; M, mirror; G1, G2, guard slits; S, specimen cell; B, beam stop; D, detector.

II-3-2 Estimation of the new apparatus

The following experiments were carried out to test the performance of the new apparatus by using the following samples whose structures were characterized by the electron microscopic observation, the hydrodynamic study and so on.

a) Latex particle

From the theory of the X-ray scattering, it is clear that the scattering intensity distribution of spherical particles has some subsidiary maxima (equation (I-19), Φ). A latex particle sample (Dow Chemical Co.Ltd.) is often utilized for the calibration of the optical system. The particles in solution have the spherical shape of the identical size. The X-ray intensity scattered by the latex particles was initially observed by Danielson, Shenfil and DuMond (8) and coincided well with the theoretical scattering intensity profile at higher order (i.e. at high angle). However the subsidiary maximum of the first or second order at very small angle could not be observed. In order to confirm that the distribution of the scattering intensity from the spherical particles has really some subsidiary maxima such as first or second order maximum in very small angle region, the small-angle X-ray measurement of the latex suspension with 5% concentration (w/w) was carried out by the new apparatus. The diameter of the latex particle was about 1100 Å, which was obtained by electron microscopic observation. The result of the X-ray measurement is shown in Fig. II-4. Scattering intensity

data without correction for the slit effects has clearly two subsidiary maxima such as the first and second order maximum. And then scattering intensity data corrected for the slit effects, desmeared data, is good consistent with the theoretical scattering intensity data for a sphere of 1100 Å in diameter. Consequently, the new apparatus makes it possible to measure small-angle intensity data for particles of below 1100 Å diameter with sufficient accuracy.

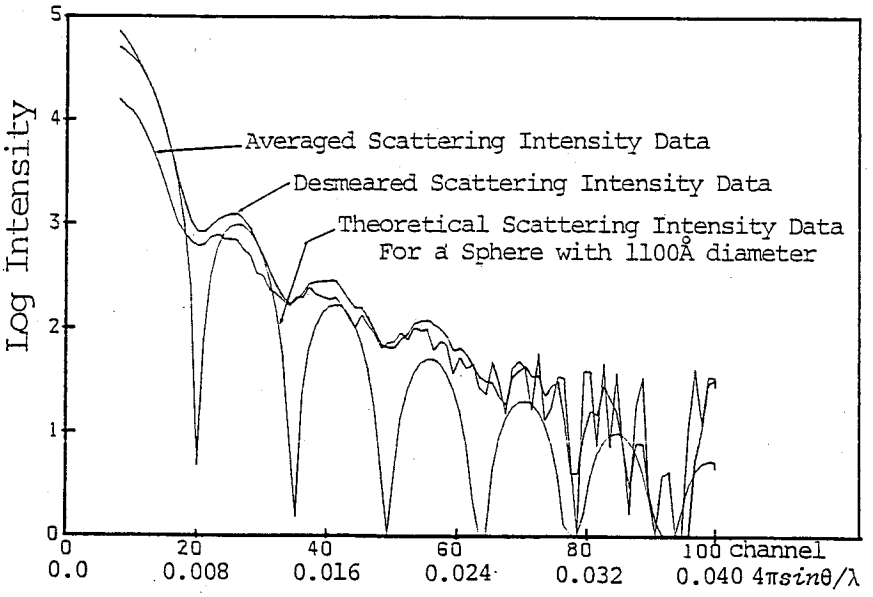

Fig. II-4. Scattering intensities for the Latex particle; Log I versus h plot.

b) Human immunoglobulin M (IgM)

Immunoglobulins are proteins playing important roles in the mechanism of the immunity, but their structures have not been reported enough. Immunoglobulin M (IgM) consists of five subunits, each of which structurally resembles immunoglobulin G (IgG) and is one of the largest proteins in the size and molecular weight (950,000 dalton) (9). In order to make it clear whether the shape of the pentameric IgM is spherical or oblate, the experiments of the small-angle scattering were carried out. Fig. II-5(a) represents a log-log plot of the observed scattering intensity data corrected for the effects of the slits together with the plots of the theoretical scattering intensities of ellipsoids of revolution. As shown in this figure, the observed scattering intensity curve is sufficiently consistent with the theoretical curve by a oblate particle (axis ratio = 0.1) rather than that of a spherical particle. The distance distribution function, P(r), is shown in Fig. II-5(b). The maximum dimension of the IgM is derived from this figure and found to be 367 Å. The radius of gyration is 108 Å from the Guinier plot and 111 Å from the P(r) function. It means that five subunits assemble around the terminal of Fc-part and form a pentamer as the IgM molecule. Thus, the shape of the IgM molecule can be approximated well by a oblate particle model with axis ratio of 0.1 represented in the figure.

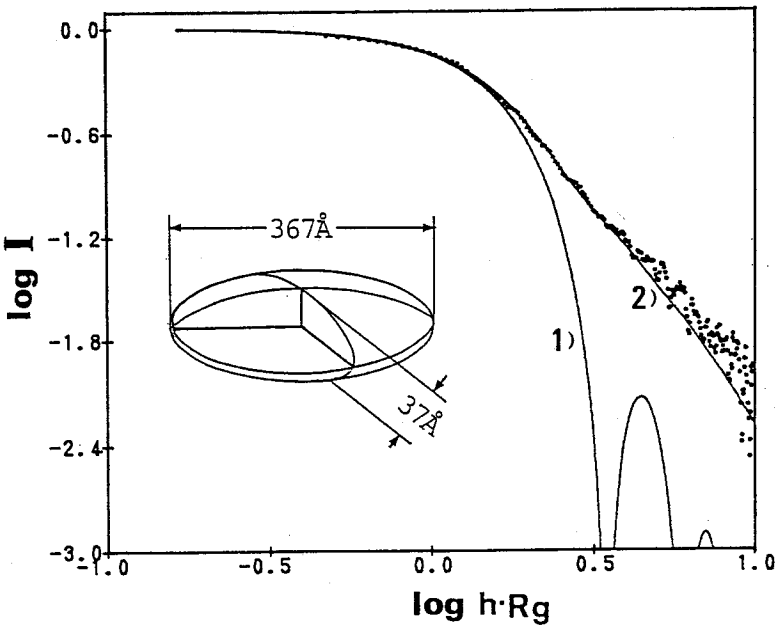

Fig. II-5(a). Log I - log (h Rg) plot of desmeared scattering intensities of Human Immunoglobulin M. Superimposed are the theoretical scattering functions (solid lines) of the oblate ellipsoids with the eccentricities, ω of 1) ω = 1.0 (sphere) and 2) ω = 0.1. The elliptic model (ω = 0.1) is inserted.

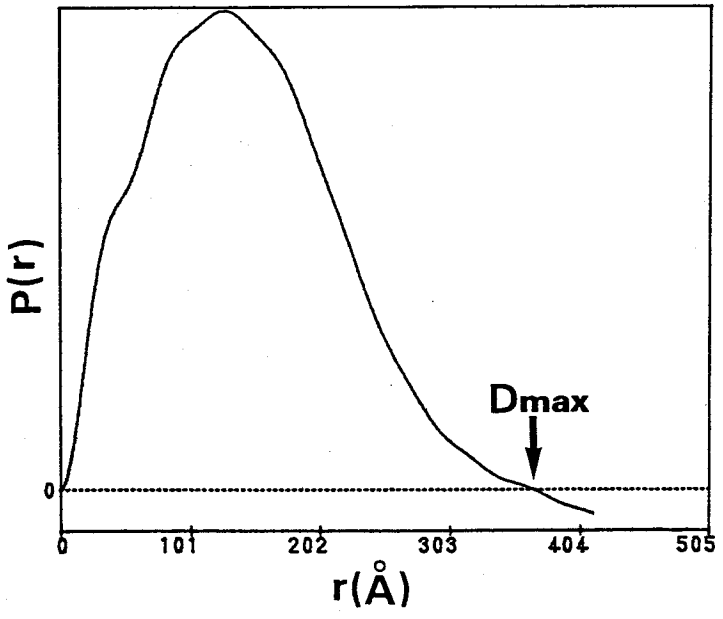

Fig. II-5(b). Distance distribution function, P(r) for the IgM molecule; r = distance; Dmax = maximum dimension of the particle.

c) Human α_2-macroglobulin (α_2M)

This protein is a tetramer and its molecular weight is 760,000 (10). The log-log plots are shown in Figs. II-6(a) and (b). The two radii of gyration obtained by the different ways and the maximum dimension of the protein are 84.6 Å (from Guinier plot), 86.2 Å (from P(r)) and 298 Å, respectively. Fig. II-6(a) suggests that the molecular shape is close to a prolate ellipsoid (ω = 3.0) rather than a sphere. However, in the range of 0.5-1.0 of the abscissa in Fig. II-6(a), the scattering intensity data of this protein disagrees with the theoretical curve of the prolate ellipsoid. The disagreement may be caused by some reasons: the accuracy of the data, the correction of the slit effect, ambiguity of the approximation to the ellipsoid of revolution, ununiformity of the electron-density distribution within the particle and so on. From the values of the radius of gyration and the maximum dimension, this protein molecule can be taken as a hollow body. One of the methods to confirm this is a comparison of the scattering data with the theoretical curves of some hollow ellipsoid particles. Fig. II-6(b) shows that the experimental data approximate to the theoretical curves of hollow bodies rather than an ellipsoid with uniform electron density. Thus, the overall structure of this protein can be approximately expressed by the hollow bodies rather than the uniform body. This result is supported by the electron microscopy.

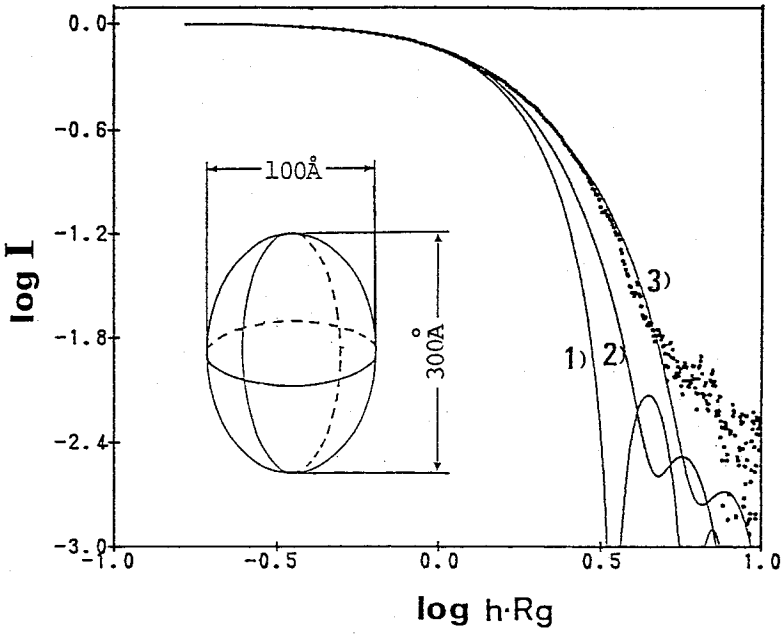

Fig. II-6(a). Log I - log (h Rg) plot of desmeared scattering intensities of Human α_2-Macroglobulin. Superimposed are the theoretical scattering functions (solid lines) of the prolate ellipsoids with the eccentricities, ω of 1) ω = 1.0 (sphere), 2) ω = 2.0 and 3) ω = 3.0. The elliptic model (ω = 3.0) is inserted.

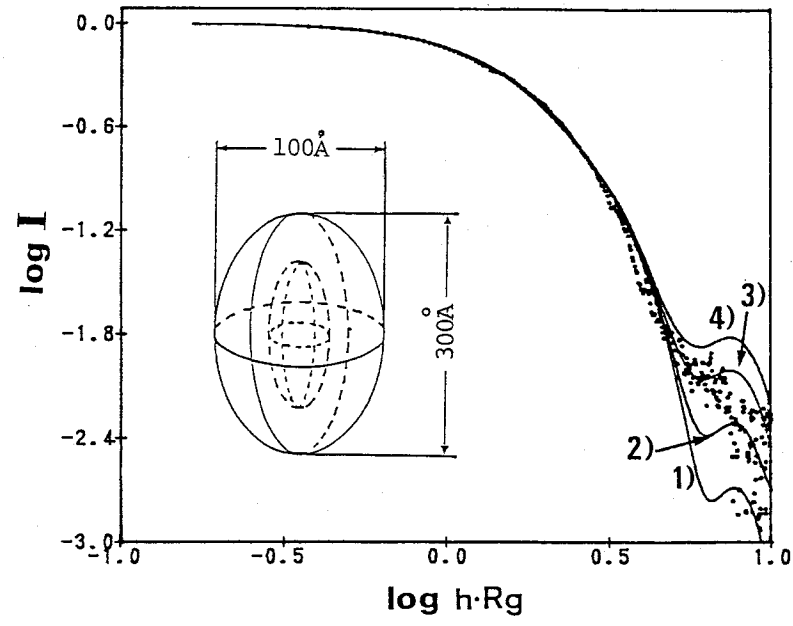

Fig. II-6(b). Log I - log (h Rg) plot of desmeared scattering intensities and hollow particles (ω = 3.0). 1) Ri/Ra = 0.0, 2) Ri/Ra = 0.4, 3) Ri/Ra = 0.6, 4) Ri/Ra = 0.8; Ri, Ra, inner and outer semi-axes of the hollow ellipsoid.

II-4 The middle- or large-angle X-ray scattering

X-ray scattering attributed to the structure of a protein molecule appears not only in a small angle region but also in a middle- or large-angle region. Since the resolution in the large-angle region is higher than that in the small angle region, information on internal structure rather than overall structure of the protein molecule may be obtained by analyzing a distribution of the scattering intensity. The internal structure may give information on the secondary or super-secondary structure of the protein, and analysis of the middle- or large-angle scattering intensity may be regarded as a method to clarify the secondary or super-secondary structure of the protein. For this reason, the experimental device used for the middle- or large-angle scattering method was developed. The X-ray source is a 0.1 x 1.0 mm spot on the copper rotating anode of a Rigaku Denki (FR-B) X-ray generator operated at 50 kV-70 mA. The spot is foreshortened to 0.1 x 0.1 mm at a glancing angle 6°. The camera (distributed by Marconi Elliott Avionics System) was used with a gold-coated toroidal mirror (Elliott-type) (11). The point beam focused by the toroidal mirror is so brilliant that scattering intensities at the large angle can be measured with sufficient accuracy. In a case of point beam, X-ray scattering from the protein solution displays the circular distribution around the position of the incident beam. An X-ray film is available for the detection of such pattern,

while the position-sensitive proportional counter (PSPC) is not suitable because of a smearing effect by the depth of the counter. A specimen cell and its temperature-control unit are same as those in sections II-2 and II-3. The film holder and the specimen cell are placed in vacuo (5×10^2Pa.). A sample-to-detector distance is 63 mm. This apparatus is able to cover a scattering range of 25 to 400 mrad, corresponding to Bragg spacing of 65 to 4 Å.

II-5 Data treatments and analyses of the solution X-ray scattering intensities

Data treatments and analyses of the solution X-ray scattering intensities are summarized in Fig. II-7.

a) Average of the scattering intensities

The X-ray scattering intensities from a protein solution recorded by the PSPC are averaged around the position of the direct X-ray beam after the background correction which is a subtraction of intensity of the buffer from that of the protein solution. The center of the position of the direct X-ray beam (zero-angle) is then precisely searched so as to realize the best coincidence of the scattering intensities at equivalent positions around the zero-angle. The extent of the coincidence is expressed by a reliability factor, Rsym:

$$R_{sym} = \left(\left(\sum_{i=1}^{N} (I_i - I_i')^2 \right) / \left(\sum_{i=1}^{N} \bar{I}_i^2 \right) \right)^{\frac{1}{2}} \qquad \text{(II-1)}$$

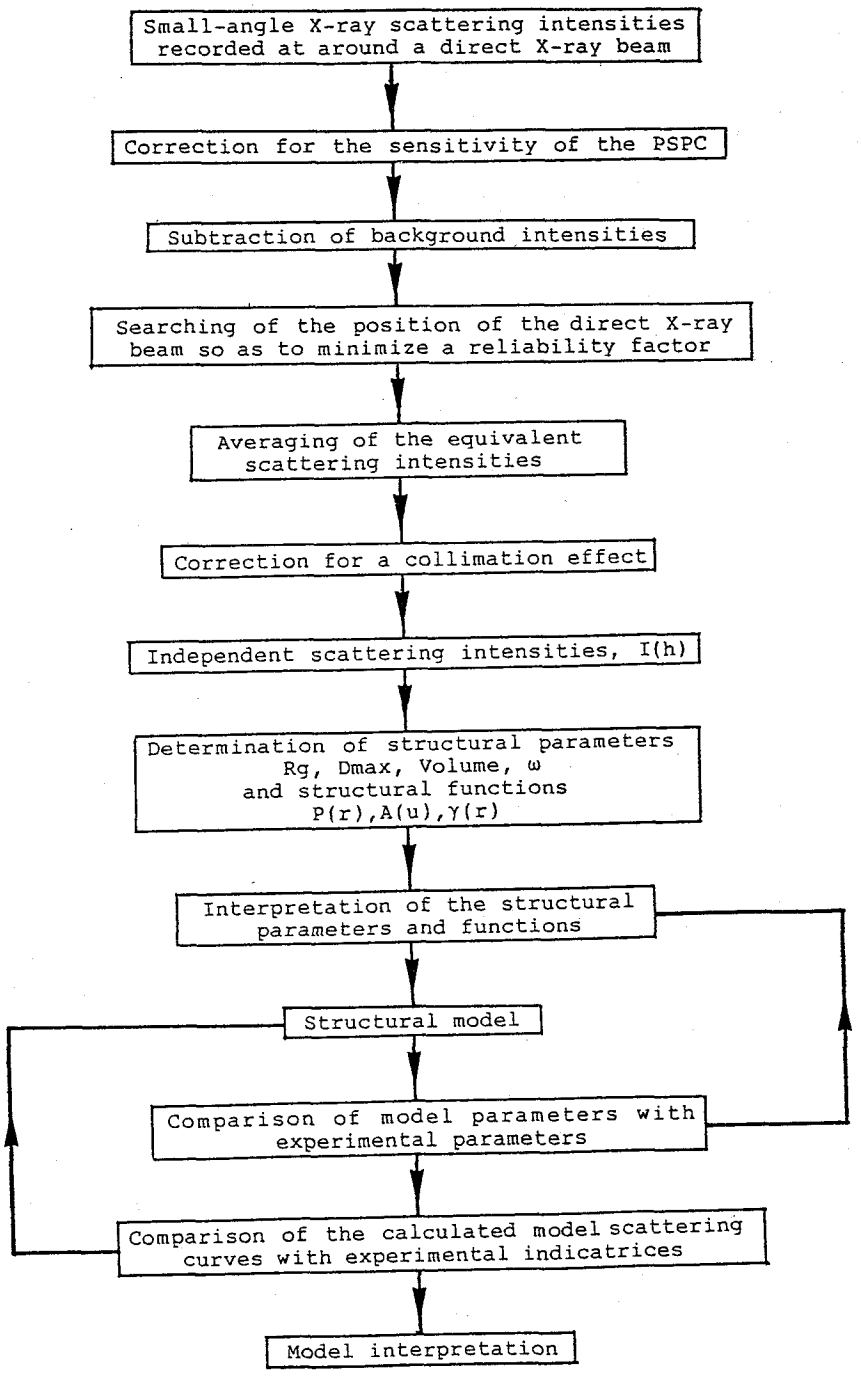

Fig. II-7. Schematic flow-chart of data treatment and processing procedure for solution X-ray scattering intensities

where I_i and I_i' are i-th equivalent scattering intensities around the direct X-ray beam, $\bar{I}_i$ the average of I_i and I_i', and N the number of the scattering intensities to be averaged. In case of measurements by a film, the photographic densities (optical densities) are measured with a Optronics P-1000 drum scanner and are converted to intensity data. The circular distributions of the scattering intensities recorded on the film are averaged by using all of the scattering intensities in one of N shells separated circularly around the direct X-ray beam. The independent scattering intensities are then obtained and they are corrected for collimation effects (described in next section).

b) Correction for collimation effect (Desmearing)

In order to obtain sufficient scattering intensity distribution in the measurements of small-angle X-ray scattering, a slit collimation system is normally used. The scattering intensities obtained by the slit collimation must be corrected for effects of slit width and length. The scattering intensity $I_{exp}(h)$ obtained by X-ray experiments can be expressed as a convolution of two functions. One of the functions is a distribution pattern of the X-ray scattering by use of an infinitely small incident beam and the other is a function of the shape of the incident beam at the position of the sample. It can be expressed as the following equation with I(h) considered as the scattering intensity by the infinitely small incident

beam:

$$I_{exp}(h) = 2 \int_{x=-\infty}^{\infty} \int_{t=0}^{\infty} Q(x)P(t)\ I(\sqrt{(h-x)^2 + t^2})\ dtdx \qquad \text{(II-2)}$$

where P(t) is a distribution function of the incident X-ray intensity along a direction of a slit length and Q(x) the distribution function along a direction of a slit width. The scattering intensity, I(h), is required for a data analysis in a structural investigation and is obtained by deconvolution of the equation (II-2). This procedure is called desmearing or correction for collimation effects.

Recently, a new iterative method has been developed by O. Glatter to estimate the scattering intensity I(h) (13). This method is made up of the following procedures: an unknown function I(h) is mainly regarded as a N-th approximation function $I_N(h)$: a smeared scattering intensity $\chi_N(h)$ is derived from the equation (II-2); relative error at a given h between a experimental intensity $I_{exp}(h)$ and the $\chi_N(h)$ including a correct sign is assigned to $D_N(h)$. The $D_N(h)$ is expressed by:

$$D_N(h) = \mathrm{sign}\left(I_{exp}(h) - \chi_N(h)\right)\left(\left(\frac{I_{exp}(h) - \chi_N(h)}{I_{exp}(h)}\right)^2\right)^{\frac{1}{2}} \qquad \text{(II-3)}$$

; the $D_N(h)$ is made to be smooth and becomes to be $D'_N(h)$, then the (N+1)-th approximation function $I_{N+1}(h)$ is derived from following equation:

$$I_{N+1}(h) = \left(D'_N(h) + 1\right) I_N(h) \qquad \text{(II-4)}$$

; if the $D_N(h)$ is converged, the iteration can be finished and a final approximation function, I(h), is thought to be a desmeared scattering intensity data which are observed by the infinitely small incident beam. First of all, $I_{exp}(h)$ is used for a starting function of the iteration as $I_1(h)$. The I(h) corrected for collimation effects is then used for the successive data analysis.

c) Data analysis

In order to derive the structural information on proteins, two ways are available for the data analysis of the solution X-ray scattering intensities corrected for the slit effects. One of them is the method of looking into the scattering intensity distribution, the other is that of the Fourier transforms of the intensity data. The former mainly gives the radius of gyration or the eccentricity of a molecule by use of the Guinier plot or the log-log plot, respectively, and also derives a volume and molecular weight from the analysis of the scattering intensity data. The latter gives also the radius of gyration and the maximum dimension by the distance distribution function in which the structural morphology may be revealed in a particular case. Such parameters obtained by the analysis of experimental data directly reflect structural information on the proteins in solution.

As the next step, a molecular model is build, which has the parameters obtained by the experimental data. If the molecular shape may be approximated by an ellipsoid of

revolution, it can be made closer to the true molecular shape by changing its eccentricity. Further improved models can be obtained by changing three semi-axes of the ellipsoid and also can be expressed as a hollow body by taking account of its hollow indexes. And the model can be build as an assembly of many spheres. This method makes it possible to clarify the internal structure of the molecule which has regions of variable electron density. Computer programs developed for the data analysis are listed in Table II-1.

II-6 Conclusion

In order to investigate the structure of protein molecules in solution, three types of experimental systems have been developed. Two of them are systems to clarify the macroscopic structure attributed to the overall structure of the protein molecule by means of the small-angle X-ray scattering. The high resolution small-angle scattering camera has a small-angle resolution of 1 mrad (= 1500 Å), while the conventional camera has that of 4 mrad (= 400 Å). The former experimental system gives support to detection of the scattering intensities in the small angle region which cannot be detected by the latter system. On the other hand, the third type of the experimental system is a large-angle X-ray scattering camera which has resolution from 24 to 400 mrad, corresponding to Bragg spacing from 65 to 4 Å. The

scattering intensities in the large angle region reflect a microscopic structure of the protein molecule. Moreover, the analyses of the architecture of subunits assembly, the secondary structure and super-secondary structure in the object are expected to be attained by using this system. These three types of experimental systems are complementary to one another in the measurement of the scattering intensities. The intensities scattered by the protein solution must be measured in the scattering range as widely as possible. Fig. II-8 shows the distribution of scattering intensities of the immunoglobulin M molecule measured by using the apparatuses described in the section (II-2), (II-3) and (II-4). The detectable range of X-ray scattering intensities is 1-400 mrad of the scattering angle, corresponding to Bragg spacing of 1600 to 4 Å. The scattering intensity data observed by three cameras can be combined by scaling overlapped data among one another. The observed intensities are so many that they are available for studying the structural features and reducing termination errors in the Fourier transforms.

Data treatments and data analyses are performed by micro-computer which uses FORTRAN programs according to the flow-chart (Fig. II-7). These programs follow the theories in the evaluation of the reliabilities of data (section II-5), correction of slit effects (section II-5) and estimation of the structural parameters of Rg, Dmax, Volume and ω (section I-4) and structural functions of P(r), A(u) and γ(r) (section I-2). The parameters obtained are

interpreted and the biological model can be constructed by trial and error.

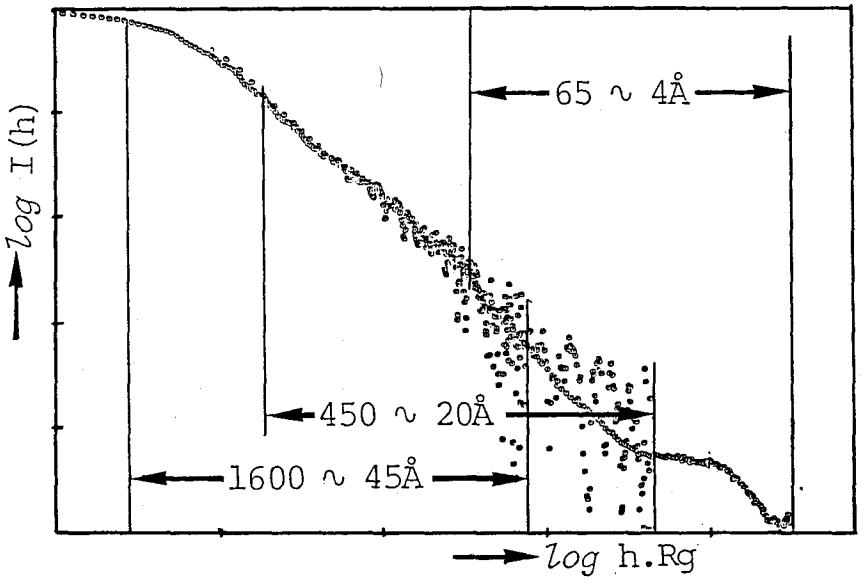

Fig. II-8. Scattering intensity profile for the Human Immunoglobulin M; 1600 - 45 Å, by high resolution small-angle scattering camera; 450 - 20 Å, commercially available small-angle scattering camera; 65 - 4 Å, large-angle scattering camera; scattering intensities are normalized.

Table II-1

Programmes developed for the process and the analysis of solution X-ray scattering intensity data

Programme Name	Function
PROX1 (PROX2)	Transmission of measured solution X-ray scattering intensities from PSPC to micro-computer
AVERAGE1 (AVERAGE2)	Subtraction of background intensities, correction for the sensitivity of PSPC and averaging of equivalent scattering intensities
AVERAGE3	Average of scattering intensities recorded on film
AVERAGE4	Average of asymmetrical scattering intensities distribution recorded on film
SBDIF	Subtraction of background intensities
ABSC	Scaling of A-film and B-film
GATHER	Gathering the scattering intensity data sets
SMOOTH	Smoothing the scattering intensity data by use of B-spline function
MSCOMB	Combination of small-angle scattering data with large-angle scattering data
DESGLATM	Desmearing of smeared scattering intensities
GUINIER1	Guinier plot of scattering intensities
PRNV	Calculation of distance distribution function, P(r)
RRNV	Calculation of autocorrelation function, A(u)
VOLRG	Estimation of radius of gyration and volume
SUBTRACT (SUBEIGEN)	Subtraction of Gaussian function from scattering intensity data by least square method
BLINE	Subtraction of B-spline function from scattering intensity data
HIRES	Data extension according to Porod's law

Table II-1 (continued)

ELLIP	Calculation of theoretical scattering intensities of rigid or hollow ellipsoid
MULTIBOD	Calculation of theoretical distance distribution function and scattering intensity from arbitrary model composed of spheres
LGLGPLOT	Log versus log plot of scattering intensity data
GRAPHNV	Plotting of various kinds of data by computer display
NEWPLOT	Plotting of various kinds of data by X-Y plotter
NEW3D	Plotting of three-dimensional data by X-Y plotter

Chapter III

Structural studies on cytochrome oxidase and cytochrome $\underline{bc_1}$ complex isolated from beef heart

III-1 Introduction

In all organisms, the electron transfer in the cell is performed very skillfully. It means that the electron-transfer system plays a very important role in the organisms. Cytochrome $\underline{c}$ in the electron-transfer system functions as an electron carrier in the mitochondria. The structure of cytochrome $\underline{c}$ has been clarified by the X-ray crystallography, and the relation between the structure and function has been discussed in detail. When the function of a given enzyme is considered and discussed, it is very important to take into account of the structure of the enzyme and any kind of the structural information is very useful. From these points of view, two important enzymes cytochrome oxidase and cytochrome $\underline{bc_1}$ complex beside cytochrome $\underline{c}$ in the electron transfer system have been studied by the solution X-ray scattering method.

Cytochrome oxidase (ferrocytochrome c : oxygen oxidoreductase EC 1.9.3.1) is the terminal component of the electron-transfer chain in mitochondria of eukaryotes and in plasma membranes of prokaryotes. It catalyzes the electron transfer from ferrocytochrome $\underline{c}$ to molecular oxygen and functions as an energy transducer which converts the energy of electron transfer to a driving force for ATP

synthesis. Cytochrome oxidase isolated from beef heart mitochondria has a minimal molecular weight of about 130,000 and consists of three large hydrophobic and four small hydrophilic subunits. It contains two heme a groups (heme a and heme a_3) and two copper atoms.

Cytochrome bc_1 complex (ubiquinol : cytochrome c reductase EC 1.10.2.2) is a multi-subunit enzyme involved in mitochondrial oxidative phosphorylation. This enzyme catalyzes the reduction of ferricytochrome c by reduced ubiquinone, and conserves the redox energy by translocating protons across the inner mitochondrial membrane. This enzyme is isolated from the beef heart mitochondria in a dimeric state and has a molecular weight of about 560,000. Each monomer contains ten different subunits which include an iron-sulfur protein, b and c_1 cytochromes.

The location of cytochrome oxidase, bc_1 complex and cytochrome c in mitochondrial membrane are shown in Fig. III-1. Four enzymes ,except for cytochrome c, in the electron-transfer chain are called complex I, II, III and IV. Among these, the complex III is cytochrome bc_1 complex and the complex IV is cytochrome oxidase. The complexes III and IV can be bound to cytochrome c and contain 20-30% (w/w) of phospholipids (14) which reduce the small-angle X-ray scattering intensities. In order to enhance the scattering intensities, it is prerequisite to remove phospholipids bound to the enzymes. Recently, Ozawa et al. have reported a procedure for purification of these enzymes by hydrophobic-interaction chromatography with phenyl-

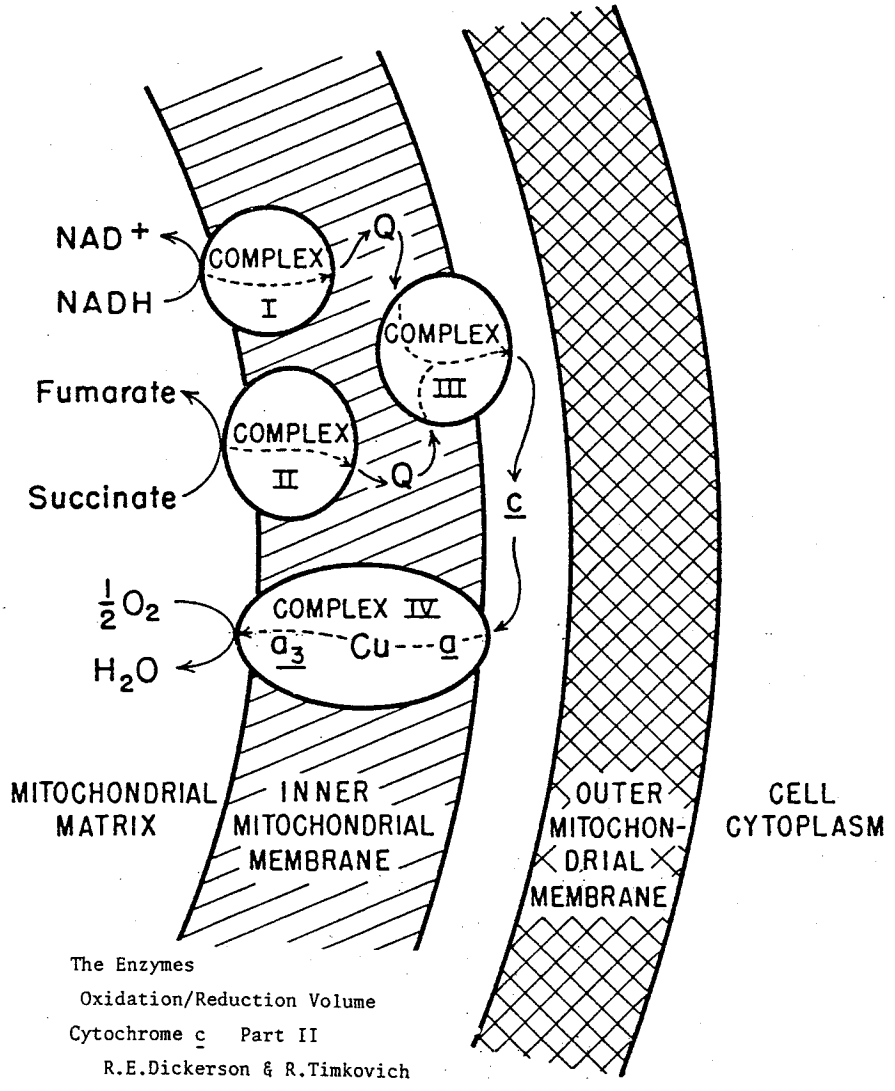

Fig. III-1. Possible spatial arrangement of components of the respiratory chain in the inner mitochondrial membrane. Adapted from reference 46.

Sepharose (15) and affinity chromatography with Sepharose-bound cytochrome c (16). By the chromatographic procedures, it became possible to obtain phospholipid-depleted enzymes.

These enzymes dissolve in physiological solutions by binding detergents. The electron densities of the detergents are generally lower than those of the proteins. When there is a difference between electron densities of two substances, the structural information about one substance can be obtained by adjusting the electron density of the solvent to that of the other. The contrast variation method can reveal the shape of the dissolved molecule and the binding sites of detergents to the enzymes.

Binding of cytochrome c to cytochrome oxidase has been proposed to control the rate of electron transport through the terminal segment of the respiratory chain in mitochondrial inner-membrane (17). It is of great importance to determine the structures in solution of the oxidase and its complex with cytochrome c. In this chapter, the structures of cytochrome oxidase isolated from beef heart mitochondria and its complex with cytochrome c in solution have been investigated and the structures of the cytochrome bc_1 complexes by means of small-angle X-ray scattering have been investigated also.

III-2. Experimental

III-2-1. Cytochrome oxidase and its complex with cytochrome c

III-2-1-1. Isolation and Purification of cytochrome oxidase and cytochrome c

Isolation and purification procedures of cytochrome oxidase are presented in Table III-1. Protein concentration was determined by the Biuret method (18) calibrated by bovine serum albumin. Heme a concentration was determined from the spectrum of the reduced oxidase using $\Delta\varepsilon_{605-630} = 16.5\ mM^{-1}cm^{-1}$ (19). Phosphorus was determined by the method of Chen et al. (20), and the amount of phospholipids was estimated from the average molecular weight of 775.

Cytochrome oxidase was isolated from beef heart mitochondria according to the method of Fowler et al. (21), and was refractionated with ammonium sulfate in the presence of 1% cholate by the method of Tzagoloff and MacLennan (22). The refractionated oxidase was further purified by phenyl-Sepharose CL-4B hydrophobic chromatography (15) and cytochrome c-Sepharose 4B affinity chromatography (16). The oxidase was passed through a column of Sephacryl S-300 equilibrated with 10 mM Tris-HCl buffer, pH 7.5 , containing 0.1% Triton X-100. The elution pattern from the Sephacryl S-300 column is shown in Fig. III-2. The eluted solution mainly contained oxidase

Table III-1

Isolation and purification procedure of cytochrome oxidase

Beef heart

↓ + 1 M Phosphate buffer, containing 0.25 M sucrose

↓ Homogenized in a blender

↓ Centrifuged at 1600 x g for 25 min

supernatant

↓ Centrifuged at 33000 x g for 60 min

precipitate

Mitochondria fraction

↓ Suspended in 10 mM Tris-HCl, pH 7.5, containing 0.25M sucrose

↓ Homogenized in an ultradisperser

↓ Centrifuged at 10500 x g for 40 min

precipitate

↓ Suspended in 50 mM Tris-HCl, pH 8.0, containing 0.25 M sucrose

↓ Homogenized in the ultradisperser

↓ Centrifuged at 10500 x g for 30 min

precipitate

↓ Suspended in 50 mM Tris-HCl buffer, pH 8.0, containing 0.66 M sucrose and 1 mM histidine

↓ + DOC (0.3 mg/mg protein)

↓ + KCl (72 g/ 1) and incubated for 15 min

Green residue

↓ Washed with 2 volumes of 50 mM Tris-HCl buffer, pH 8.0, containing 0.66 M sucrose and 1 mM histidine

↓ Centrifuged at 10500 x g for 20 min

Table III-1 (continued)

Green pellet

↓ + DOC (0.5 mg/mg protein)

↓ + KCl (74.5 g/l)

↓ Centrifuged at 10500 x g for 20 min

Green supernatant

↓ Dialyzed against 30 volumes of 10 mM Tris-HCl buffer, pH 8.0 for 90 min

↓ + 0.19 volume of sat. AS and incubated for 10 min

↓ Centrifuged at 10500 x g for 20 min

supernatant

↓ + 0.04 volume of sat. AS and incubated for 10 min

↓ Centrifuged at 10500 x g for 20 min

precipitate

↓ Dissolved in 50 mM Tris-HCl buffer, pH 8.0 and adjusted the protein concentration to 20-30 mg/ml

↓ + 0.2586 volume of 20% cholate (3% cholate)

↓ + 0.4655 volume of sat. AS (27% sat.)

↓ Incubated at 4^{o} C for 4 h

↓ Centrifuged at 78000 x g for 10 min

supernatant

↓ Incubated for 2 h at 30^{o} C

↓ Centrifuged at 78000 x g for 10 min

supernatant

↓ + equal volume of 50 mM Tris-HCl buffer, pH 8.0

↓ + 0.384 volume of sat. AS (37.5% sat.)

↓ Incubated at 4^{o}C for 2 h

Table III-1 (continued)

Centrifuged at 78000 x g for 20 min

precipitate

↓ Dissolved in 50 mM Tris-HCl buffer, pH 8.0

↓ + 0.5 volume of sat. AS (33% sat.)

↓ Centrifuged at 78000 x g for 20 min

precipitate

↓ Dissolved in 0.1 M sodium bicarbonate buffer, ph 8.3, containing 0.1 M NaCl and 1% DOC

↓ Applied to a phenyl-Sepharose CL-4b column (2.5 x 20 cm) equilibrated with 0.1 M sodium bicarbonate buffer, pH 8.3, containing 0.1 M NaCl and 1% DOC

↓ Washed with 500 ml of the equilibrium buffer

↓ Eluted with 0.1 M sodium bicarbonate buffer, pH 8.3, containing 0.1 M NaCl and 1% Triton X-100

↓ Diluted ten times with 10 mM Tris-HCl buffer, pH 7.5, containing 0.1% Triton X-100

↓ Applied to a cytochrome c-Sepharose 4B (1 x 50 cm) equilibrated with 10 mM Tris-HCl buffer, pH 7.5, containing 0.1% Triton X-100

↓ Washed with 50 ml of the equilibrium buffer

↓ Washed with 10 mM Tris-HCl buffer, pH 7.5, containing 0.1% Triton X-100 and 25 mM NaCl

↓ Eluted with 10 mM Tris-HCl buffer, pH 7.5, containing 0.1% Triton X-100 and 100 mM NaCl

↓ Applied to a Sephacryl S-300 column (2.5 x 70 cm) equilibrated with 0.1 mM Tris-HCl buffer, pH 7.5, containing 0.1% Triton X-100 and 100 mM NaCl

↓ Eluted with 0.1 M Tris-HCl buffer, pH 7.5, containing 0.1% Triton X-100 and 100 mM NaCl

Purified cytochrome oxidase

---

sat. AS : saturated ammonium sulfate

molecules in the dimeric form and then was used for X-ray measurements. The concentration of heme a of the purified oxidase was 14.2 nmol/mg and its phospholipid content was 2.0% (w/w). The densitometric tracing of SDS-polyacrylamide gel electrophoresis profile of the purified oxidase is shown in Fig. III-3.

Cytochrome c (isolated from horse heart), purchased from Sigma (Type III), was purified by the method of Hagihara et al. (23).

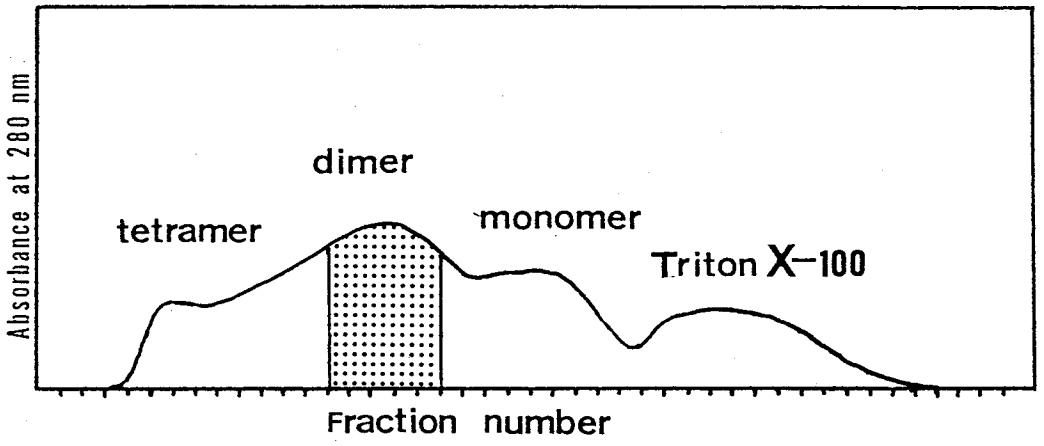

Fig. III-2. Elution profile of the cytochrome oxidase from a Sephacryl S-300 column; flow rate, 20 ml/h; fraction size, 3 ml/tube. Dotted area indicates fractions pooled, which is the purified cytochrome oxidase.

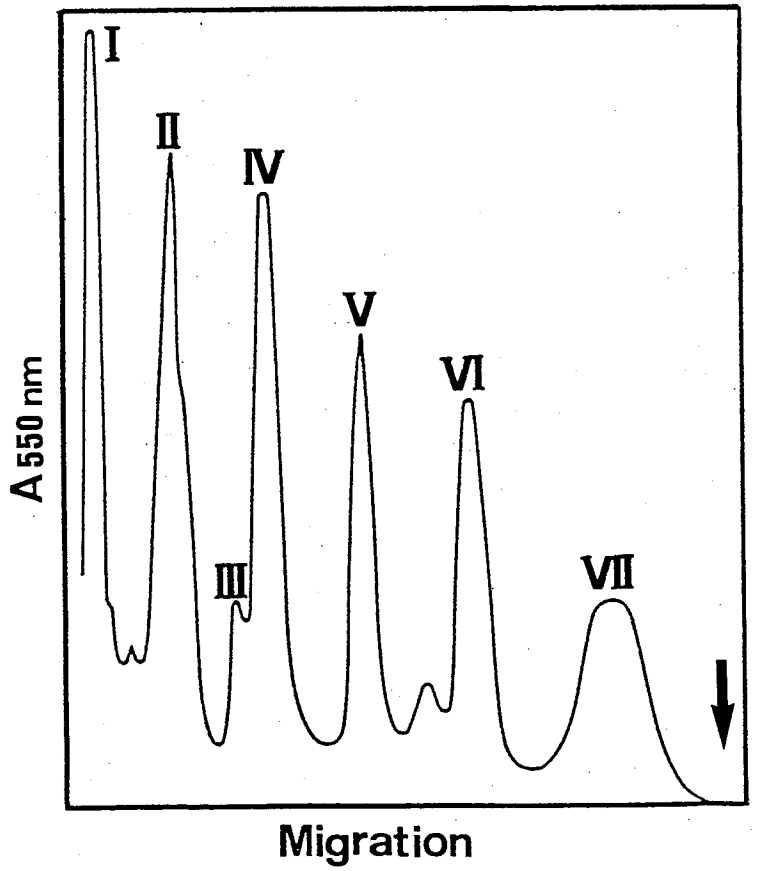

Fig. III-3. Densitometric tracing of SDS-polyacrylamide gel electrophoresis profile of purified cytochrome oxidase. The arrow indicates the front of electrophoresis.

III-2-1-2 Cytochrome oxidase - cytochrome c complex

The cytochrome oxidase eluted from a Sephacryl S-300 column with 100 mM Tris-HCl buffer, pH 7.5, containing 0.1% Triton X-100, 100 mM NaCl was dialyzed to remove salt against 10 mM Tris-HCl buffer, pH 7.5, containing 0.1% Triton X-100. Cytochrome c was added to the oxidase solution in heme c : heme a ratio of 1 : 2 (1 : 1 mol /mol). The mixture was passed through a Sephadex G-75 column to remove the extra cytochrome c which did not bind to the oxidase. This procedure is shown in Table III-2.

Table III-2

Purification procedure of cytochrome oxidase - cytochrome c complex

Purified cytochrome oxidase	
↓	Dialyzed against 10 mM Tris-HCl, pH 7.5, buffer containing 0.1% Triton X-100 and no salt
↓	+ purified cytochrome c (1 : 1 mol / mol)
↓	Applied to a Sephadex G-75 (1 x 20 cm) equilibrated with 0.1 mM Tris-HCl buffer, pH 7.5, containing 0.1% Triton X-100
↓	Eluted with 0.1 mM Tris-HCl buffer, pH 7.5, containing 0.1% Triton X-100
↓	Concentrated
Cytochrome oxidase - cytochrome c complex	

III-2-1-3 Preparation of samples for the contrast variation method

Electron densities of the protein and the detergent in the cytochrome oxidase and of the cytochrome *c* are listed in Table III-3. The numbers of electrons of each moiety were calculated from their chemical formulas. The partial specific volume of cytochrome oxidase-detergent complex was estimated by taking account of the amount of detergent bound to the oxidase (180 molecules of Triton X-100 / heme aa_3, which value was estimated from the extinction coefficient). In order to apply the contrast variation method the electron density of the solvent was increased to that of protein or detergent by addition of a sucrose solution. The sucrose solution was prepared by dissolving sucrose powder in buffer solution (without Triton X-100) so as to become 63% (w/w) of sucrose concentration. Fig. III-4 shows a plot of the concentration of sucrose *versus* the electron density of the solvent.

The enzyme solution was initially concentrated to avoid change of the protein concentration by addition of the sucrose solution. The buffer solution which contains the detergent was also concentrated under the same condition as that for the enzyme solution. Various amount of the sucrose solution and 10 mM Tris-HCl buffer, pH 7.5, were added to concentrated solutions in order to keep the concentrations of protein and detergent constant. Values of these amounts are listed in Table III-4.

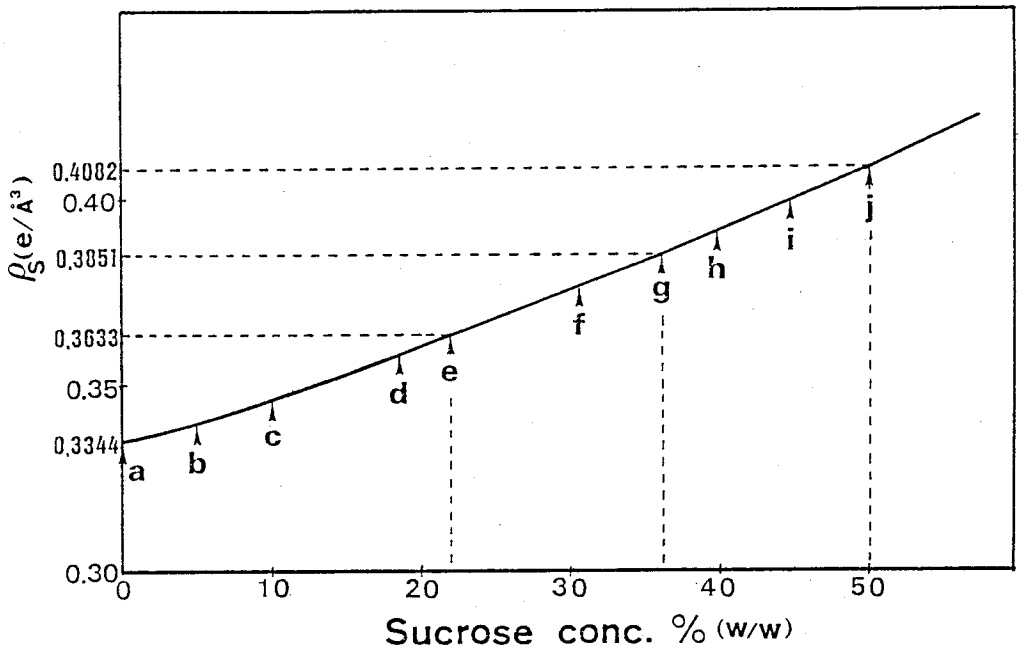

Fig. III-4. Variation of the electron density of the solvent, ρ_s as a function of the sucrose concentration. X-ray measurement was carried out under the condition of each arrow.

Table III-3

Values of electron density for each moiety

Cytochrome oxidase	0.4082 e/Å^3
Triton X-100	0.3633
Cytochrome oxidase - Triton X-100 Complex	0.3851*
Cytochrome <u>c</u>	0.4092

* assuming that the amount of bound detergent is 180 molecules / heme <u>aa$_3$</u>

Table III-4

Preparation of samples for the contrast variation measurements

sample	sucrose concentration	solution	sucrose solution	buffer solution
	%(w/w)	µl	µl	µl
a	0.0	25	0	75
b	5.0	25	6	69
c	10.0	25	12.5	62.5
d	18.5	25	24	51
e	22.0	25	29	46
f	30.7	25	42	33
g	36.3	25	51	24
h	40.0	25	57	18
i	45.0	25	65.5	9.5
j	50.0	25	75	0

solution : concentrated enzyme or buffer solution

sucrose solution : 63% (w/w) sucrose in 10 mM Tris-HCl buffer, pH 7.5

buffer solution : 10 mM Tris-HCl buffer, pH 7.5

III-2-1-4 Measurement of small-angle X-ray scattering intensities

Measurement of small-angle X-ray scattering intensities was carried out by using the system with a one-dimensional position sensitive proportional counter, described in the section II-1. Measurement time was 5000 sec for one specimen of the cytochrome oxidase or its complex with cytochrome c and the same specimen was measured eight times. The distribution of the scattering intensities was observed in the range of 4.0 to 76.7 mrad of the scattering angle and was processed according to the procedures described in the section II-5. In order to correct the background X-ray scattering, the buffer solution was also measured. All of the measurements were carried out at 5±0.5°C. The protein concentration was 5 mg/ml and the millimolar extinction coefficient used was 16.5 for $A_{604-630}$ for heme a. The reliability factors (R-values, equation II-1) were listed in Table III-5.

Table III-5

Reliability factors, R_{sym}, of the small-angle X-ray scattering intensities from cytochrome oxidase-cytochrome c complex, cytochrome oxidase solutions

Concentration of sucrose (%)	R_{sym}^{1}	R_{sym}^{2}
0.0	0.0468	0.0346
5.0	0.0772	0.0572
10.0	0.1164	0.0839
18.5	0.1724	0.1591
22.0	0.1092	0.1539
30.7	0.2475	0.3120
36.3	0.5198	0.4928
40.0	0.5266	0.7242
45.0	0.4776	0.6011
50.0	0.2137	0.3135

R_{sym}^{1} : Cytochrome oxidase-cytochrome c complex
R_{sym}^{2} : Cytochrome oxidase

III-2-2 Cytochrome bc_1 complex

III-2-2-1 Isolation and purification of cytochrome bc_1 complex

Isolation and purification procedures of cytochrome bc_1 complex are presented in Table III-6. The concentrations of cytochromes *b* and c_1 were estimated by the difference absorption spectra of dithionite-reduced *minus* ascorbate-reduced form and ascorbate-reduced *minus* ferricyanide-oxidized form, respectively (24). The millimolar extinction coefficients used were 28.5 for A_{563}-A_{577} in cytochrome *b* (25) and 17.5 for A_{554}-A_{540} in cytochrome c_1 (26). The protein concentration was determined by the Lowry's method with a slight modification (27) using bovine serum albumin as the standard. The total phospholipid content was calculated from the total amount of phosphorus determined by the method of Chen *et al.* (20), assuming that the average phospholipid molecular weight is 775.

Cytochrome bc_1 complex was prepared from beef heart mitochondria by the method of Rieske *et al.* (28). Isolated cytochrome bc_1 complex was refractionated with ammonium acetate in the presence of 1% cholate. Successively, cytochrome bc_1 complex was purified by applying to columns of a phenyl-Sepharose CL-4B hydrophobic chromatography and a cytochrome *c* Sepharose 4B affinity chromatography. The densitometric tracing of SDS-polyacrylamide gel electrophoresis profile of the highly purified cytochrome

bc_1 complex is shown in Fig. III-5. The total molecular weight of the 10 subunits was 236,200.

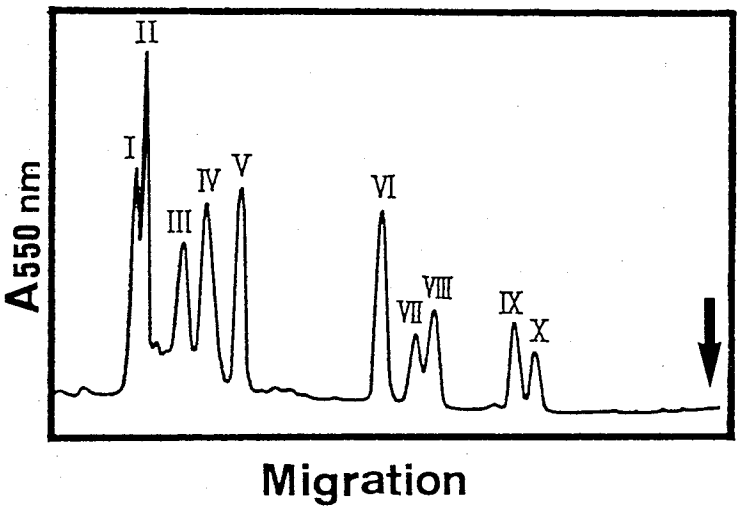

Fig. III-5. Densitometric tracing of SDS-polyacrylamide gel electrophoresis profile of purified cytochrome bc_1 complex. The arrow indicates the front of electrophoresis.

Table III-6

Isolation and purification procedure of cytochrome bc_1 complex

Beef heart

↓ + 1 M Phosphate buffer, containing 0.25 M sucrose

↓ Homogenized in a blender

↓ Centrifuged at 1600 x g for 25 min

supernatant

↓ Centrifuged at 33000 x g for 60 min

precipitate

Mitochondria fraction

↓ Suspended in 10 mM Tris-HCl, pH 7.5, containing 0.25M sucrose

↓ Homogenized in an ultradisperser

↓ Centrifuged at 10500 x g for 40 min

precipitate

↓ Suspended in 50 mM Tris-HCl, pH 8.0, containing 0.25 M sucrose

↓ Homogenized in the ultradisperser

↓ Centrifuged at 10500 x g for 30 min

precipitate

↓ Suspended in 50 mM Tris-HCl buffer, pH8.0, containing 0.66 M sucrose and 1 mM histidine

↓ + DOC (0.3 mg/mg protein)

↓ + KCl (72 g/ 1) and incubated for 15 min

Red components

↓ Dialyzed against 10 mM Tris-HCl pH 9.0 for 60 min

↓ Centrifuged at 10500 x g for 75 min

precipitate

Table III-6 (continued)

↓ Suspended in 50 mM Tris-HCl buffer, pH 8.0, containing 0.66 M sucrose and 1 mM histidine

↓ Homogenized in an ultradisperser

↓ + DOC (0.5 mg / mg protein)

↓ + 50% saturated ammonium acetate (0.165 ml/ml above suspension)

↓ Incubated for 15 min

↓ Centrifuged at 10500 x g for 30 min

supernatant

↓ + 50% saturated ammonium acetate (0.035 ml / ml supernatant)

↓ Incubated for 12-13 min

↓ Centrifuged at 10500 x g for 30 min

supernatant

↓ + 50% saturated ammonium acetate (0.03 ml / ml supernatant)

↓ Incubated for 12-13 min

↓ Centrifuged at 10500 x g for 30 min

supernatant

Complex III rich-fraction

↓ + solid ammonium acetate (0.45 g / ml supernatant)

↓ Incubated for 12-13 min

↓ Centrifuged at 10500 x g for 40 min

precipitate

↓ Suspended in 50 mM Tris-HCl buffer, pH 8.0, containing 0.66 M sucrose and 1 mM histidine

↓ Homogenized in the ultradisperser

↓ + Cholate (0.25 mg / mg protein)

↓ + 0.54 volume of saturated ammonium sulfate

Table III-6 (continued)

↓ Incubated for 10 min

↓ Centrifuged at 10500 x g for 15 min

supernatant

↓ + 0.0835 volume of saturated ammonium sulfate

↓ Incubated for 10 min

↓ Centrifuged at 10500 x g for 15 min

supernatant

↓ + 0.0345 volume of saturated ammonium sulfate

↓ Incubated for 10 min

↓ Centrifuged at 10500 x g for 15 min

supernatant

↓ + 0.115 volume of saturated ammonium sulfate

↓ Incubated for 10 min

↓ Centrifuged at 10500 x g for 15 min

precipitate

↓ Suspended in 25 mM Tris-HCl pH 8.0, 20% glycerol

intact complex III

↓ Applied to a phenyl-Sepharose CL-4B column (1 x 25 cm) equilibrated with 25 mM Tris-HCl pH 8.0, containing 0.25% DOC, 0.2 M NaCl, 1 mM EDTA, 20% glycerol

↓ Washed with 20 ml / 420 nmol of complex III

↓ Eluted with 25 mM Tris-HCl pH 7.5, containing 3% Tween 20, 20% glycerol

↓ Applied to a cytochrome c-Sepharose 4B (1 x 25 cm) equilibrated with 25 mM Tris-HCl pH 7.5, containing 20% glycerol, 0.1% Tween 20

↓ Eluted with 25 mM Tris-HCl pH 7.5, containing 20% glycerol, 0.1% Tween 20, 0.1 M NaCl

Purified cytochrome bc_1 complex

III-2-2-2 Preparation of samples for the small-angle X-ray scattering measurement

Cytochrome bc_1 complex isolated by the method of Rieske was purified by the following two ways. One was purified by means of hydrophobic chromatography followed by affinity chromatography. The other was purified only by the affinity chromatography. The difference between two ways is the procedure of the hydrophobic chromatography. This procedure depletes the phospholipids bound to the bc_1 complex. Concentration of heme and the amount of phospholipids in each sample are listed in Table III-7.

Table III-7

Composition of the purified cytochrome bc_1 complex

	Heme/Protein		Phospho-lipid	Phosphorus
	b (μmol/mg	c_1 protein)	%	(μg/mg protein)
Complex III	7.00	4.03	17.7	7.08
PS	8.12	4.47	7.5	2.98
CS	7.39	4.40	16.0	6.40

III-2-2-3 Measurement of small-angle X-ray scattering intensities

Measurement of small-angle X-ray scattering intensities for cytochrome $\underline{bc_1}$ complex was carried out by using the same system as that in the experiments of cytochrome oxidase. Measurement time was 5000 sec. The temperature of the specimen was kept at 5±0.2°C. The protein concentrations of PS and CS-sample were 5.7 and 3.7 mg/ml, respectively. The millimolar extinction coefficients used were 28.5 for $A_{563-577}$ for heme $\underline{b}$ and 17.5 for $A_{553-540}$ for heme $\underline{c_1}$. The distribution of scattering intensities was observed by the conventional small-angle scattering camera and the high resolution small-angle scattering camera in a range of scattering angle of 1.2 to 76.7 mrad. In order to correct background, the buffer solution for cytochrome $\underline{bc_1}$ complex was also measured with the same condition as that for the enzyme. Reliability factors (R-values) are listed in Table III-8.

Table III-8

Reliability factors, R_{sym}, of the small-angle X-ray scattering intensities from cytochrome $\underline{bc_1}$ complex

	R_{sym}^{1}	R_{sym}^{2}
PS	0.0881	0.2184
CS	0.1054	0.1837

R_{sym}^{1} : small-angle X-ray scattering camera
R_{sym}^{2} : high resolution small-angle X-ray scattering camera

III-3 Results

III-3-1 Cytochrome oxidase and its complex with cytochrome c

The radii of gyration, Rg, of the cytochrome oxidase and its complex with cytochrome c are listed in Table III-9. The change of the Rg value in this table depends on the variation of the contrast, or that of the sucrose concentration, because this value is given as a function of the contrast (equation I-36). Information on cytochrome c binding to the oxidase can be obtained from a comparison in the Rg values of the complex and the oxidase. The Rg values of the complex in each sucrose solution are larger than those of the oxidase. If cytochrome c is buried in the oxidase molecule, the differences in the Rg value may be very small and independent of the sucrose concentration. Moreover, the difference of 5 Å in the Rg values in 18.5-22% sucrose solution without the detergent contribution (Table III-9, d-e) is larger than that of 2 Å in 0-10% sucrose solution with the detergent contribution (Table III-9, a-c). This means that the significant differences can be observed independently of the detergent contribution. These results suggest that cytochrome c is not buried in the oxidase molecule but binds on the surface of the molecule.

Table III-9

Molecular parameters for the cytochrome oxidase and its complex with cytochrome c deduced from small-angle X-ray scattering

sample	sucrose	complex				oxidase			
	%(w/w)	Rg (Å)	Rg_A (Å)	Dmax (Å)	V x10^5 (Å^3)	Rg (Å)	Rg_A (Å)	Dmax (Å)	V x10^5 (Å^3)
a	0.0	55.5(1)	55(1)	165(8)	6.5	53.8(1)	54(1)	165(8)	5.6
b	5.0	55.4(1)	54	160	6.2	53.5(2)	54	161	7.1
c	10.0	55.7(2)	55	156	4.7	52.3(4)	52	152	2.9
d	18.5	55.2(2)	54	156	8.0	49.7(2)	49	141	2.9
e	22.0	54(2)	53(2)	147(6)	4.9	48.2(2)	49(2)	149(6)	3.6
f	30.7	41.4(3)	44	140	1.1	35.2(2)	36	135	0.6
g	36.3	18.3(1)	29(2)	42(5)	0.5	/	/	41	0.2
h	40.0	/	/	42	0.2	/	/	41	0.2
i	45.0	17.6(1)	13	53	0.5	/	/	41	/
j	50.0	28.7(1)	28(2)	130	0.3	/	/	51	0.1

Rg : Radius of gyration calculated from Guinier plot
Rg_A : Radius of gyration calculated from distance distribution function
Dmax : Maximum dimension
V : Scattering volume
complex: Cytochrome oxidase - cytochrome c complex
oxidase: Cytochrome oxidase
Standard deviations are shown in parentheses.

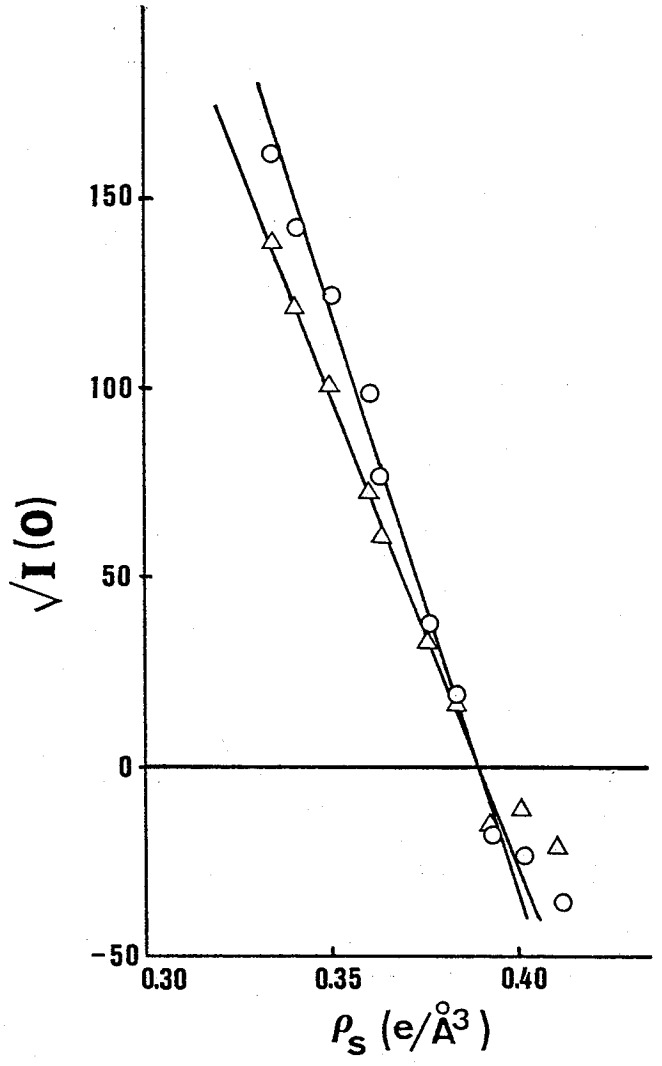

Fig. III-6. Variations of $\sqrt{I(0)}$ for the cytochrome oxidase (△) and its complex with cytochrome c (○) as a function of electron density of the solvent, ρ_s.

Fig. III-6 shows a plot of the electron density of the solvent against square root of zero-angle scattering intensity, $\sqrt{I(0)}$. In the equation (I-33), if h is very close to zero, the term of $\exp(i\vec{h}\vec{r})$ becomes unity approximately, and the equation (I-32) can be rewritten to the following equation by the equation (I-31):

$$I(0) \simeq \Delta\rho^2$$

This shows that the zero-angle scattering intensity is proportional to square of the effective number of electrons of the molecule and $I(0)=0$ if $\Delta\rho=0$. A point of intersection with abscissa in the $\sqrt{I(0)}$ versus ρ_s plot indicates the mean electron density of the molecule, and it is evaluated to be 0.38-0.39 $e/\mathring{A}^3$. This is coincident with the mean electron density calculated for the oxidase-detergent complex, as presented in Fig. III-4. The result shows that the estimation of the amount of detergent bound to the oxidase is sufficiently correct .

The intramolecular distance distribution function, P(r), can be calculated by the Fourier transform of the scattering data (equation (I-13)). Fig. III-7 shows the distance distribution functions of the oxidase and the complex. By plotting P(r) versus r, the maximum dimension, Dmax, of one particle can be obtained directly from the value on the abscissa where the P(r) function curve intercepts (Fig. III-7). The Dmax values of the oxidase and the complex are listed in Table III-9.

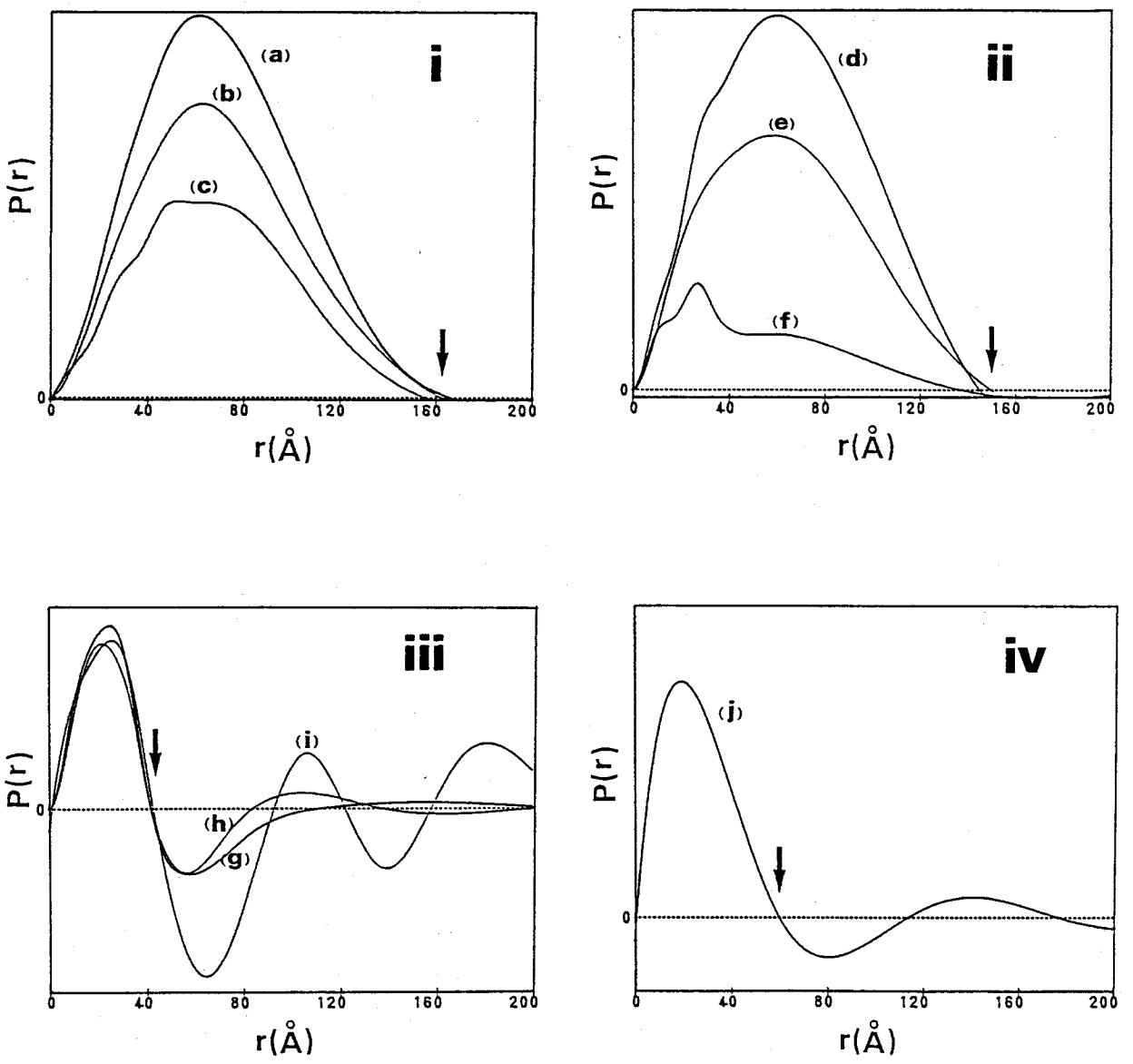

Fig. III-7-1. Distance distribution functions, P(r) for the cytochrome oxidase in various sucrose concentrations; (i) first, (ii) second, (iii) third and (iv) fourth group; letters, (a)to (j), correspond to those of Table III-4. Arrows indicate the maximum dimensions of the cytochrome oxidase particle.

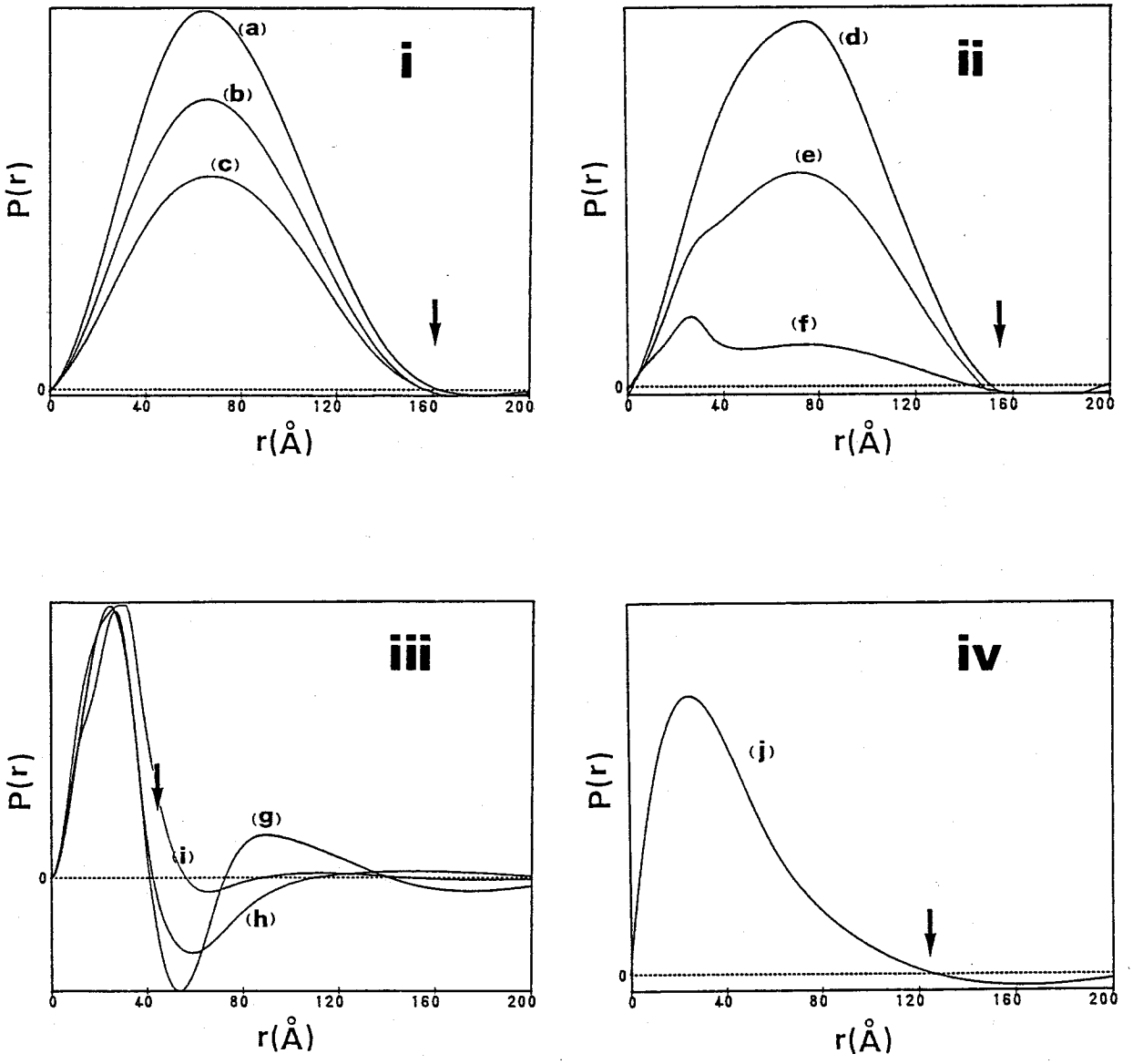

Fig. III-7-2. Distance distribution functions, P(r) for the cytochrome oxidase - cytochrome c complex in various sucrose concentrations; (i) first, (ii) second, (iii) third and (iv) fourth group; letters, (a) to (j), correspond with those of Table III-4. Arrows indicate the maximum dimensions of the cytochrome oxidase - cytochrome c complex particle.

The P(r) functions may be grouped into four classes according to the concentration of sucrose. The P(r) functions of the first group are those from the 0-10% sucrose solutions which contain the oxidase or the oxidase-detergent complex, as shown in Fig. III-7-1(i) or Fig. III-7-2(i). The P(r) functions of this group present an attribute of the overall structure of the oxidase molecule or the oxidase-detergent complex molecule, since the electron density of the solvent including sucrose is lower than that of the oxidase, ρ_{ox} or that of the detergent, ρ_{tx}. The radii of gyration derived from the Guinier plot was about 53 Å and 55 Å for the oxidase and the complex, respectively. The difference in the Rg values between the oxidase and the complex is about 2 Å. However, the great difference in the maximum dimensions between the oxidase and the complex is not detectable.

The scattering intensity curves of the oxidase solution and the complex solution without sucrose are shown in Fig. III-8. The theoretical intensity curves of ellipsoids with the eccentricities of 1.0, 2.0 and 3.0 are also plotted in the same figure. It is seen that the experimental scattering curves of the oxidase and the complex coincide with the theoretical scattering curve of the ellipsoid of revolution whose eccentricity is 2.0. However, on the basis of the discussion on Fig. II-6, the disagreement in the range of 0.5-1.0 of the abscissa suggests that the electron densities within these particles are remarkably ununiform.

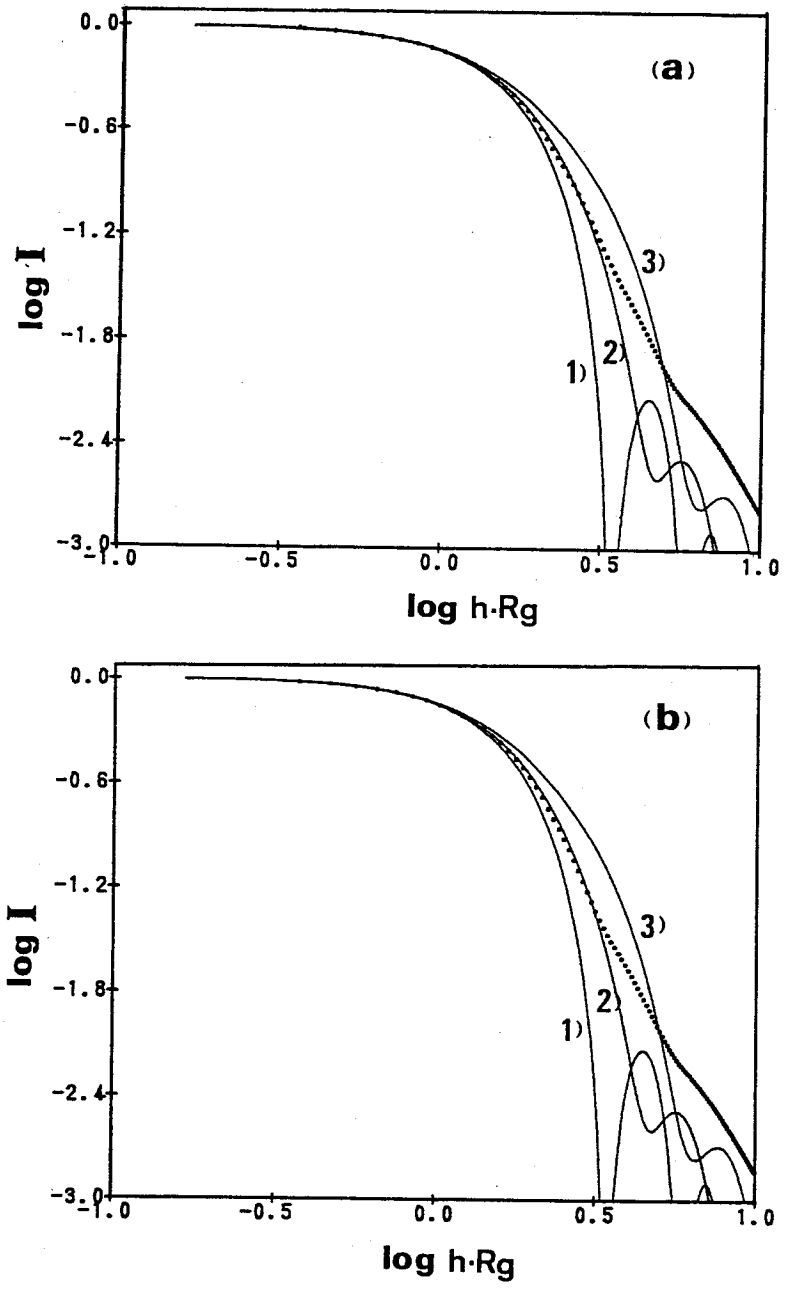

Fig. III-8. Log I - log (h Rg) plots of desmeared scattering intensities of cytochrome oxidase and its complex with cytochrome c in 0% sucrose solution; (a), cytochrome oxidase; (b), complex with cytochrome c. Superimposed are the theoretical scattering functions (solid lines) of the prolate ellipsoids with the eccentricities, ω of 1) ω = 1.0 (sphere), 2) ω = 2.0 and 3) ω = 3.0.

The P(r) functions of the second group are obtained from the 18.5-30.7% sucrose solutions. As shown in Fig. III-7-1(ii) or Fig. III-7-2(ii), these functions present the distance distribution of the protein moiety in the oxidase or the complex, since the ρ_s is close to the ρ_{tx}. The figures (a) through (e) in the Fig. III-7 show that the maximum dimensions of the protein particles do not change greatly in the solution up to 22% of sucrose concentration. This means that the detergents are bound not to both ends of the prolate particle of the oxidase but to somewhere on the surface of the oxidase within the maximum dimension of about 160 Å.

The P(r) functions in the third group which were obtained from the 36.3-45% sucrose solutions have positive and negative regions. Such oscillation of P(r) corresponds to fluctuation of the electron density in the particle, since the ρ_s is close to the mean electron density ρ_{mx} of the oxidase-detergent or the complex-detergent particle. The positive region of the P(r) function is attributed to the protein structure and the negative region is the detergent structure. The original maximum dimension no longer exists at such sucrose concentrations, since the boundary defining the molecular shape disappears from the molecule. The apparent maximum dimension close to 40 Å may be considered to be the average size of each subunit whose assembly forms the oxidase. The last group in the 50% sucrose solution supplies the structural information about the detergent moiety bound to the oxidase, since the ρ_s is

equal to the ρ_{ox} and the portion of the protein disappears. From these results of the contrast variation method, the relation of the electron density between the detergent and the oxidase has been proposed, as shown in Fig. III-9. In this figure, ρ_{tx}, ρ_{mx} and ρ_{ox} represent the mean electron density of the detergent, detergent-oxidase and oxidase, respectively. Letters of (a), (b), (c) and (d) correspond to the group i, ii, iii and iv described previously. When the electron density of the solvent is close to 0.3344 e/Å^3 (in the case of (a)), both the detergent and the oxidase contribute to the X-ray scattering. In the case of (b), the scattering intensities are attributed only to the oxidase, while in the case of (d), the scattering intensities are from the detergent which causes negative amplitude. The case of (c) is regarded as an intermediate step of the case of (b) and (d).

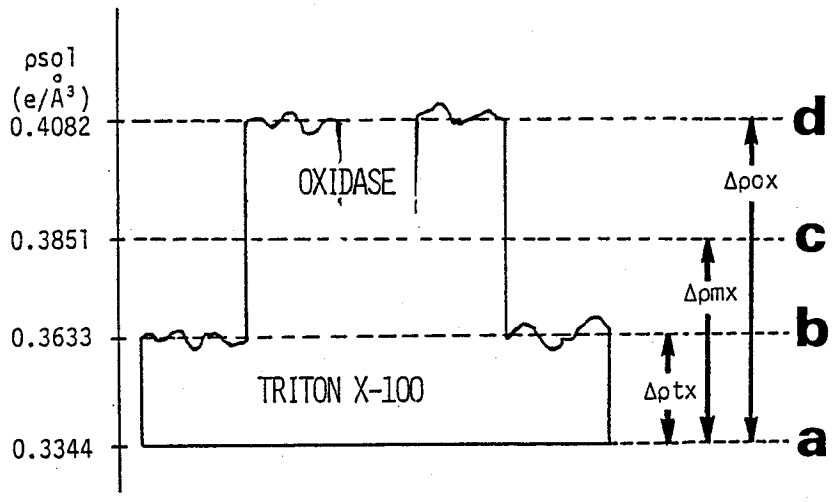

Fig. III-9. Schematic representation of the electron density level for the cytochrome oxidase and the bound detergent; ρ_{sol}, electron density of the solvent; $\Delta\rho_{tx}$,$\Delta\rho_{mx}$,$\Delta\rho_{ox}$, difference electron densities between Triton X-100, Oxidase - Triton X-100 complex, Oxidase and the solvent.

The P(r) function of the complex in 0% sucrose solution (Fig. III-7-2) involves the vectors of the oxidase, the detergent, the cytochrome c and their cross-vectors. In order to scrutinize the location of the cytochrome c in the complex, a difference-distance distribution function, $\Delta P(r)$, was calculated. The $\Delta P(r)$ of 22% sucrose solution was shown in Fig. III-10-1. This function presents the distance distribution from the cytochrome c to the oxidase, since many extra vectors which are self-vectors of the oxidase and the detergents disappear. In this figure, the maximum dimension can be regarded as the longest distance from the cytochrome c to the oxidase and can be evaluated to be 140 Å. This means that the center of the cytochrome c is located in a place which is about 40 Å distant from the end of the oxidase, assuming that radius of the cytochrome c is 20 Å. The place is also suggested to be on the molecular surface of the oxidase, because cytochrome c binds to the oxidase by an ionic interaction between the two enzymes. The schematic representation of this arrangement is shown in Fig. III-10-2.

Fig. III-11 shows the Stuhrmann plot (Rg^2 versus $1/\Delta\rho$) representing a negative quadratic curve. This plot suggests that the oxidase dimer has a dense region in the molecule and forms an asymmetrical dimer whose center of gravity is apart from the electronic center of the dimer molecule, because β (in equation I-36) $\neq 0$.

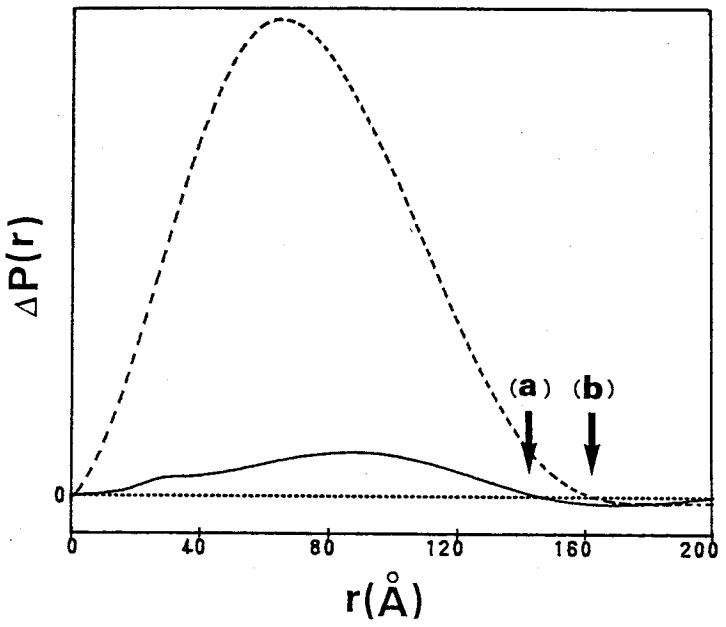

Fig. III-10-1. Difference-distance distribution function ΔP(r) between the cytochrome oxidase - cytochrome c complex and the cytochrome oxidase in 22% sucrose solution (solid line). Superimposed is the P(r) function for the cytochrome oxidase in 0% sucrose solution (dashed line).
Arrows (a) and (b), maximum dimensions of the ΔP(r) and P(r).

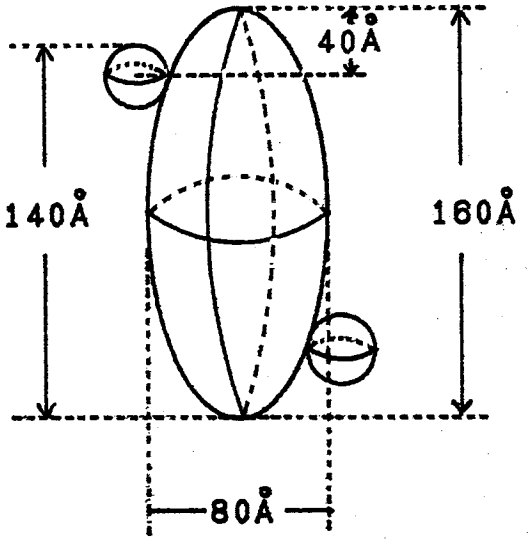

Fig. III-10-2. Proposed arrangement of the cytochrome oxidase and cytochrome c; ellipsoid, cytochrome oxidase as the dimer form; sphere, cytochrome c

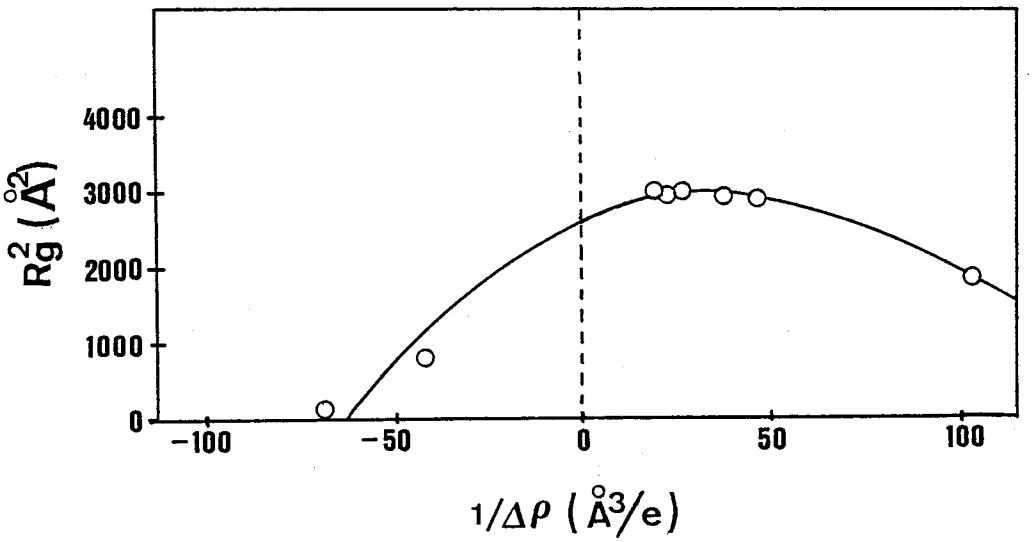

Fig. III-11. Stuhrmann, Rg^2 *versus* $1/\Delta\rho$, plot for the cytochrome oxidase - cytochrome *c* complex.

III-3-2 Simulation of model of cytochrome oxidase and its complex with cytochrome c

The interpretation of small-angle scattering data is mainly based on the comparison of experimental data with structural functions (29). Computer simulation was carried out in order to confirm the results of the X-ray measurement. The sphere method is widely used in practical application. The scattering intensity I(h) of an aggregate of n spheres can be computed by the Debye formula:

$$I(h) = \sum_{i=1}^{h} g_i^2 \Phi_i^2(h) + 2 \sum_{i=1}^{n-1} \sum_{k=i+1}^{n} g_i g_k \Phi_i(h) \Phi_k(h) \frac{\sin(d_{ik}h)}{d_{ik}h}$$

where g_i is the weighting factor of the i-th sphere, $\Phi_i(h)$ the form factor of the i-th sphere, d_{ik} the distance between the centers of the i-th and k-th spheres ,and h is the same as that described previously.

$$g_i = \rho_i V_i = \rho_i \frac{4\pi}{3} R_i^3$$

where ρ_i is the electron density of the i-th sphere (radius R_i) and V_i the volume of this sphere. The shape factor $\Phi_i(h)$ is given by:

$$\Phi_i(h) = 3 \frac{\sin(R_i h) - (R_i h)\cos(R_i h)}{(R_i h)^3}$$

As a first approximation, a biological macromolecule is composed of many spheres of well-defined size representing different globular subunits. In this case, the shape factors of the subunits are actual parameters of the model. However, in most cases, there is no such possibility and the method of finite elements has to be used, i.e. the model must be made with a large number of sufficiently small spheres of equal size and, if necessary, different weight. The shape factor of the small sphere is not an actual parameter of the model and introduces a limit of resolution. The size of the sphere used was determined to be 24 Å in the diameter by taking account of the resolution in the X-ray measurements. Simulations were carried out by using the distance distribution function presenting information on the architecture of the molecule.

The oxidase particle dissolves as a dimeric form in the buffer solution containing 0.1% Triton X-100. The shape of the particle can be approximated by an ellipsoid of revolution (prolate) with the eccentricity of 2.0-3.0 (Fig. III-8), the prolate model composed of 56 spheres was built as a dimeric form of the oxidase. The 56 spheres were assembled in the close contact with each other. The results of the experiment of the group ii suggested that the detergent might be bound not to the both ends of the oxidase dimer, but to the interface of the dimer. The detergent was considered to be located around the interface and then its corresponding sphere was given a value of 0.3633 $e/Å^3$ as the electron density, while the other sphere

representing the oxidase molecule was given a value of 0.4082 e/$\mathring{A}^3$. The distance distribution function of the model composed of 56 spheres with the electron densities of the detergent and the oxidase was calculated by an algorithm of the sphere method described previously and was compared with the corresponding experimental P(r) function. Some spheres with identical size were added to the model so as to exclude differences between the calculated and the experimental P(r) functions. Finally, 74 spheres were used to make the model as shown in Fig. III-12. In this figure, the detergents are shown by blue circle and the oxidases shown by green ones. Red circle is cytochrome c molecule whose position was determined by the distance distribution of this enzyme in the ΔP(r) and the P(r) function in 22% and 0% sucrose solution, respectively. Variations of the P(r) functions of the model by increasing the electron densities of the solvent correspond to those of the experimental function, which are shown in Fig. III-13. This means that estimation of the binding sites of the detergents and cytochrome c molecule is correct.

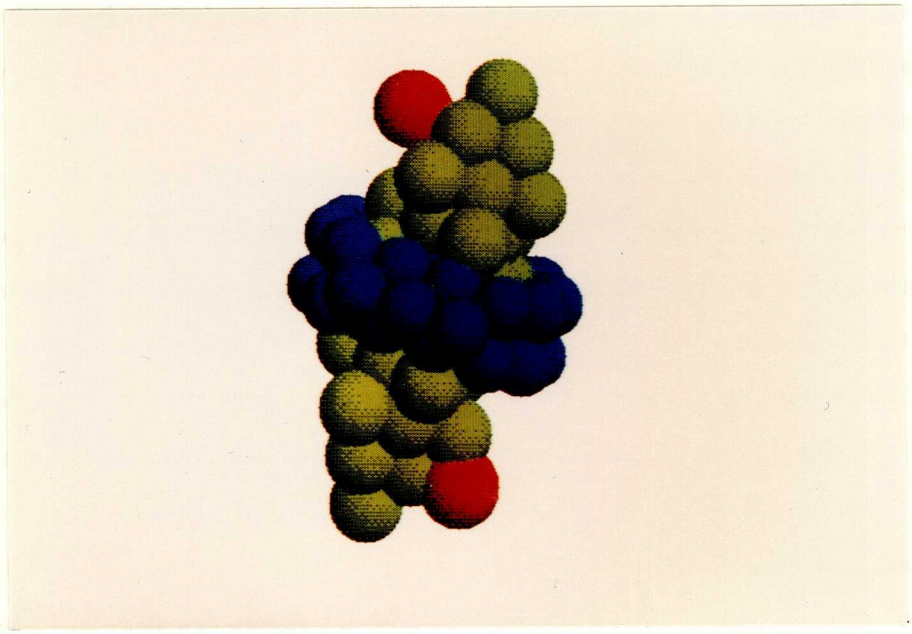

Fig. III-12. Proposed model for the cytochrome oxidase and the bound detergent as a dimeric form; green, cytochrome oxidase; blue, Triton X-100; red, cytochrome c.
Radius of each sphere is 12 Å.

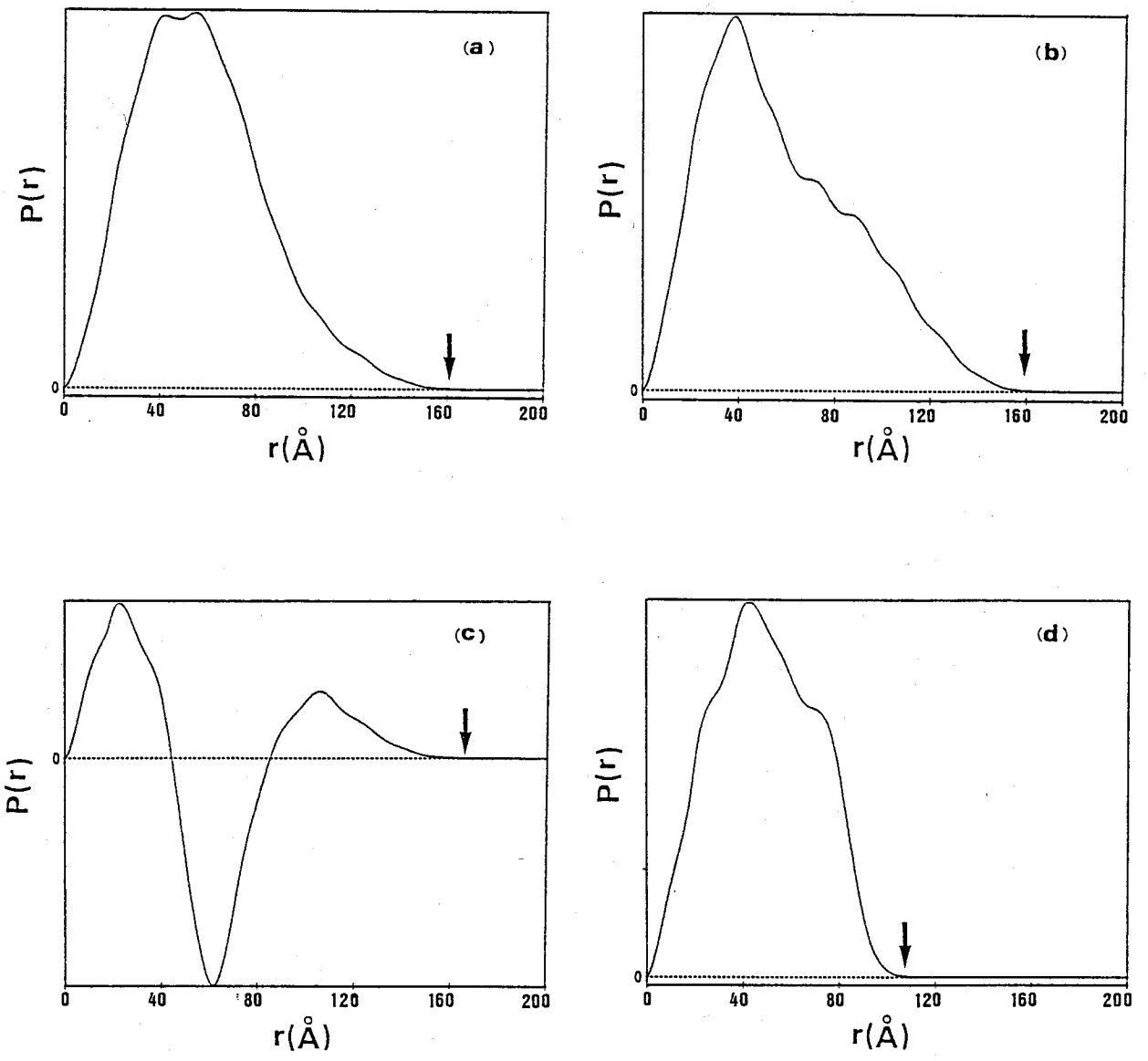

Fig. III-13. Distance distribution functions, P(r) for the model composed of 74 spheres; (a), 0% sucrose (Group i); (b), 22% sucrose (Group ii); (c), 36.3% sucrose (Group iii); (d), 50% sucrose (Group iv). Arrows indicate the maximum dimensions.

III-3-3 Cytochrome bc_1 complex

For the small-angle X-ray scattering measurement, two kinds of samples of cytochrome bc_1 complex isolated from beef heart mitochondria were prepared. One of them was highly purified by using two column chromatography, hydrophobic and affinity chromatography (PS-sample). The other (CS-sample) was prepared by only affinity chromatography. These two procedures of the purification gave difference of the amount of phospholipids in the cytochrome bc_1 complex. The PS-sample contained 7.5% (w/w) phospholipids while the CS-sample contained 16% (w/w) phospholipids.

Small-angle X-ray scattering data of the cytochrome bc_1 complex were measured in 25 mM Tris-HCl buffer, pH 7.5 containing 20% glycerol, 0.1% Tween 20 and 0.1 M NaCl. The scattering intensities in the small-angle region were plotted according to Guinier (log (I) *versus* h^2) to obtain the radius of gyration, Rg. Fig. III-14 shows these plots for the slit-smeared curves. The radii of gyration can be calculated from these plots and are listed in Table III-10. The molecular weight of the enzyme is very large, so that the scattering intensities distribute at very small angle around the incident X-ray. Two ((c) and (d)) of four plots in Fig. III-14 were made of the data observed by the high resolution small-angle scattering apparatus. Therefore, the reliabilities of the (c) and (d) data are better than those of the (a) and (b) data.

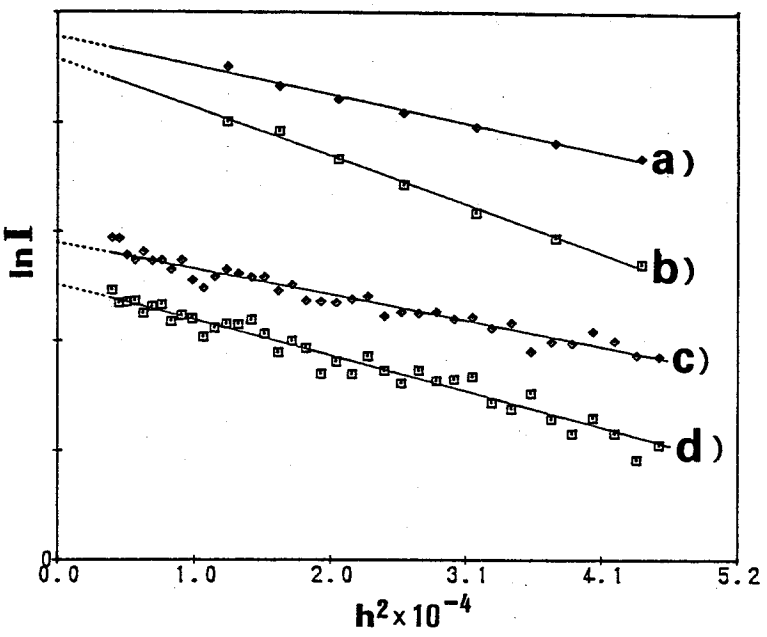

Fig. III-14. Guinier plots of average scattering intensities from cytochrome bc_1 complex; a) PS-sample, b) CS-sample measured by small-angle X-ray scattering camera; c) PS-sample, d) CS-sample measured by high resolution small-angle X-ray scattering camera.

Table III-10

Radii of gyration and standard deviations of the cytochrome bc_1

	Rg^1	s(Rg)	Rg^2	s(Rg)
PS	67	1.5	67	1.2
CS	87	1.4	79	1.2

Rg^1 : small-angle X-ray scattering camera
Rg^2 : high resolution small-angle X-ray scattering camera
s(Rg) : standard deviation of the radius of gyration

The radii of gyration calculated from the desmeared scattering curves are listed in Table III-11, and the Guinier plots of the curves are shown in Fig. III-15. The radius of gyration can also be calculated from an intramolecular distance distribution function derived from the desmeared scattering curve by the method of Fourier transform. These values coincide with those from the Guinier plots using desmeared scattering intensities. Fig. III-16 shows the P(r) functions of two samples.

Table III-11

Molecular parameters for the cytochrome $\underline{bc}_1$ complex deduced from small-angle X-ray scattering

	Rg(Å)	Rg_A(Å)	Dmax (Å)	Vol $\times 10^6$ (Å^3)	f	H_2O (g/g)
PS	69.5(5)	68.8	222	1.89	3.01	1.49
CS	82.1(9)	83.9	300	2.81	4.16	2.34

Rg : Radius of gyration calculated from Guinier plot
Rg_A : Radius of gyration calculated from distance distribution function
Dmax : Maximum dimension
Vol : Scattering volume
f : degree of hydration
H_2O : amount of water
Standard deviations are shown in parentheses.

The maximum dimension, Dmax, can be estimated from the P(r) functions. The P(r) function becomes zero where the r is equal to or greater than the maximum dimension Dmax. The Dmax was determined to be 222 Å and 300 Å for the PS- and CS-sample, respectively.

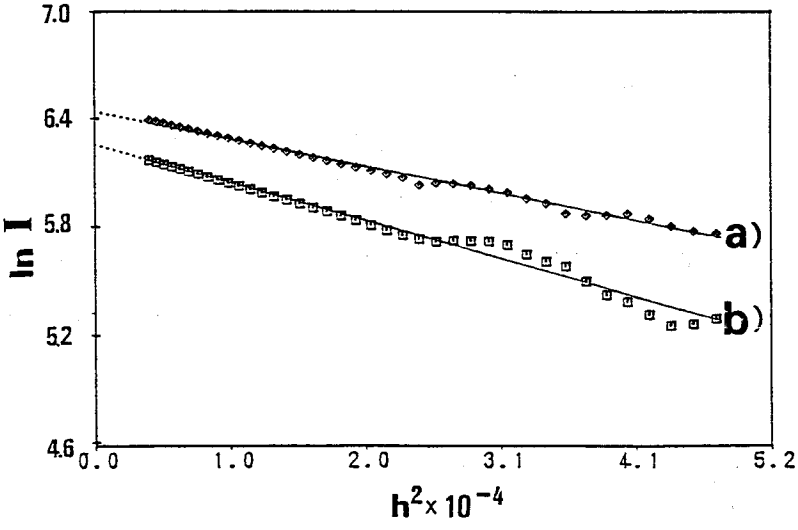

Fig. III-15. Guinier plots of desmeared scattering intensities from cytochrome $\underline{bc_1}$ complex; a) PS-sample, b) CS-sample.

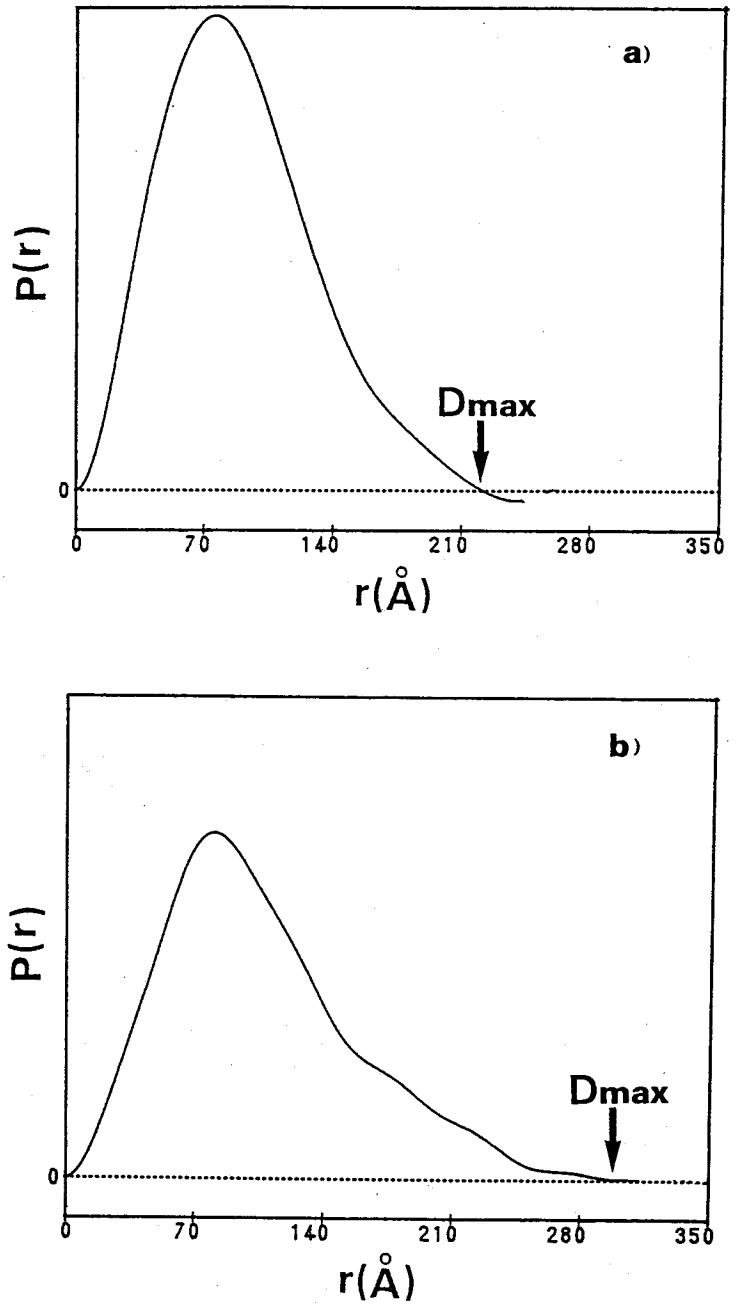

Fig. III-16. Distance distribution functions, P(r) for the cytochrome bc_1 complexes; r = distance; Dmax = maximum dimension of the particle; a) PS-sample, b) CS-sample.

A hydrated volume of the protein molecule can be determined from the intensity at zero-angle and the invariant Q according to Porod (described in the section I-4). A comparison of the hydrated volume with the unhydrated volume calculated from the molecular weight (about 472,400) and the partial specific volume gives the swelling factor, f, and the mass of water (45), whose values are listed in Table III-11. Since the evaluation of the swelling factors do not take into account of the detergents (Tween 20) bound to the cytochrome $\underline{bc_1}$ complex, the mass of water should include the mass of the detergent as an unknown parameter.

By making a comparison between the experimental and the theoretical scattering curves, the shape, that is, the overall structure of the enzyme can be estimated. Fig. III-17 shows log (I) <u>versus</u> log (hRg) plots in which dotted curves represent the experimental data of PS- and CS-sample and solid curves indicate the theoretical values for some ellipsoids of revolution. This figure shows that the shape of the enzyme can be approximated by an oblate ellipsoid rather than a sphere and the electron density within the particle is remarkably ununiform.

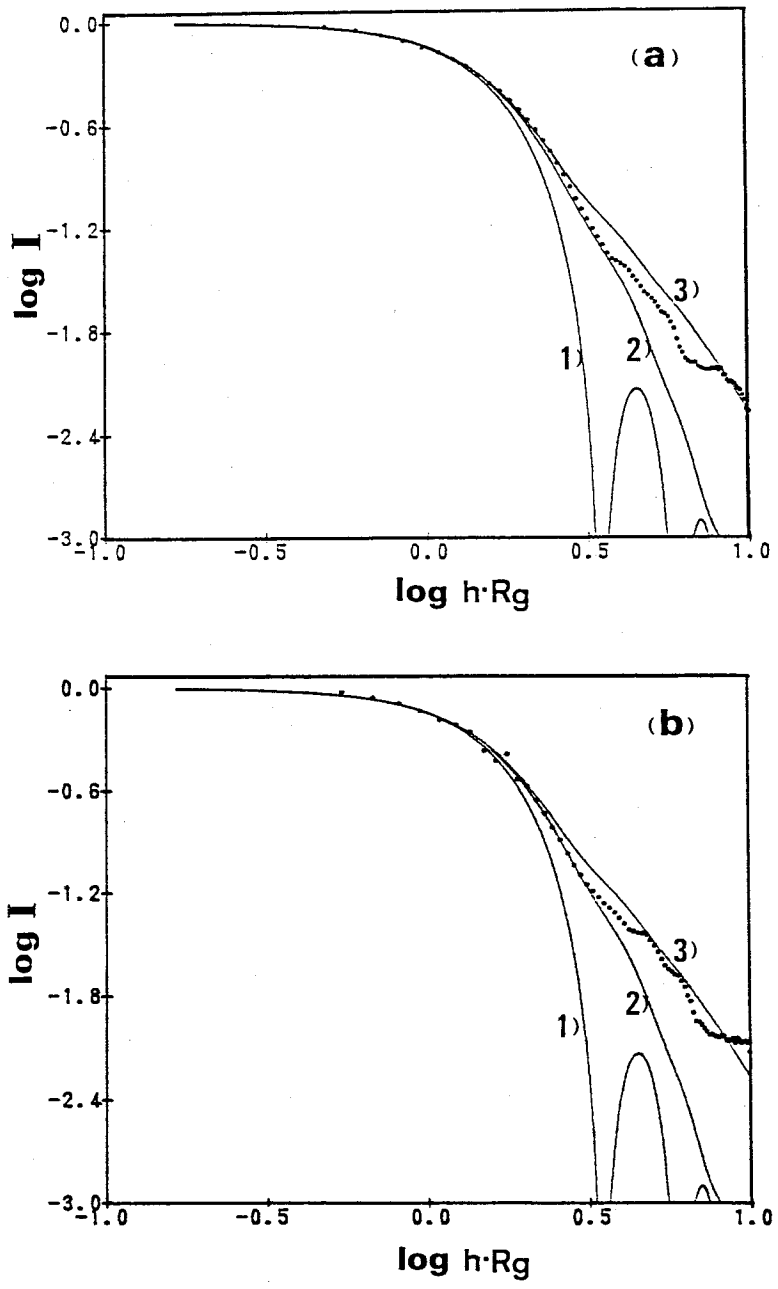

Fig. III-17. Log I - log (h Rg) plots of desmeared scattering intensities of the cytochrome $\underline{bc}_1$ complex; (a) PS-sample, (b) CS-sample. Superimposed are the theoretical scattering functions (solid lines) of the oblate ellipsoids with the eccentricities, ω of 1) ω = 1.0 (sphere), 2) ω = 0.3 and 3) ω = 0.1.

III-4 Discussion

Recent development of the X-ray source such as synchrotron radiation makes it possible to study the molecular structure of proteins in solution by the small-angle X-ray scattering method. However, this technique has never been applied to intrinsic membrane proteins. The primary difficulty in studying the structure of intrinsic membrane proteins arises from phospholipids bound to the proteins (14). The phospholipids make it difficult to obtain highly purified preparations of the intrinsic membrane proteins. In addition, if the proteins are covered with phospholipids, the phospholipid-protein-detergent complexes give poor information about the structure of the proteins to the X-ray scattering. The second difficulty is concerned with detergents. When the detergent forms large micelles, the high background scattering from the detergent micelles may interfere with the precise measurement of scattering intensities. And if a large amount of the detergent is bound to the protein in proportion to the amount of the phospholipids, change of the scattering intensities caused by binding of cytochrome c may not be detected by this technique. For these reasons, the oxidase and bc_1 complex were highly purified and depleted of phospholipids by hydrophobic interaction chromatography so as to minimize the contribution of the phospholipids and the detergents to the X-ray scattering.

Protein solutions with concentration of 5 - 3 mg/ml

were used to obtain the structural parameters of the oxidase and the $\underline{bc_1}$ complex from the measurement of the small-angle X-ray scattering. Such structural parameters as the radius of gyration Rg and the maximum dimension Dmax obtained in this experiment were those estimated in a given concentration of the protein solution, not at infinite dilution. Thus, it is necessary to discuss the dependence of the Rg value on the concentration of the protein solution.

Effects of the protein concentration on the distribution of the X-ray scattering intensities are explained by the equation (I-25) described in chapter I. The coefficient $8v_0/v_1$ in the equation depends on the concentration, and its change affects the distribution of the scattering intensities at very small angle region. At infinite dilution, the coefficient is close to zero, and influence of the concentration on the Guinier plot disappears. In other cases, it may be considered that the Rg value is somewhat dependent on the protein concentration. The extent can be discussed by two experimental examples of serratia protease and ovomacroglobulin. Guinier plots of these two proteins are shown in Figures A and B.

For serratia protease with the molecular weight of 45,000, in Figure A, the protein solutions of 10 - 5 mg/ml concentration were used in the experiment where the coefficient was in a range of 0.18 - 0.09. The Rg value in each concentration was in a range of 26.6±0.2 Å. For

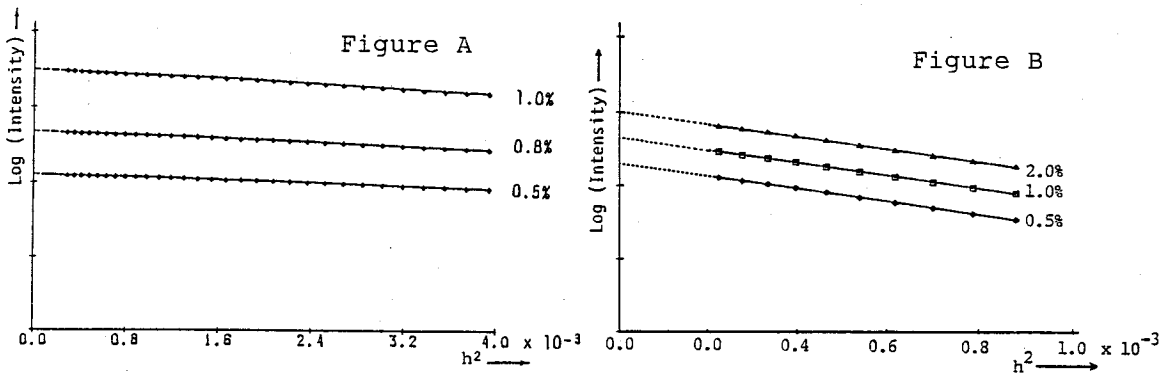

ovomacroglobulin with the molecular weight of 750,000, in Figure B, the measurement was carried out under the condition that the coefficient was in a range of 0.48 - 0.12, and the Rg value was estimated to be 75.5±1.0 Å with the standard deviation of 0.5 Å. Since the respective plots in Figures A and B are parallel to one another, it can be considered that the influence of the concentration on the scattering intensities is negligibly small under these conditions. Because the coefficients of the oxidase and the $\underline{bc_1}$ complex solutions were about 0.1, the Rg values obtained here were considered to be independent of the protein concentration.

The radius of gyration and the maximum dimension of the oxidase in 0% sucrose solution were 53 Å and 165 Å, respectively. These values suggest that the oxidase should form a dimer in the solution state. Henderson and Capaldi showed by electron microscopy and image reconstruction that the span of the oxidase molecule in the mitochondrial membrane was about 70-80 Å (30). Also in nonionic detergents (Triton X-100, Tween 20) and at physiological

pH, beef heart cytochrome oxidase forms a stable dimer with high electron-transfer activity (31,32). The molecular weight can be calculated from its scattering volume (Table III-9) with the following equation:

$$M = N_A V / v_c(X + 1)$$

where M is the molecular weight of the oxidase, N_A the Avogadro's number, V the scattering volume of the oxidase-detergent complex, v_c the partial specific volume of such a complex and X the grams of bound detergent per gram of oxidase. The v_c and X are estimated by spectrophotometric study (section III-2-1-3), and then the molecular weight of the oxidase is calculated to be about 250,000. This value is consistent with the molecular weight calculated from the amino acid composition of the oxidase and implies that the oxidase has little hydration under these conditions. The difference between two scattering volumes in 0% and 22% sucrose solutions corresponds to the volume of the bound detergents, because the detergents were invisible from the oxidase-detergent complex molecule when the electron density of the solvent is equal to that of the detergents. These values of the oxidase and the complex are 1.95×10^5 and 1.66×10^5 $Å^3$, respectively. The Triton X-100 has a molecular weight of 646 and a partial specific volume of 0.908, so that such volume differences correspond to the number of bound Triton X-100 molecules of 200 and 170, respectively. These values are consistent with the value

estimated by the spectrophotometric study.

The shape of the oxidase dimer can be approximated by a prolate ellipsoid with the eccentricity of 2.0 (Fig. III-8). However, the experimental scattering curve in this figure deviates largely from the theoretical curve at scattering angles of 15 mrad or larger angle which correspond to Bragg spacing smaller than 100 Å. The disagreement between the two curves may be caused by such reasons as the interference between two monomers, the deviations from uniform electron density of the ellipsoid and the ambiguity of the approximation to the ellipsoid of revolution. From the results in the experiments with the contrast variation technique, it has been made clear that the detergents are bound to the surface around the interface where the monomers come in close contact with each other. The binding site is considered to be located at a surface of hydrophobic parts such as the subunits I and III. To the contrary, the part near each end (in the direction of long axis) of the dimer may be hydrophilic, involving the subunit II. Cytochrome c may be bound by the hydrophilic interaction under conditions of low ionic strength.

The P(r) function represents the intramolecular distance distribution. In case of the solubilized oxidase molecule, the P(r) function contains the distribution of not only the intra-oxidase but also intra-detergent and detergent-oxidase distances. However, the last two kinds of distance distribution can be neglected if the electron

density of the solvent is equal to that of the detergents, or $\Delta\rho_{tx}$ is zero. Under this condition, the difference-distance distribution function $\Delta P(r)$ between the oxidase-cytochrome c complex and the oxidase reveals distances from the cytochrome c to the oxidase and its maximum dimension corresponds to the distance from cytochrome c to the one end of the oxidase dimer. This value was found to be 140 Å and difference between this value and the maximum dimension of the oxidase dimer in 0% sucrose solution was about 20 Å. Therefore, the binding sites of the cytochrome c to the oxidase dimer are considered to be located on the surfaces which are about 40 Å distant from the each end of the oxidase dimer. The distance of 40 Å corresponds to the summation of the radius (20 Å) of the cytochrome c and the value (20 Å) described above. The molecular region involving this binding site is called the cytoplasmic (C-) site.

On the basis of these considerations, a typical oxidase model is constructed by an aggregate of spheres (Fig. III-12). The model is represented as a dimeric form whose cytoplasmic sites direct their course toward outsides. Stuhrmann plot indicates that the center of gravity of the oxidase dimer may be apart from the electronic center of the dimer. It means that the dimer has an asymmetrical form. Henderson and Capaldi showed also that the oxidase dimer in mitochondrial membrane had two cytoplasmic sites at the same side (30), while this investigation proposed that two cytoplasmic sites were

located in the opposite direction to each other. The structural difference of these two dimers may depend on the difference in the cytoplasmic site, in membrane or in solution.

Structural parameters of cytochrome $\underline{bc_1}$ complex isolated from beef heart have been obtained by the small-angle X-ray scattering. Two samples of the complex were prepared: one is the highly purified $\underline{bc_1}$ complex (PS-sample) containing 7.5% (w/w) phospholipids and the other is CS-sample with 16% phospholipids. The difference in the preparation procedures between two samples is only a hydrophobic-interaction chromatography step.

The radii of gyration of the PS- and CS-samples obtained from Guinier plot were in good agreement with those from distance distribution function. This agreement means the values of the radius of gyration should be correct. The P(r) functions also gave the maximum dimensions of the complexes which were 222 Å and 300 Å for the PS- and CS-samples, respectively. The maximum dimension of the CS-sample was longer than that of the PS-sample though the peak of the function for the CS-sample was lower than that of the PS-sample. The difference between two peak-heights (at a position of r=80 Å) may be caused by the difference in the protein concentration between the two samples. However, even when the scales of the P(r) functions for the CS- and the PS-samples were adjusted to each other, the maximum dimension of the former sample is larger than that of the latter. It may be

caused by the amount of the detergent (Tween 20) bound to the $\underline{bc_1}$ complex. The P(r) function of the complex gives an asymmetrical profile. The shape of the complex deduced from this profile is deviated from a sphere.

In order to estimate the shape of the complex, the experimental scattering curve was compared with theoretical curves for ellipsoids of revolution with various eccentricities (Fig. III-17). The experimental scattering data used in this study was obtained by combining two different data sets obtained separately by a new high resolution small-angle scattering apparatus and by a commercially available camera. The figure shows that the dotted curves of two preparations (PS and CS) are agreement with theoretical curves of oblate ellipsoids (ω = 0.3-0.1). Disagreement at the high angle region may be caused by the same reasons as those for the case of the oxidase.

The scattering volumes of the PS- and the CS-samples were 18.9×10^5 Å^3 and 28.1×10^5 Å^3, respectively (Table III-11). These values are much greater than unhydrated volumes of 6.0×10^5 Å^3 and 6.3×10^5 Å^3 calculated from the molecular weight, the partial specific volume of 0.74 ml/g and the respective quantity of the phospholipids. These differences correspond to the amount of Tween 20 molecules, if the hydration of the $\underline{bc_1}$ complex is as little as that of the oxidase molecule. The differences between the scattering volumes and the unhydrated volumes were estimated to be 12.9×10^5 Å^3 and 21.8×10^5 Å^3, respectively. These figures mean that the respective

complexes have about 550 and 930 molecules of Tween 20, assuming that the molecular weight of Tween 20 is 1228 and its partial specific volume is 0.869. Since the maximum dimension is extended to 300 Å with the increase in the amount of the detergents, the detergents are bound to the circumference of the complex. J. S. Rieske reported that an approximate diameter of the $\underline{bc_1}$ particle considered as a sphere was about 100 Å by electron microscopic examination with negative-stained enzyme (33). This figure supports that the PS- and CS-samples form dimers in solution.

From these results, it can be assumed that the $\underline{bc_1}$ complex have the hydrophilic subunits of each monomer in the center of the dimer. Consequently, the hydrophobic subunits are located on each end of the dimer and the detergents are bound to the ends. This was also supported by results of the experiments for the CS-sample by means of contrast variation, in which the maximum dimension indicated a decrease of 60-70 Å when the detergents were vanished by increasing electron density of the solvent. This means that the detergents are bound to the circumference of the complex dimer to form the model built in this study. Such a dimeric model is a dissymmetrical model of the cytochrome oxidase (Fig. III-12).

Chapter IV

Secondary structure analysis of proteins by means of the solution X-ray scattering

IV-1 Introduction

The X-ray crystal-structure analysis clarify the internal structure of proteins at high resolution and make it possible to deduce the structure-function relationships. However, this analysis in the solid state is not suitable to obtain the information on the dynamic behavior of protein molecules in solution. Besides there are a number of biologically interesting proteins which cannot be crystallized so as to be studied crystal structure. The X-ray solution scattering method extracts the structural information from the diffused scattering intensity distribution around incident X-rays. The intensity distribution is usually analyzed in two scattering angle regions (the so-called small angle and large angle regions). The analysis of the scattering profile in the small angle region (small-angle X-ray scattering) gives the information on the overall shape of the molecule which is described by such physical parameters as the radius of gyration, the volume, the mass, and the maximum dimension (described in the chapter II), while the analysis of the large-angle region gives the internal structure of the molecule. Therefore, the application of the large-angle X-ray scattering to the study of a protein structure should

lead to the analysis of the information on the secondary and/or super-secondary structure of the protein.

The small-angle X-ray scattering method has been applied successfully to clarify the molecular morphologies and the time-resolved structural changes of the proteins in solution. By contrast, the structure analysis by the large-angle X-ray scattering method has not been done so much, because the large-angle X-ray scattering intensity is too weak to be measured with accuracy enough to study the protein structure in solution.

The measurement system for large-angle X-ray scattering method has been set up recently in our laboratory as described in the section II-4. This system consists of a high brilliant rotating-anode X-ray generator and a focusing camera equipped with a toroidal mirror, by which it is possible to record the large-angle X-ray scattering intensities with enough accuracy. Experiments to investigate the correlation between the profile of the large-angle scattering intensity and the internal structure of a protein in solution have been carried out by use of this apparatus.

In this chapter, we will report how the information on the secondary structure of proteins can be obtained from the profile of the large-angle scattering intensity. For this experiment, the following six proteins were used: triosephosphate isomerase (35), taka-amylase A (36), pyruvate kinase (37), lactate dehydrogenase (38), cytochrome c (39) and myoglobin (40). Roughly speaking,

there are two types of secondary structures in proteins, that is, α-helix and β-sheet. The first four have β-sheets. However, the last two have only α-helix structure and no β-sheet.

IV-2 Experimental

IV-2-1 Preparation of protein solutions

Triosephosphate isomerase , pyruvate kinase and lactate dehydrogenase were purchased from Boehringer Mannheim, and myoglobin and cytochrome c were from Sigma Chemical Company. Taka-amylase A was extracted from Takadiastase by the method of Akabori et al. (34) and purified with DEAE-cellulose column chromatography. The eluted protein solutions were dialyzed overnight against a large volume of the buffer solution used for the final purification procedures and concentrated to 80-130 mg/ml by use of an ultrafiltration method with Diaflo membrane, YM-10. The concentrations of the six proteins prepared for X-ray measurement are listed in Table IV-1.

IV-2-2 Large-angle X-ray scattering measurement

A system used for the experiments of the large-angle X-ray scattering was described in the section II-4. Scattering intensities were recorded on 45 x 45 mm films of Sakura Cosmic Ray Film and measured with the Optronics P-1000 drum scanner. The temperature of the specimen was kept at $(4.0\pm0.2)^{\circ}C$ by circulating the chilled water

inside the cell holder. The specimen to film distance was 63.34±0.02 mm which was calibrated with the powder diffraction pattern of sodium myristate. The measurement time was 3600 sec for each protein or buffer solution.

IV-2-3 Small-angle X-ray scattering measurement

Small-angle X-ray measurement was carried out to measure intensities which could not be obtained by the large-angle X-ray scattering camera. A system used for the measurements of the small-angle X-ray scattering intensities was described in the section II-2. The specimen was kept at (4.0±0.2)^{o}C by the same method described previously. The measurement time was 2000 sec for each protein solution and buffer. The specimen-to-detector distance was 300.0mm.

Table IV-1

Protein concentrations and sources

Protein (source)	Concentration (mg/ml)
Triosephosphate isomerase (Chicken muscle)	131
Lactate dehydrogenase (Pig muscle)	89
Pyruvate kinase (Cat muscle)	100
Taka-amylase A (Aspergillus oryzae)	110
Myoglobin (Sperm whale)	84
Cytochrome c (Horse heart)	91

IV-3 Results

IV-3-1 Data reduction

For the large-angle scattering ($0.1<h<1.5$), the X-ray diffraction by the protein solution was recorded with the circular distribution of the scattering intensities on the film. The scattering intensities were made by such two steps, that is, measuring blackness of the film and averaging the measured intensities at every equivalent scattering angle. The procedures of the average was described in the section II-5. The reliability factors representing accuracy of the measurements are listed in Table IV-2. Net intensity of the protein was evaluated by subtracting the scattering intensity of the buffer from that of the protein solution.

On the other hand, for the small-angle scattering ($0.01<h<0.1$), the net intensity was initially obtained by subtracting the intensity of the buffer from that of the protein solution, and then averaged. The reliability factors are listed in Table IV-2. The slit effects were corrected by the Otto Glatter's Method described in the section II-5 (13). The small-and large-angle scattering intensity data were combined with each other by scaling the data at the overlapped region ($0.1<h<0.2$). The whole scattering intensity data for each protein are shown in Fig. IV-1.

Table IV-2

Reliability factor of small- and large-angle scattering

Protein	small-angle	large-angle
Triosephosphate isomerase	0.0243	0.03694
Lactate dehydrogenase	0.0424	0.03203
Pyruvate kinase	0.0443	0.03504
Taka-amylase A	0.0242	0.03272
Myoglobin	0.0294	0.02263
Cytochrome c	0.0263	0.02605

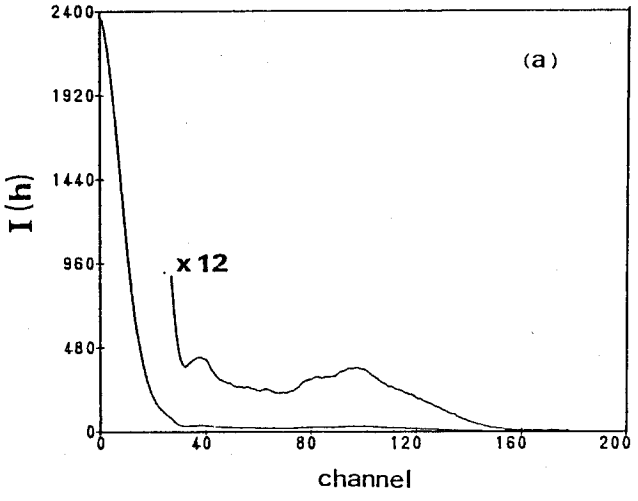
(a)
I(h)
x 12
channel
2400
1920
1440
960
480
0
0
40
80
120
160
200

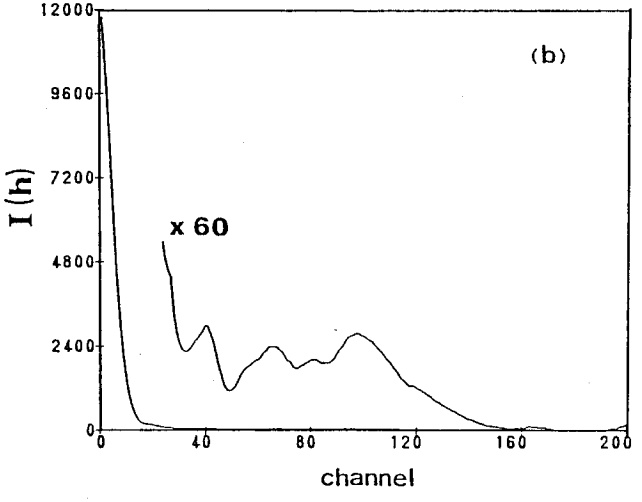
(b)
I(h)
x 60
channel
12000
9600
7200
4800
2400
0
0
40
80
120
160
200

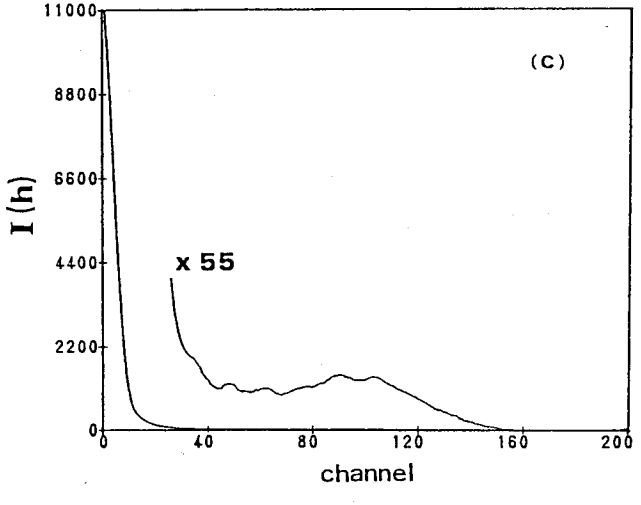
(c)
I(h)
x 55
channel
11000
8800
6600
4400
2200
0
0
40
80
120
160
200

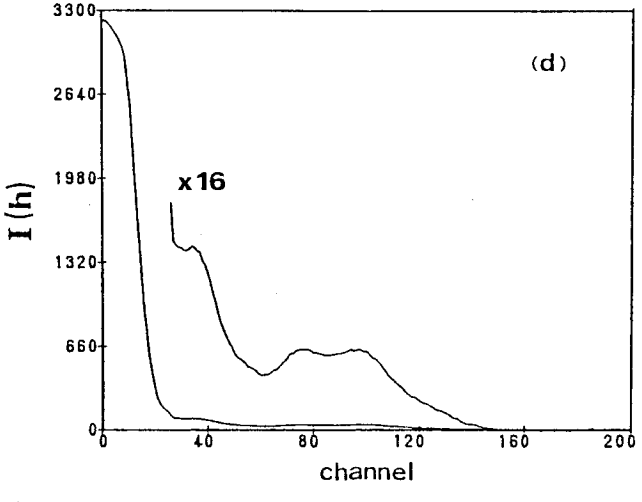
(d)
I(h)
x16
channel
3300
2640
1980
1320
660
0
0
40
80
120
160
200

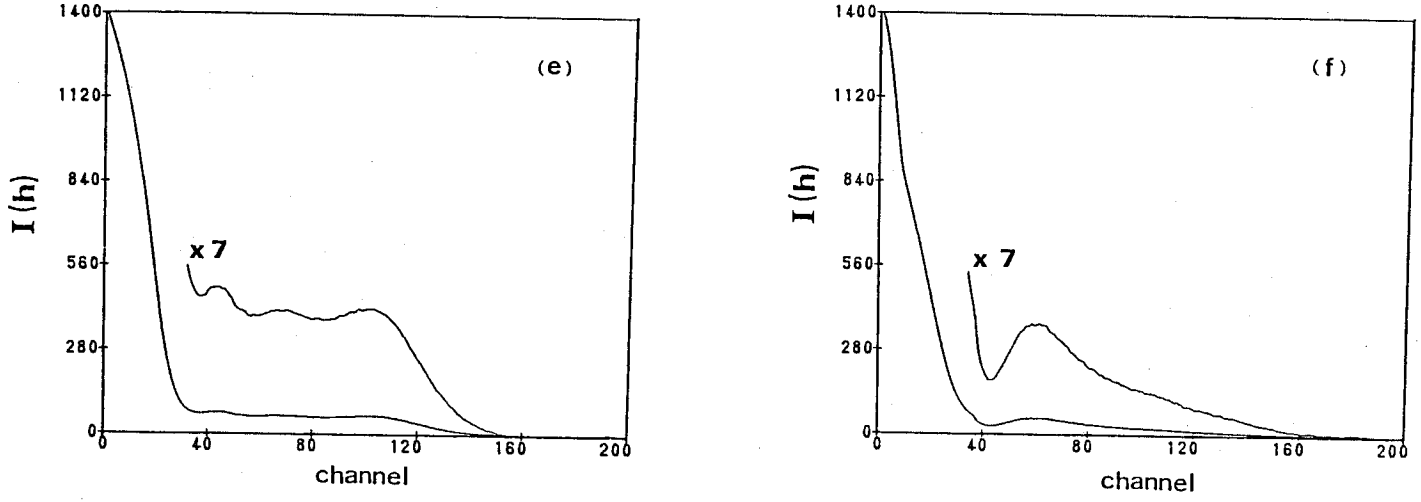

Fig. IV-1. Scattering intensities, I(h) for the six proteins; (a) Triosephosphate isomerase, (b) Lactate dehydrogenase, (c) Pyruvate kinase, (d) Taka-amylase A, (e) Myoglobin, (f) Cytochrome c. Superimposed are the magnified intensities. Channel corresponding to the scattering angle; $2\theta = \tan^{-1}(\text{channel}/63)$.

IV-3-2 Data analysis

Diffractions attributed to internal structures of proteins are observed in the large-angle region. Therefore, it is a reasonable method to investigate the internal structure of proteins by the analyses of scattering intensity distribution in this region. In order to obtain the information on the structure of the protein, the autocorrelation function A(u) is calculated by the conventional Fourier transformation method, as usually formulated by the following equation:

$$A(u) = \int_0^\infty \frac{1}{2\pi} I(h)\ h^2 \frac{\sin(hu)}{hu}\ dh \qquad \text{(IV-1)}$$

where I(h) is the scattering intensity data. This function is identical to the characteristic function, $\gamma(r)$ (3), described in the chapter I (equation (I-11)).

The A(u) function calculated with the whole scattering intensity distribution as shown in Fig. IV-1 may be similar to the Gaussian function depending on the properties of the whole scattering intensity curve because lots of pairs of atoms are summed up over the molecule. Accordingly, it makes difficult to find out the information on internal structure of proteins directly from this A(u) function. Since the internal structures are considered as deviation from a homogeneous electron density giving the overall structure of the protein molecule, the intensities attributed to the overall structure are not necessary for the analysis of the internal structure. Therefore, such intensities have to be excluded from the whole scattering

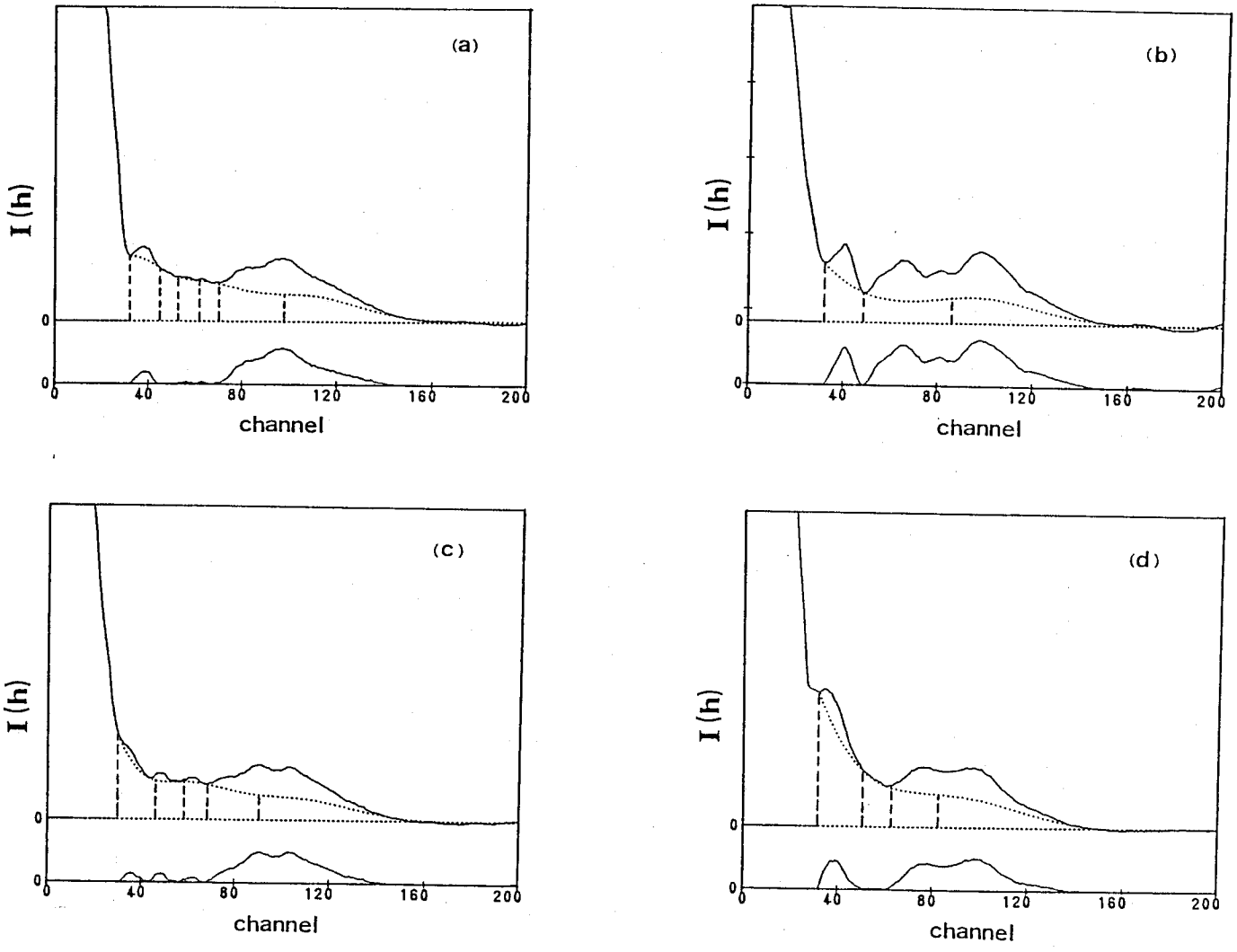
(a)
(b)
(c)
(d)
I (h)
0
0
0
40
80
120
160
200
channel

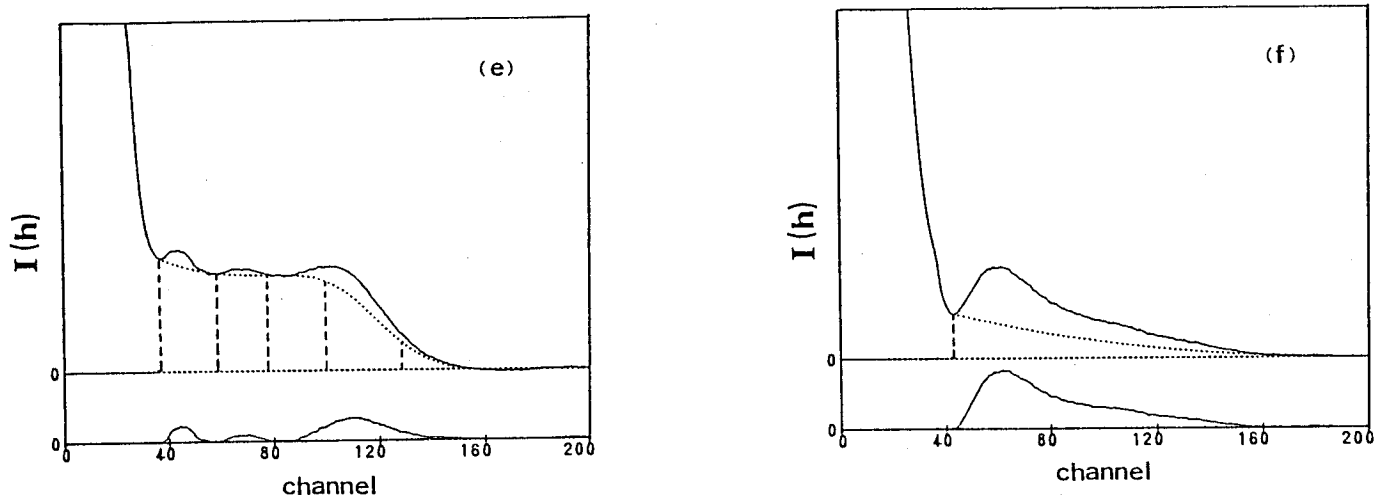

Fig. IV-2. Scattering intensity curves, I(h) (solid lines) and B-spline curves, $I_B(h)$ (dot lines) for the six proteins; (a) Triosephosphate isomerase, (b) Lactate dehydrogenase, (c) Pyruvate kinase, (d) Taka-amylase A, (e) Myoglobin, (f) Cytochrome c; (- - -), knots for the B-spline function. Superimposed are the $I_R(h)$ curves; $I_R(h) = I(h) - I_B(h)$.

intensities. The distinct diffraction patterns have to be kept in the large-angle region. From this consideration, it is expected that a curve which should be subtracted from the whole intensity curve must be varied in proportion to the increase of the scattering angle. One of the methods to approximate the curve is an utilization of a B-spline function. The B-spline function is very suitable for the extraction of the characteristic peaks from the whole scattering intensity curve. This function can be used to define the reasonable smooth-base line in each scattering curve, as shown in Fig. IV-2. In the present analysis the number and position of knots for the B-spline function were selected so as to reserve the distinct fluctuations. The number and the position of the knots, which define the B-spline functions, are listed in Table IV-3.

Table IV-3

Number and position of knots for the B-spline function

Knots No.	Protein						
	TIM	LDH	PK	TAA	Mb	Cyt.c	
1	32	32	30	32	37	43	channel
2	44	49	43	51	59	160	
3	50	84	56	60	79	200	
4	60	150	68	82	101	204	
5	68	171	90	138	135		
6	100	204	162	150	154		
7	150		180	180	164		
8	177		204	204	180		
9	204				204		

TIM : Triosephosphate isomerase
LDH : Lactate dehydrogenase
PK : Pyruvate kinase
TAA : Taka-amylase A
Mb : Myoglobin
Cyt. c : Cytochrome c

$I_R(h)$ curve representing the distinct fluctuations of the scattering intensity data is expressed by the following equation and is shown in the Fig. IV-2.

$$I_R(h) = I(h) - I_B(h) \qquad \text{(IV-2)}$$

where $I_B(h)$ is the B-spline function. A difference autocorrelation function, $\Delta A(u)$, was calculated by the Fourier transform of the $I_R(h)$ curve instead of the coefficient I(h) in the equation (IV-1). The results of the six proteins are shown in Fig. IV-3. These difference autocorrelation functions are expected to contain the information on the internal structure of the proteins, because the coefficients have no extra intensities due to the overall structure. In the four $\Delta A(u)$ functions (Figs. IV-3(a), (b), (c) and (d)), there is common peak without reference to the molecular size at a distance of about 12 Å attributed to something in the protein molecules involving some β-sheets, while other two functions have no common features.

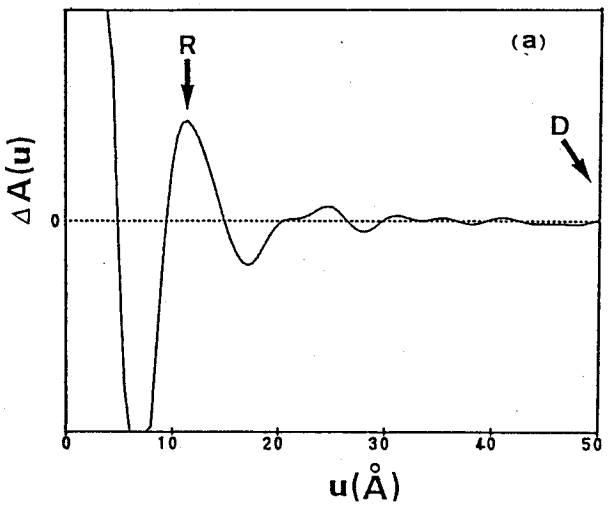
R
(a)
D
ΔA(u)
0
0
10
20
30
40
50
u(Å)

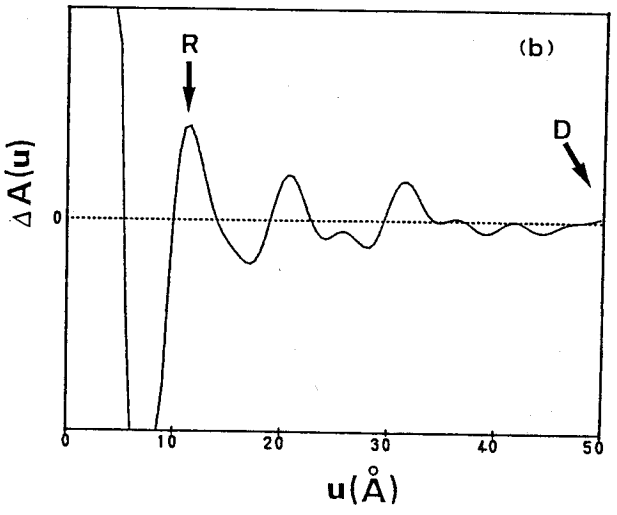
R
(b)
D
ΔA(u)
0
0
10
20
30
40
50
u(Å)

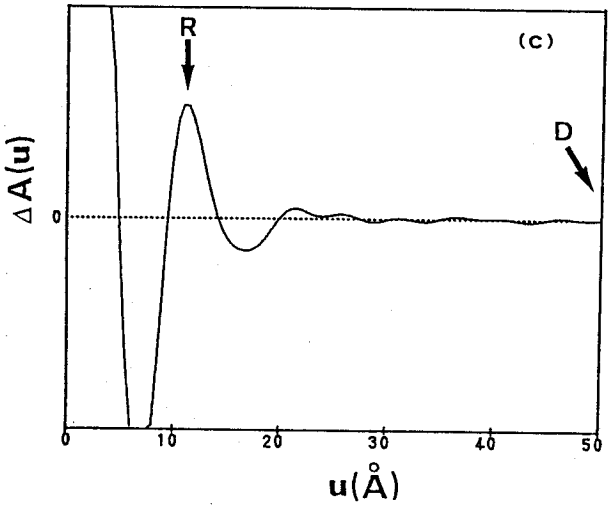
R
(c)
D
ΔA(u)
0
0
10
20
30
40
50
u(Å)

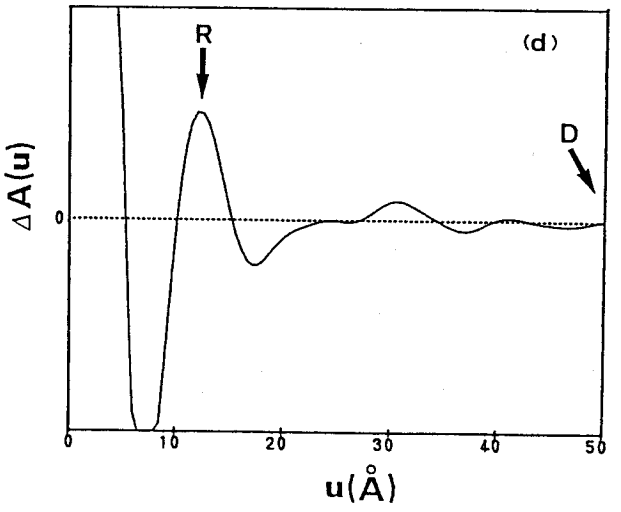
R
(d)
D
ΔA(u)
0
0
10
20
30
40
50
u(Å)

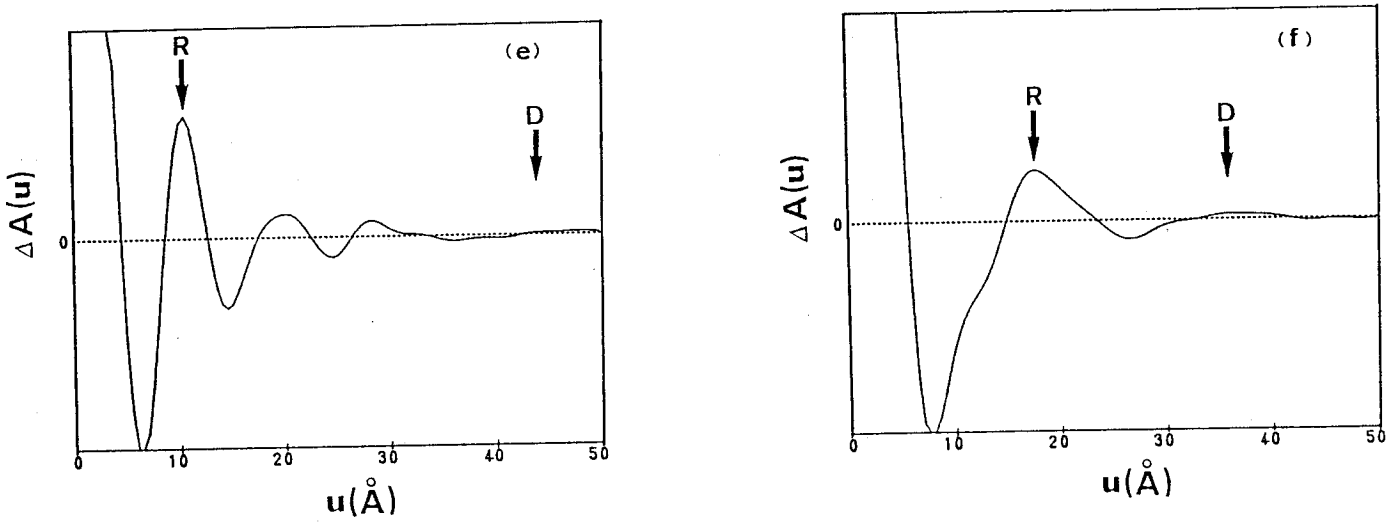

Fig. IV-3. Experimental difference autocorrelation functions, ΔA(u) for the six proteins; (a) Triosephosphate isomerase, (b) Lactate dehydrogenase, (c) Pyruvate kinase, (d) Taka-amylase A, (e) Myoglobin, (f) Cytochrome c; R, D, ΔA(u) peak and maximum dimension;

	R		D	
(a)	11.5	(Å)	72.5	(Å)
(b)	11.5		77.5	
(c)	11.5		68.5	
(d)	12.0		68.0	
(e)	10.0		44.0	
(f)	18.0		34.5	

IV-3-3 Simulation

To confirm the results of the Fig. IV-3, the $\Delta A(u)$ functions of the protein models were calculated and compared with the corresponding experimental functions. The model scattering intensities of the six proteins were calculated from the atomic scattering factors and the atomic coordinates obtained by X-ray crystallographic analyses which have been registered in the Brookhaven National Laboratory Protein Data Bank. All atoms excluding the heme group and binding water were used for the calculations of the scattering intensities except pyruvate kinase which has the only α-carbon atoms registered in the data bank. Atomic scattering factors evaluated by Thomas-Fermi or Hartree-Fock Method were available. The $I_R(h)$ curves from the calculated scattering intensities are shown in Fig. IV-4. The difference autocorrelation functions calculated from the $I_R(h)$ curves are represented in Fig. IV-5. The $\Delta A(u)$ functions ($\Delta A(u)_{calc}$) have also the peak at the distance of about 12 Å in the figures of the proteins containing β-sheets. From the results of the X-ray measurement and the model calculations, it was clarified that the protein containing β-sheets gave the 12 Å peak to the distance distribution in the protein molecule.

Further advanced simulation was carried out in order to clarify the cause to give the distance of 12 Å. An atomic-pair distance distribution was calculated about following four groups: intra-β-strands of the proteins

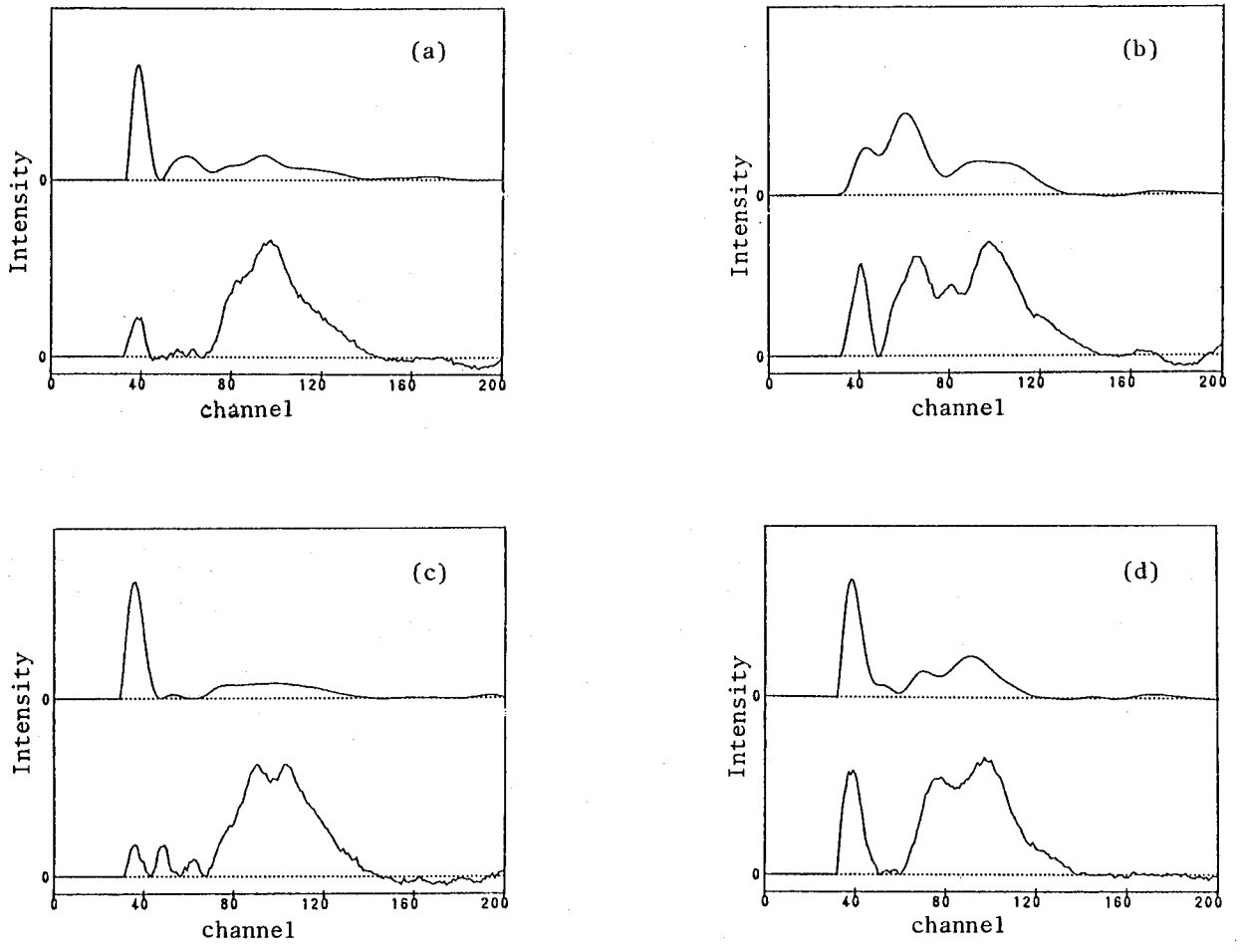
(a)
(b)
(c)
(d)
Intensity
0
0
0
40
80
120
160
200
channel

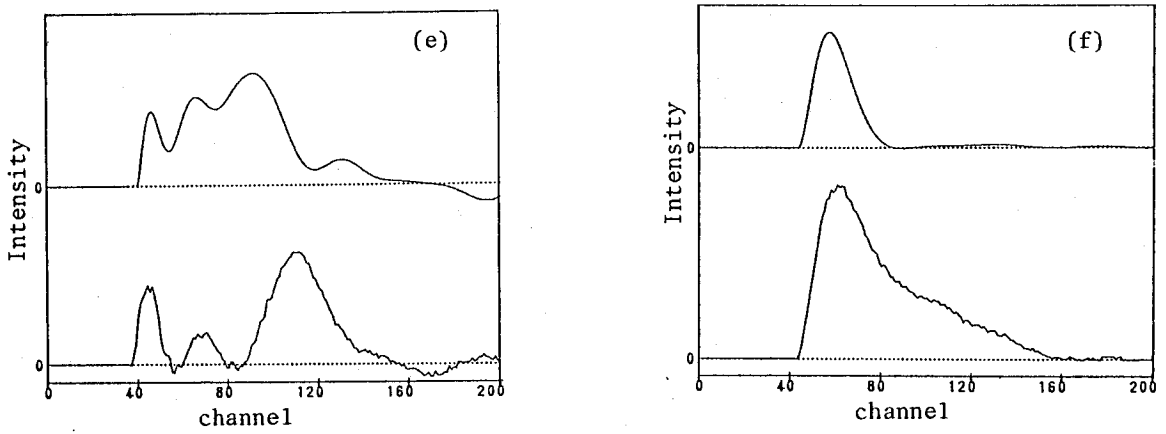

Fig. IV-4. $I_R(h)$ curves for the six proteins; (a) Triosephosphate isomerase, (b) Lactate dehydrogenase, (c) Pyruvate kinase, (d) Taka-amylase A, (e) Myoglobin, (f) Cytochrome c; upper, $I_R(h)$ for calculated model scattering curves; lower, $I_R(h)$ for observed scattering curves. Intensities directed by ordinates are given in arbitrary units.

(a)
D
R
0
10
20
30
40
50
u(Å)
Δ A(u)

(b)
D
R
0
10
20
30
40
50
u(Å)
Δ A(u)

(c)
D
R
0
10
20
30
40
50
u(Å)
Δ A(u)

(d)
D
R
0
10
20
30
40
50
u(Å)
Δ A(u)

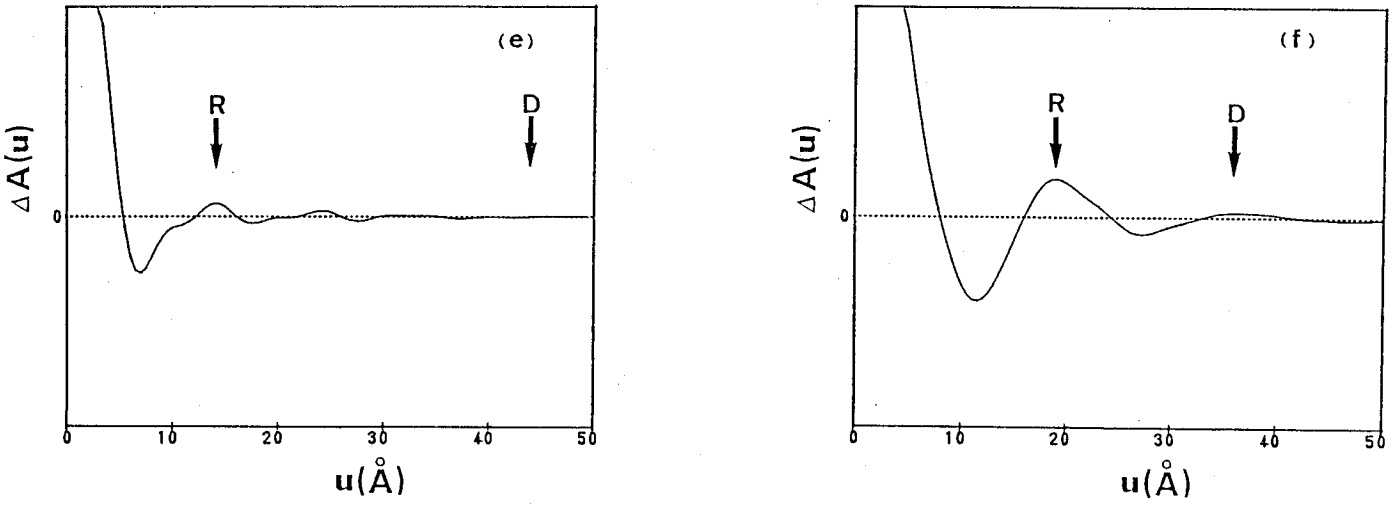

Fig. IV-5. Calculated difference autocorrelation functions, ΔA(u) for the six proteins; (a) Triosephosphate isomerase, (b) Lactate dehydrogenase, (c) Pyruvate kinase, (d) Taka-amylase A, (e) Myoglobin, (f) Cytochrome c; R, D, ΔA(u) peak and maximum dimension;

	R		D	
(a)	12.0	(Å)	72.5	(Å)
(b)	12.0		77.5	
(c)	11.5		68.5	
(d)	12.5		68.0	
(e)	14.0		44.0	
(f)	19.0		34.5	

containing α-helices and β-sheets; inter-β-strands of the same proteins; inter-α-helices of the same proteins; inter-α-helices of the proteins containing only α-helices. The results are shown in Fig. IV-6. The atomic-pair distance distribution of the inter-β-strands presents a maximum peak at about 12-14 Å without reference to the molecular size, while the distribution of the intra-β-strands presents it at about 5 Å and in a case of the α-helices, the distribution maximum is varying in proportion to the molecular size. This means that the distance of 12-14 Å is considered as the average distance of the inter-β-strands in the protein molecule.

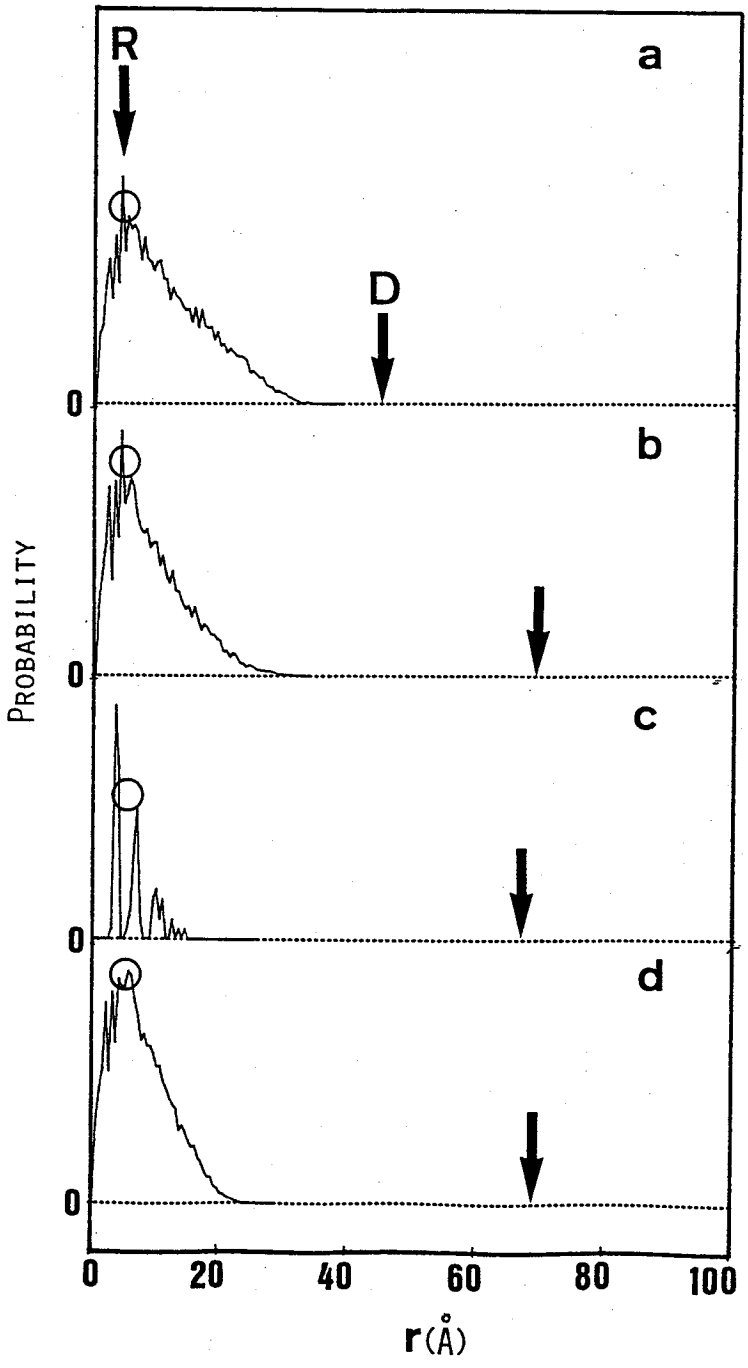

Fig. IV-6-1. Atomic-pair distance distribution: intra-β-strands; (a) Superoxide dismutase, (b) Triosephosphate isomerase, (c) Pyruvate kinase, (d) Taka-amylase A; R, D, distribution peak and molecular dimension.

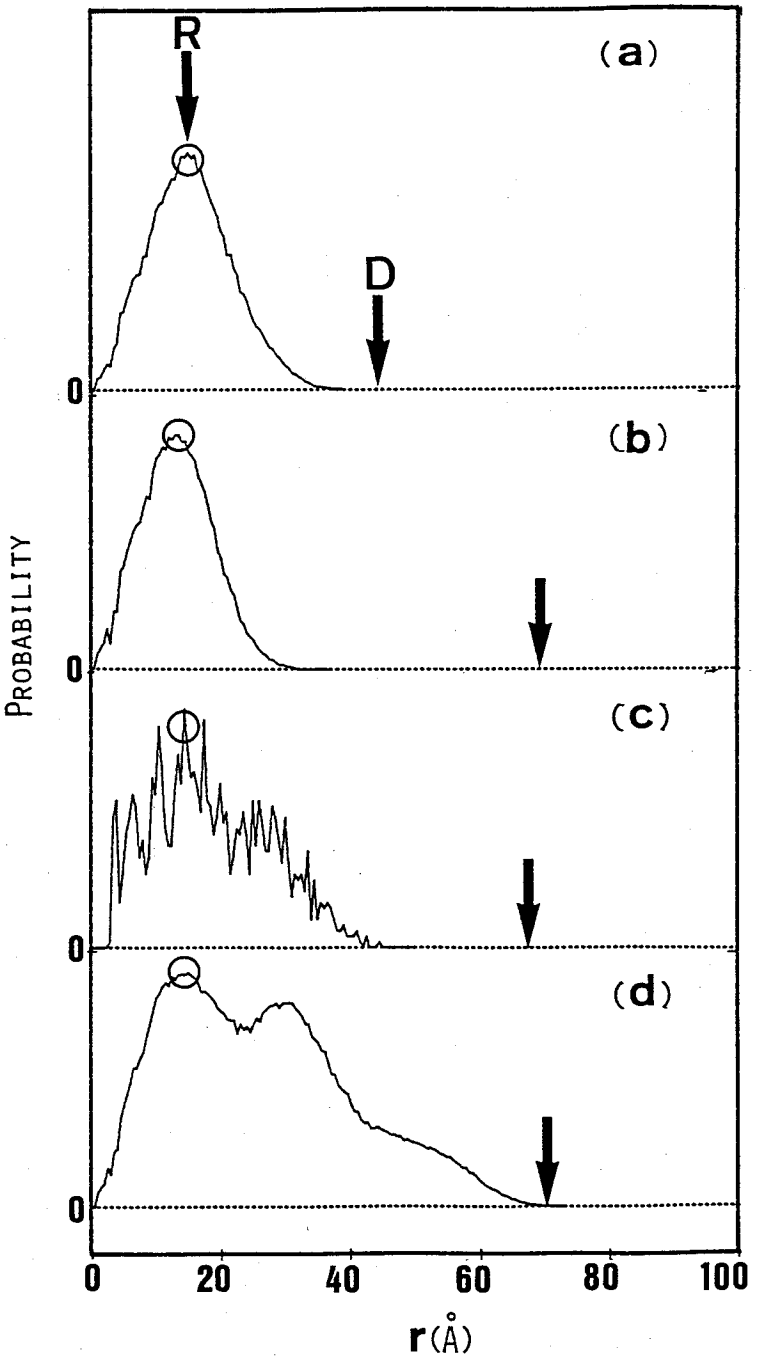

Fig. IV-6-2. (continued):
inter-β-strands; (a) Superoxide dismutase,
(b) Triosephosphate isomerase, (c) Pyruvate kinase,
(d) Taka-amylase A.

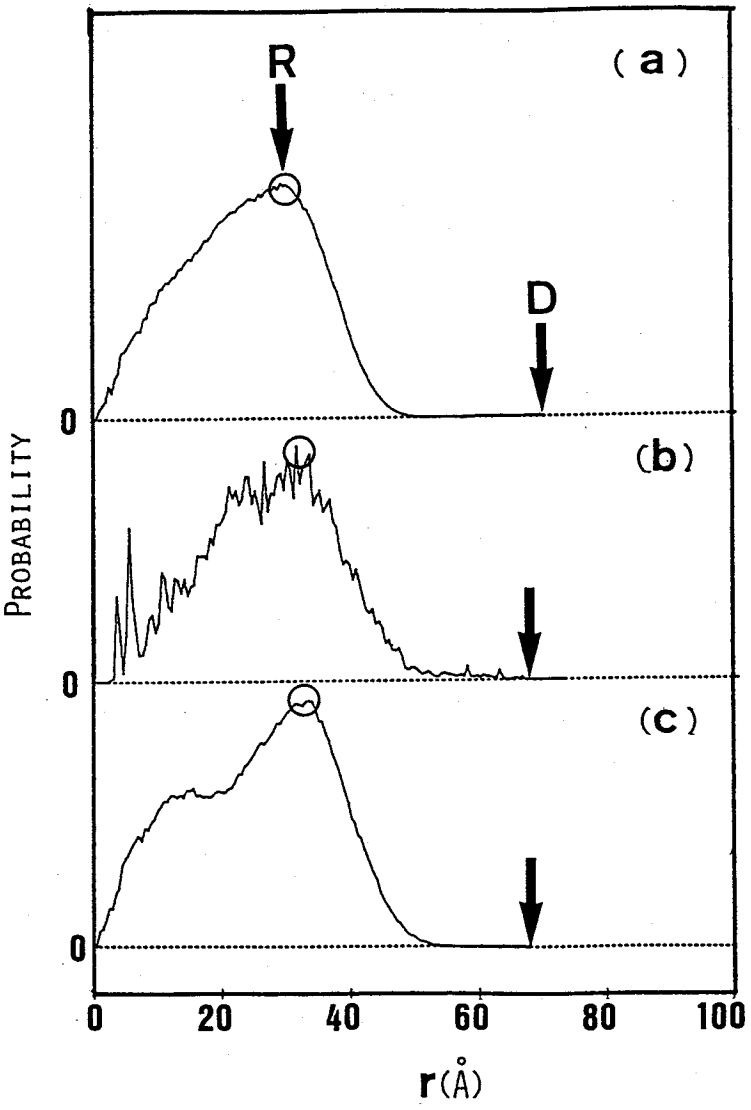

Fig. IV-6-3. (continued):
inter-α-helices; (a) Triosephosphate isomerase, (b) Pyruvate kinase, (c) Taka-amylase A.

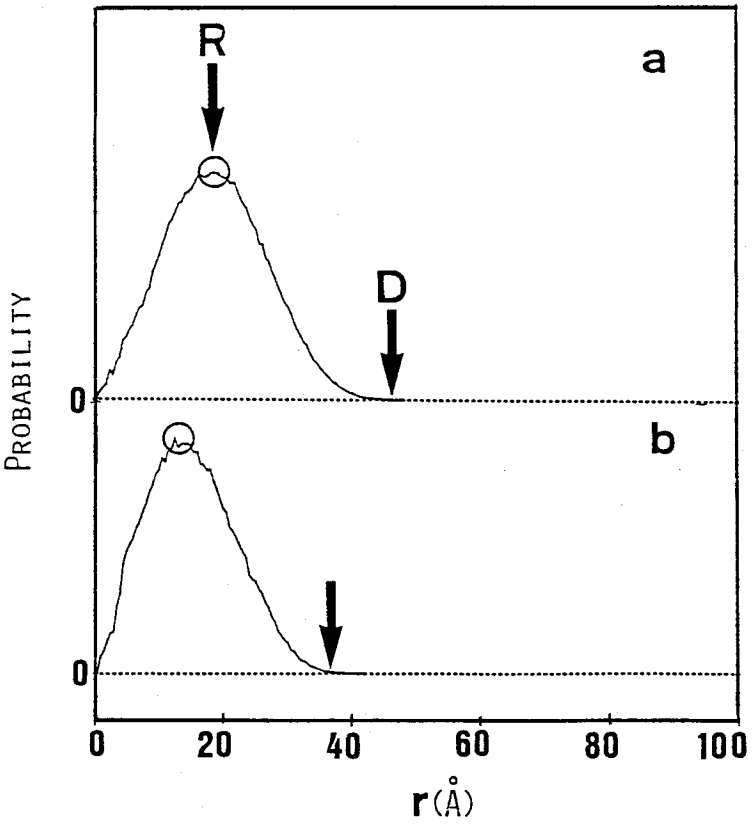

Fig. IV-6-4. (continued):
inter-α-helices; (a) Myoglobin, (b) Cytochrome c.

IV-4. Discussion

The X-ray scattering from a protein solution contains information on the overall structure and internal structure which can be analyzed separately by dividing the scattering intensity into the two scattering angle regions (the small angle and the large angle regions).

The radius of gyration and the eccentricity specifying the overall structure of proteins are estimated by the analysis of the scattering intensity data in the small angle region and have also some influence on the scattering intensity in the large-angle region. The internal structure of a protein affects the scattering intensity profile in the large-angle region. However, the intensity fluctuations in the large-angle region are very small in comparison with the intensity in the same region due to the overall structure of the protein, and it is very difficult to find out the characteristics of the profile. The autocorrelation function, A(u), calculated with such scattering intensity data is also very hard to be interpreted. Therefore, these fluctuations are required to be extracted by subtracting extra intensity due to the overall structure from the intensity in the large-angle region.

The scattering intensity I(h) from the particle was derived firstly by Debye as a following equation:

$$I(h) = \sum_{ij}^{N}\sum f_i f_j \frac{\sin(d_{ij}h)}{d_{ij}h} \qquad \text{(IV-3)}$$

where f is the atomic scattering factor, d_{ij} is the distance between the centers of the i-th and j-th atoms, and N is the number of atoms. Since the atomic scattering power f is proportional to the number of electrons, it is approximately taken the place of form factor ($\rho V\Phi$) of a sphere , where ρ is the electron density of the sphere, V is the volume of the sphere and Φ is the scattering amplitude of the sphere. If a molecule is composed of the equivalent spheres (radius=R), the equation (IV-3) is rewritten as a following equation by use of the difference of electron density ($\Delta\rho_i$) from the mean electron density of the molecule:

$$I(h) = I_V(h) + I_{VF}(h) + I_F(h) \qquad \text{(IV-4)}$$

$$I_V(h) = \rho_m^2 V^2 \Phi^2(h) \sum_{ij}^{N} \frac{\sin(d_{ij}h)}{d_{ij}h}$$

$$I_{VF}(h) = \rho_m V\Phi(h) \sum_{ij}^{N} \frac{(\Delta\rho_i + \Delta\rho_j)\sin(d_{ij}h)}{d_{ij}h}$$

$$I_F(h) = V^2\Phi^2(h) \sum_{ij}^{N} \frac{\Delta\rho_i\Delta\rho_j \sin(d_{ij}h)}{d_{ij}h}$$

$$\sum_{ij}^{N}(\Delta\rho_i + \Delta\rho_j) = 0$$

where ρ_m is the mean electron density of the molecule. $I_V(h)$ is the scattering intensity from the particle containing the uniform electron density, $I_F(h)$ reflects the fluctuation of the electron density in the particle and $I_{VF}(h)$ is their cross-term.

Internal structure may be expressed as fluctuations from the uniform electron density of the molecule. $\Delta A(u)$ function transformed from $I_R(h)$ is shown in Fig. IV-3. These figures present information on the internal structure of protein molecule, because the $I_R(h)$ data contain the interference terms of many $\Delta\rho$ representing the fluctuation of the electron density of the intramolecule. This function may be likely similar to the Patterson function in X-ray crystallography, and represents the vector distribution probability inside the particles.

As shown in Figs. IV-3(a), (b), (c) and (d), $\Delta A(u)$ curves have a common feature such as a maximum of 12 Å due to the β-sheets, but the curve of the LDH is not similar to other three curves in the range of 18-50 Å. This result shows that the tertiary structure of the LDH is different from those of other three proteins. It is a plain truth as proposed by J. S. Richardson that the LDH is classified into a type of doubly wound parallel β-sheets according to the tertiary structure, while the TAA, the TIM and the PK are classified into a type of a singly wound parallel β-barrels (41). Though the LDH is structurally different from the TAA, the TIM and the PK, they have obviously common structural units of the secondary structures such as the β-strand. Therefore, maximum at 12 Å in the $\Delta A(u)$ function likely corresponds to the length of β-strand and to the distance of inter-/intra-strand. And in the range of 18-50 Å, the $\Delta A(u)$ reveals each characteristic distance distribution attributed to the relatively large structural

units such as parallel β-sheet and β-barrel.

Two proteins, Mb and Cyt.c, have only α-helices as secondary structures and a single heme in their molecules. If the position of peaks in ΔA(u) function corresponds to the distance of inter-/intra-helices, the ΔA(u) of the Mb and the Cyt.c curves should be similar to each other. However, the two ΔA(u) curves have no similarities. The differences of their ΔA(u) curves are caused by the different helical content of two proteins.

On the other hand , from results of crystal structure analyses, it is possible to calculate the scattering intensities of protein models from their atomic coordinates. The calculated scattering intensities were processed by the same way as that used for the observed data. Fig. IV-4 shows the $I_R(h)$ curves produced by subtracting B-spline function from the calculated scattering curve, and also shows the observed scattering curves. The differences between calculated and experimental scattering data are detected in these figures, for example migration of the maxima positions and variation of relative maxima heights. It is probably caused by the difference between such scattering intensities from a protein in the aqueous state and from its model with atomic scattering factors in vacuo. If the calculated scattering curve is made to fit the experimental one, it must be necessary to take account of the solvent effect for atomic scattering factor. One of the methods to correct the solvent effect is to use 'effective atomic

scattering factor' (42), in place of atomic scattering factor in vacuo. This method is used in the improved cube method (42,43). Though the solvent effect was not taken into account, in the present simulation of scattering curves, characteristics of protein structures could be expressed sufficiently in each scattering curve. Then, the $\Delta A(u)$ function could be derived from $I_R(h)$ curve. It was noticed previously that each $\Delta A(u)$ function in Fig. IV-5 was not directly obtained from atomic coordinates of corresponding protein model, but calculated from scattering intensity from which B-spline function was subtracted. In the Fig. IV-5, the behavior of each curve is similar to that of experimental curve except for small differences which are the deviations of the maximum position and its relative height. The shifts of maxima and minima in the proteins containing β-sheets are within 2 Å. The results in the simulations correspond to those of the experimental curves. The $\Delta A(u)$ curve of Cyt.c conserves the features of the experimental curve, but the $\Delta A(u)$ curve of Mb seems to slide by 4 Å to the larger value in comparison with its observed curve. This fact plausibly indicates that the molecular structure of myoglobin in the aqueous state is different from that in the crystalline state (44), if $\Delta A(u)$ function gives information on the secondary structure such as α-helix.

The atomic-pair distance distribution profile directly gives intramolecular distance distribution (Fig. IV-6) because of no assumption in the calculation. These

profiles indicate that proteins containing some β-sheets have distribution maxima of 12-14 Å without reference to each molecular size while proteins containing only α-helices have such maxima in proportion to molecular size. The former distance corresponds to that of the ΔA(u) function, for the functions also have common peaks without reference to the molecular size (Figs. IV-3 and IV-5). The distance of 12-14 Å can be considered as the average distance between β-strands and may play an important role for the protein folding, or the main-chain packing.

From results described above, it can be followed that information on the internal structures such as secondary or super-secondary structures can be derived from ΔA(u) functions transformed from the large-angle scattering intensities. The interferences of the β-strands give the X-ray scattering in the large-angle region and it is expressed as the distance distribution peak of 12 Å by the analysis of the scattering data. In case of α-helices in Cyt.c and Mb, common features of their internal structures could not be obtained from their ΔA(u) functions. The reason may be that the contribution of the helices to the X-ray diffraction is much smaller than that of β-sheets. Furthermore, the existence of the peaks attributed to the β-sheets are confirmed and recognized by the atomic-pair distance distribution profile. This fact shows the efficiency of the subtraction by the B-spline function and the new method of the analysis in the large-angle scattering from protein solution.

Chapter V

General conclusion

The solution X-ray scattering technique was applied to investigate the structure of cytochrome oxidases, cytochrome bc_1 complexes and also used for the analyses of secondary structure of globular proteins.

In Chapter I, the general and fundamental theories of the X-ray scattering were described. The contrast variation method is a new technique to investigate the structure of biological macromolecules in solution and can increase information of the solution X-ray scattering. Chapter II dealt with the experimental systems of the solution X-ray scattering method that I have developed in order to measure the scattering intensities with enough accuracy. The experimental systems were classified into three types; One was a high resolution small-angle X-ray scattering apparatus to measure the intensities at very small angle region ($0 < h < 0.14$); The second was a conventional small-angle camera to measure at a range of $0.014 < h < 0.3$ and the third was a middle-/large-angle camera at a range of $0.1 < h < 1.6$. These systems could compensate each other and afford us room for choice of an optimum condition for the measurement.

In Chapter III, the structure of cytochrome oxidase isolated from beef heart mitochondria and the complex with cytochrome c in solution were studied. In the presence of

Triton X-100 detergent, the oxidase was found to exist as an elongated dimer with the maximum dimension of 165 Å, which was composed of two structurally minimal units, and bound cytochrome c at the place which was about 40 Å distant from the both ends of the elongated one to form the electron-transferring complex without change of the maximum dimension. On the contrary, detergents were bound to the interface of the dimer and were about 180 molecules as the number of the Triton X-100. By these facts it was clarified that the hydrophobic part of the oxidase monomer was in close contact with the hydrophobic part of another monomer and hydrophilic part was kept away from the oxidase's contact region.

Also the structure of cytochrome bc_1 complexes isolated from beef heart mitochondria have been studied. The investigation clarified that the enzymes in the presence of Tween 20 existed as an oblate dimer with eccentricity of 0.3-0.1. Phospholipids involved in the enzyme were greatly depleted by hydrophobic-interaction chromatography and the depletion of the phospholipids made a maximum dimension of the enzyme decrease to 222 Å. It was suggested that the phospholipids were located in the circumference of the oblate dimer and the detergents bound there. Thus, it was shown that the hydrophilic part of the enzyme was in close contact with that of the other to form the oblate dimer.

Chapter IV dealt with one of methods to investigate the internal structure of globular proteins. X-ray

diffraction from proteins which have characteristic tertiary structure gave individual scattering profiles in the large angle region. These profiles were composed of some scattering patterns attributed to the secondary structure. Such scattering patterns were extracted from the whole scattering pattern by subtraction of B-spline curve. Difference autocorrelation function was useful to investigate the electron density fluctuation in the protein molecule. This function calculated from the extracted scattering pattern showed a peak at a distance of 12 Å. The peak was a common feature in such groups as proteins containing the β-sheets. It was also confirmed by a profile of a simple, atomic -pair distance distribution. These profiles also indicated peaks at a distance of about 12 Å for the proteins containing the β-sheets, while peaks for the intra-β-strand were about 5 Å. By these results it was thought that the distance of 12 Å was an average distance between β-strands and played an important role of the main-chain folding to form the tertiary structure.

References

(1) Debye,P. (1915) *Ann. Physik.* **46**, 809-823

(2) Guinier,A. (1939) *Ann. Phys.* **12**, 161-237

(3) Porod,G. (1952) *Kolloid-Z.* **124**, 83-114 and **125**, 51-57

(4) Green,H.S. (1947) *Proc. Roy. Soc. (London)* **A-189**, 103-117

(5) Debye,P. (1927) *Physik. Z.* **28**, 135-141

(6) Stuhrmann,H.B., and Kirste,R.G. (1965) *Z. Physik. Chemie., Frankfurt* **46**, 247-250

(7) Guinier,A. and Fournet,G. (1955) *Small Angle Scattering of X-Rays, John Wiley and Sons, New York*

(8) Danielson,W.E., Shenfil,L., and DuMond,J.W.M. (1952) *J. Appl. Phys.* **23**, 860-865

(9) Nisonoff,A., Hopper,J.E. and Spring,S.B. (1975) *The Antibody Molecule, Academic Press, New York*

(10) Barrett,A.J. and Starkey,P.M. (1973) *Biochem. J.* **133**, 709-724

(11) Elliott,A (1965) *J. Sci. Instrum.* **42**, 312-316

(12) Stuhrmann,H.B., and Miller,A. (1978) *J. Appl. Cryst.* **11**, 325-345

(13) Glatter,O. (1974) *J. Appl. Cryst.* **7**, 147-153

(14) Green,D.E., and Tzagoloff,A (1966) *J. Lipid Res.* **7**, 587-602

(15) Ozawa,T., Tada,M., and Suzuki,H. (1979) in *Cytochrome oxidase, Elsevier/North-Holland, Amsterdam*, P.39

(16) Ozawa,T., Okumura,M., and Yagi,K. (1975) *Biochem. Biophys. Res. Commum.* **65**, 1102

(17) Kawato,S., Sigel,E., Carafoli,E., and Cherry,R.J. (1981) *J. Biol. Chem.* **256**, 7518

(18) Gornall,A.G., Bardawill,C.J., and David,M.M. (1949) *J. Biol. Chem.* **177**, 751

(19) Yonetani,T. (1961) *J. Biol. Chem.* **236**, 1680

(20) Chen,P.S.Jr., Toribara,T.Y., and Warner,H. (1956) *Anal. Chem.* **28**, 1756

(21) Fowler,L.R., Richardson,S.H., and Hatefi,Y. (1962) *Biochim. Biophys. Acta* **64**, 170-173

(22) Tzagoloff,A. and MacLennan,D.H. (1965) *Biochim. Biophys. Acta* **99**, 476-485

(23) Hagihara,B., Morikawa,I., Sekuzu,I., and Okunuki,K. (1958) *J. Biochem.* **45**, 551

(24) Shimomura,Y., and Ozawa,T. (1980) *Biochemistry International* **1**, 283-289

(25) Zaugg,W.S., and Rieske,J.S. (1962) *Biochem. Biophys. Res. Commum.* **9**, 213-217

(26) Green,D.E., Järnefelt,J., and Tisdale,H.D. (1959) *Biochim. Biophys. Acta* **31**, 34-46

(27) Hartree,E.F. (1972) *Anal. Biochem.* **48**, 422-427

(28) Rieske,J.S., Zaugg,W.S., and Hansen,R.E. (1964) *J. Biol. Chem.* **239**, 3023-3030

(29) Kratky,O. (1963) *Progress in Biophys.* **13**, 105-173

(30) Henderson,R., Capaldi,R.A., and Leigh,J.S. (1977) *J. Mol. Biol.* **112**, 631-648

(31) Robinson,N.C., and Capaldi,R.A. (1977) *Biochemistry* **16**, 375-381

(32) Saraste,M., Penttila,T., and Wikström,M. (1981) *Eur. J. Biochem.* **115**, 261-268

(33) Vail,W.J., Riley,R.K., and Rieske,J.S. (1975) *FEBS LETTERS* **58**, 33-38

(34) Toda,H., and Akabori,S. (1963) *J. Biochem.* **53**, 102-110

(35) Bannar,D.W., Bloomer,A.C., Petsko,G.A., Phillips,D.C., Pogson,C.I., and Wilson,I.A. (1975) *Nature (London)* **255**, 609-614

(36) Matsuura,Y., Kusunoki,M., Harada,W., Tanaka,N., Iga,Y., Yasuoka,N., Toda,H., Narita,K., and Kakudo,M. (1980) *J. Biochem.* **87**, 1555-1558

(37) Stuart,D.I., Levine,M., Muirhead,H., and Stammers,D.K. (1979) *J. Mol. Biol.* **134**, 109-142

(38) Adams,M.J., Ford,G.C., Koekoek,R., Lentz,P.J.Jr., MacPherson,A.Jr., Rossmann,M.G., Smiley,I.E., Schevitz,R.W., and Wonacott,A.J. (1970) *Nature (London)* **227**, 1098-1103

(39) Swanson,R., Trus,B.L., Mandel,N., Mandel,G., Kallai,O.B., and Dickerson,R.E. (1977) *J. Biol. Chem.* **252**, 759-775

(40) Watson,H.C. (1969) *Prog. Stereochem.* **4**, 299-333

(41) Richardson,J.S. (1984) *Advances in Protein Chemistry Vol.34 The Anatomy and Taxonomy of Protein Structure*

(42) Müller,J.J. (1983) *J. Appl. Cryst.* **16**, 74-82

(43) Fedorov,B.A.,Ptitsyn,O.B., and Voronin,L.A. (1974) *J. Appl. Cryst.* **7**, 181-186

(44) Fedorov,B.A., and Denesyuk,A.I. (1978) *J. Appl. Cryst.* **11**, 473-477

(45) Kratky,O. (1958) *Z. Elektrochem.* **62**, 66-73

(46) Dickerson,R.E. and Timkovich,R. (1975) *The Enzymes Oxidation/Reduction volume Cytochrome c Part II*

List of publications

1. Structural Studies on Cytochrome c by the Small-Angle Scattering

   Yukio Morimoto, Tatsuhisa Kato, Yasuo Hata, Nobuo Tanaka, Yukiteru Katsube, Tatzuo Ueki, Mikio Kataoka, Yuzuru Hiragi and Yoshiyuki Amemiya (1984/85) *PHOTON FACTORY ACTIVITY REPORT*, **3**, 176

2. Structural Studies on Aldolase by means of Time-Resolved X-ray Scattering

   Yukio Morimoto, Mamoru Sato, Yasuo Hata, Nobuo Tanaka, Yukiteru Katsube, Tatzuo Ueki, Mikio Kataoka, Yuzuru Hiragi and Yoshiyuki Amemiya (1985/86) *PHOTON FACTORY ACTIVITY REPORT*, **4**, (in press)

3. Secondary Structure Analysis of proteins in solution by large-angle X-ray scattering

   Yukio Morimoto, Yasuo Hata, Nobuo Tanaka and Yukiteru Katsube (in preparation)

4. Structural Investigation of Beef Heart Cytochrome Oxidase in Solution

   Yukio Morimoto, Mamoru Sato, Nobuo Tanaka, Yukiteru Katsube, Masashi Tanaka and Takayuki Ozawa (in preparation)

5. Designing and Application of a New High Resolution Small-Angle X-ray Scattering Apparatus

   Yukio Morimoto (1986) *Kessho Kaiseki Kenkyu Senta Dayori* **7**, 21-28

6. Isolation, Characterization, and Comparison of a Ubiquitous Pigment-Protein Complex Consisting of a Reaction Center and Light-Harvesting Bacteriochlorophyll Proteins Present in Purple Photosynthetic Bacteria
Tetsuya Ueda, Yukio Morimoto, Mamoru Sato, Tomisaburo Kakuno, Jinpei Yamashita, and Takekazu Horio (1985) *J. Biochem.* **98**, 1487-1498

7. Effect of Iodination on the Purple Membrane Structure
Mikio Kataoka, Kazuo Takeda, Yukio Morimoto, Naoki Sato Nobuo Tanaka, and Fumio Tokunaga (1986) *Photobiochem. and Photobiophys.* (in press)

8. Stopped-Flow Small-Angle X-Ray Scattering Study on the Acid-Denaturation of Taka-Amylase A
Tatsuya Hozaki, Mitsunori Kato, Mamoru Sato, Nobuo Tanaka, Yukio Morimoto, Yasuo Hata, Yukiteru Katsube and Nobutami Kasai (1986) *Bull. Chem. Soc. Jpn.* **59**, 3747-3753

9. Structure of Methyl-3-C-(Acetoxymethyl)-1,4-di-O-acetyl-α-erythro-pentofuranoside
Miwako Irie, Keiichi Fukuyama, Tomitake Tsukihara, Yukiteru Katsube, Yukio Morimoto, Yoshihiro Shigemasa and Ruka Nakashima (1985) *Acta. Cryst.* **C41**, 1814-1816

The content of this thesis has been or will be published in the above papers and communications.